Durham University

Durham E-Theses

Investigation into the use of zero angle ultrasonic probe array for defect detection and location

Snowdon, Paul C.

How to cite:

Snowdon, Paul C. (2007) *Investigation into the use of zero angle ultrasonic probe array for defect detection and location*, Durham theses, Durham University. Available at Durham E-Theses Online: http://etheses.dur.ac.uk/2283/

Use policy

The full-text may be used and/or reproduced, and given to third parties in any format or medium, without prior permission or charge, for personal research or study, educational, or not-for-profit purposes provided that:

- a full bibliographic reference is made to the original source
- a link is made to the metadata record in Durham E-Theses
- the full-text is not changed in any way

The full-text must not be sold in any format or medium without the formal permission of the copyright holders.

Please consult the full Durham E-Theses policy for further details.

Academic Support Office, The Palatine Centre, Durham University, Stockton Road, Durham, DH1 3LE
e-mail: e-theses.admin@durham.ac.uk Tel: +44 0191 334 6107
http://etheses.dur.ac.uk

Copyright© 2007 by Paul C. Snowdon

The copyright of this thesis rests with the author. No quotation from it should be published without prior written consent and information derived from it should be acknowledged.

The copyright of this thesis rests with the author or the university to which it was submitted. No quotation from it, or information derived from it may be published without the prior written consent of the author or university, and any information derived from it should be acknowledged.

10 MAR 2008

Acknowledgements

I would like to thank Dr. Sherri Johnstone of the University of Durham for her supervision and support during my studies, and Professor David Wood and Professor Mike Petty for their continuous encouragements.

I would also like to thank Dr. Stephen Dewey of Corus Plc. for his support, and Corus Plc. for their financial contribution to the project.

Abstract

The steel industry like any other manufacturing process is under constant pressure to deliver higher quality defect free material at lower cost to customers. This push for zero defects has led to improved manufacturing processes and the need for more reliable, faster defect testing methods. Ultrasound fundamentally provides a mechanical stress, produced by tensile, compressive, shearing or flexural forces, which are of such low intensity that no material damage occurs.

The remit of the project was to investigate and develop the latent potential within the present automated ultrasonic immersion system using an array of normal angle probes, used for billet inspection. The work presented in this thesis describes the research undertaken to develop a system using, 10mm diameter, standard zero angled 5MHz ultrasonic transducers. The transducers were used at linear separation distances of between 22.5mm and 45mm set in a typical 8-probe array orientation.

The developed technique is potentially transferable to other ultrasonic multi-probe array applications and demonstrates that time of flight diffraction can be realised using normal probes, and termed Normal Probe Diffraction, (NPD). The technique located defects, using the intersection of ellipses, with an error of <0.5% of the signal transit distance and, with the application of a correlation filter, improved the Signal to Noise Ratio (SNR) from –2.0dB to 17.0dB.

Contents

Chapter 5. System and Initial Experimental Work

Nomenclature

Symbol	Quantity	Units
α	Attenuation coefficient	$^{N}/_{A}$
D	Diameter of a flat circular oscillator	m
λ	Wavelength	m
N	Length of near zone	m
f	Frequency	Hz
c	Acoustic velocity	m/s
γ	Half angle of divergence	$^{N}/_{A}$
v	Particle velocity	m/s
ρ	Density	kg/m^3
p	Sound pressure	Pa
μ	Poisson's ratio	$^{N}/_{A}$
E	Young's modulus	GPa
G	Modulus of shear	N/m^2
Z	Acoustic impedance	Ns/m^3
P	Acoustic power	W

Chapter 1.

Motivation for the Project

1.1. Introduction

The steel industry like any other manufacturing company is under constant pressure to deliver higher quality "defect free" material at lower cost to customers. Improvements in manufacturing processes and the use of more sophisticated measurement systems have seen a significant reduction in the number of defective products with the aim of reaching the elusive goal of zero failures [1]. This push for zero defects has lead to improved manufacturing processes and the need for more reliable, faster defect testing methods.

The standard ultrasonic technique for defect detection is the pulse/echo method, using an array of relatively low cost ultrasonic transducers. To improve on this method the steel industry is tending to move towards complex phased array technologies. These ultrasonic systems are relatively expensive and complex when compared to a basic pulse/echo system. They also have a propensity of being application specific, in that the probes or probe-coupling shoe will be tailored to a specific examination or component location.

The remit of this project was to investigate the latent potential within an existing ultrasonic defect detection system installed at Thrybergh billet mill, Corus plc. This system consists of an array of probes in which each probe sequentially fires and receives an ultrasonic pulse as a steel billet travels past. The specific research question to be addressed in this thesis is, if the system is reconfigured such that after each probe fires, all the probes are used to detect reflected pulses, can extra information about the presence, size and type of defects be improved?

Chapter 2 gives a description of the manufacturing process at Thrybergh billet mill together with the current ultrasonic defect detection system to be investigated. To put the project into context, a literature review of current technologies is presented in Chapter 3 followed by the wave propagation theory required to understand the technology researched in this project. To study the system, an experimental rig was set up in controlled laboratory conditions. This is described in Chapter 5 together with the results from initial experimental work. Chapters 6 and 7 describe the experimental data and analysis undertaken using the experimental rig to analyse the detected signals and improve the signal the noise ratio. Finally, the work is critically assessed in Chapters 8 and 9 and summarised in Chapter 10.

1.2. References

1. Wolfram, A. *Automated ultrasonic inspection.* in *15th WCNDT conference.* 2000. Rome, Italy. www.ndt.net/article/wcndt00/papers/idn197/idn197.htm

Chapter 2.

Project Definition

2.1. Introduction

This chapter firstly describes the manufacturing process at Thrybergh billet mill such that the purpose, operation and limitations of the existing defect detection system can be explained. The detailed project motivation will then be presented in context with this manufacturing process.

2.2. The Bloom and Billet Mill

The Bloom and Billet Mill consists of two distinct processes: the Primary Mill and the Finishing mill. At the Primary Mill the molten steel is continuously cast as a 400 mm square bloom. During the casting process, refractory shrouds cover the vessel to prevent atmospheric exposure, which is the main cause of inclusions being formed in the molten steel [1, 2, 3]. Oxides and sulphides are the most common inclusions found in steel; these can be quite simple in nature containing just one component (e.g. Alumina particles Al_2O_3) but very often come as a much more complex, multi-component construction, containing more than one inclusion.

The solidified steel is then re-heated and rolled into a 180 mm square billet. In addition to the chemical variations, inclusions also vary in their size and shape [4], however the hot rolling process elongates and concentrates these inclusions to the core of the billet. An initial eddy current inspection of the material (for surface breaking cracks) is done at this stage prior to the steel leaving the mill. The steel is then transferred in billet form to the Finishing Mill. At the Finishing Mill it is reheated to 1200°C and rolled down to the final size required of between 30-75mm. This process of working the steel also improves the quality of the steel by refining its crystalline structure and making the metal stronger and tougher. An ultrasonic inspection process takes place after the material has been hot rolled down to the final 30-75mm sizes and the evaluation of the ultrasonic signals is carried out with multi-channel electronics [5]. This is because the coarse grain structure of the as-cast bloom causes high attenuation of ultrasound [6]. Thus, it is more practical to inspect the steel post hot rolling.

2.3. Automated Ultrasonic Test System

The current system is a stationary multi-transducer array, consisting of two identical banks of immersion transducers set overlapping so that no part of the material is left un-inspected. These are arranged at normal incidence to the material and at 90^0 to each other, as shown in Figure 2.2. This is used for the inspection of square section, steel billets ranging in size between 40mm to 80mm. The steel billet in this particular inspection system is passed by the transducer arrays on the diamond as shown in red in Figure 2.2. Each bank of eight transducers is arranged as in Figure 2.3, the transducers were activated sequentially, testing the steel using pulse/echo procedures.

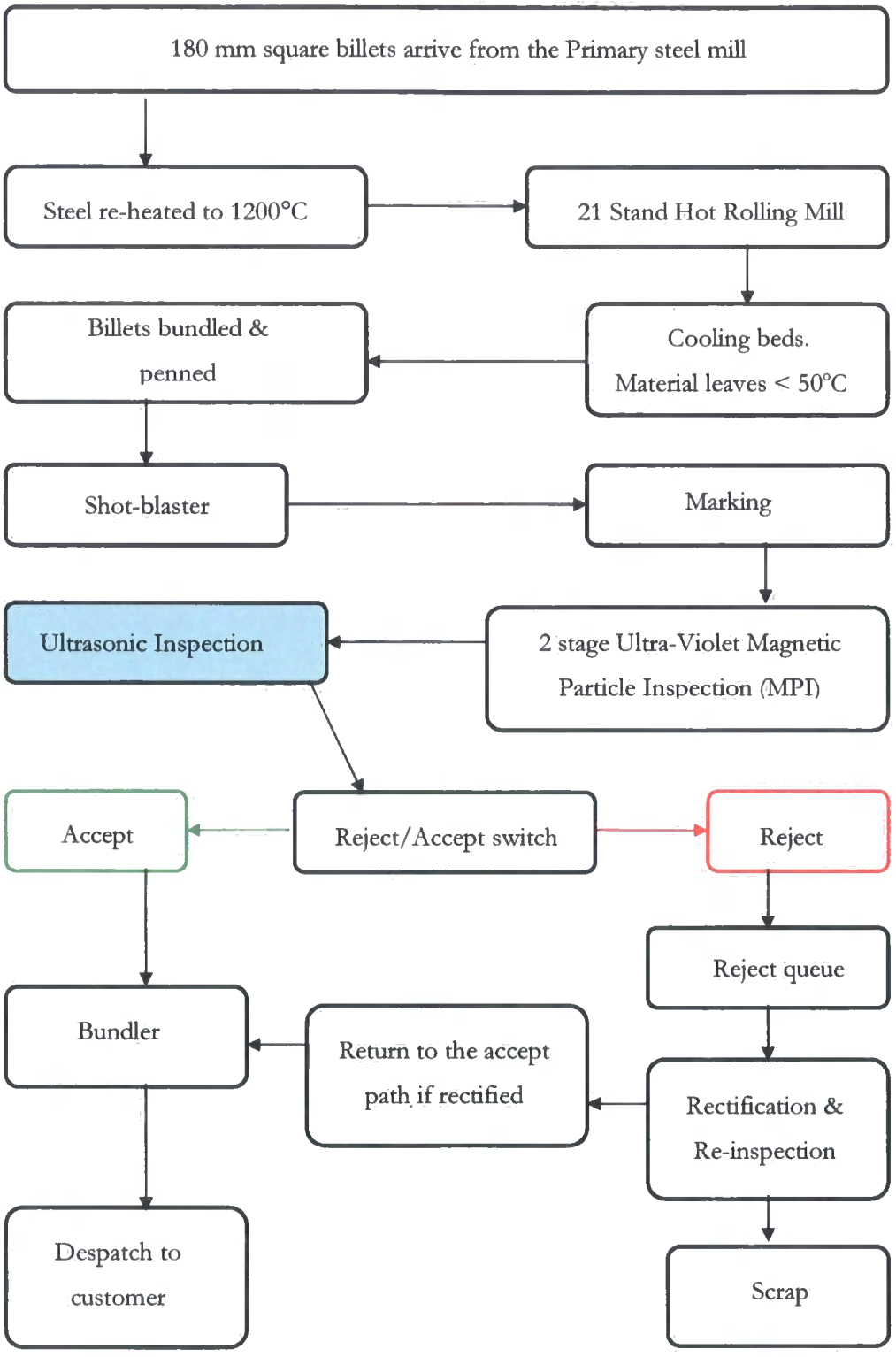

Figure 2.1. Schematic of the Bar Mill finishing line

The piezoelectric transducers have a 10mm diameter active element. This combined with the orientation and a 75mm stand off distance facilitates beam overlap at the operating speed of the system. The stand off distance of the 5MHz transducers also takes the pulse out of the Fresnel zone or near-field and into the Fraunhofer-zone or far-field [7].

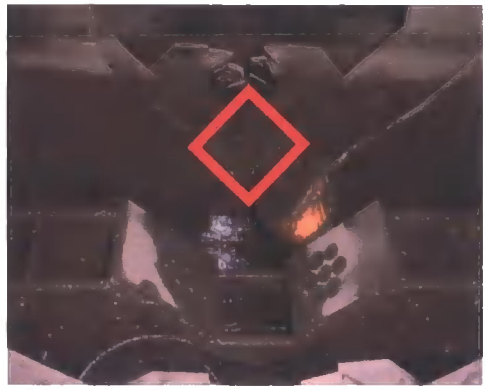

Figure 2.2. Photograph of the transducer array showing material orientation in red

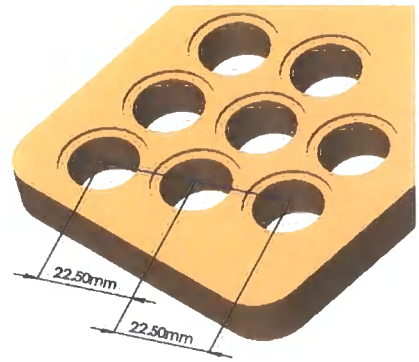

Figure 2.3. Drawing of fixture showing transducer separation

2.4. System Operation

The front end of the bar as it passed beyond the inspection transducers, enables the automated ultrasonic inspection system. This results in a short length of bar at the extreme front end which is not been inspected (50mm - 100mm typically) known as 'front end loss' and it is necessary therefore to suppress the automatic alarm output from the inspection system caused by distorted signals which would occur if the transducers pick up the abrupt edge of the bar end. Each transducer of the array works independently in pulse/echo mode i.e. each transducer is both a transmitter and receiver.

The transducers are held at a distance of approximately 70mm from the material. This is both to alleviate the possibility that they will be struck by the front end of the moving bar, and to remove the complications involved with the near field of the transducers. An automated marking system, marks all defect affected areas that are encountered by the inspection system.

The pulse repetition frequency (PRF) of the probe array is optimised to allow for signal decay [8], and to give full coverage of the billet to be inspected, whilst operating at its recommended throughput rate. Test throughput speeds are limited, not by the pulse repetition rate, but by air entrapment and turbulence. The system is capable of material throughput speeds of 2m/s, however at Thrybergh bar mill it runs between 0.8m/s to 1m/s. The inspection is terminated prior to the tail end of the bar passing over the inspection transducers and again suppressing the alarm output similar to the front end. This results in an additional un-inspected region at the tail end of the bar, known as 'back end loss'. Bars, for which the line control logic has been alerted to the defective nature of the product, are tracked through the line and subsequently sorted into good or defective groups. The defective bars are then manually re-inspected to qualify and define the nature of the defect.

2.5. Project Motivation

As the demand for cleaner steels increases every year [9] it would be desirable from both an economic and environmental position to eliminate the primary re-heating and rolling process altogether.

This would have substantial influence on costs in energy expenditure and material handling. However this would place greater demands on the downstream NDT, as the intermediate NDT stage would also have been eliminated.

The remit of the project is to investigate the core section of the material using ultrasonic techniques. The steel sections of interest are square section billets with dimensions ranging from 76mm x 76mm down to 36mm x 36mm. The initial concept was to use the Sonomatic™ system as it currently operates, but processing the received transmission using several of the probes. That is a single transmitter with multiple receivers. The initial concept was deemed worthy of further investigation because of the divergence of the ultrasonic wave as it is transmitted. When an ultrasonic probe is fired, the pulse of ultrasound is transmitted through the water coupling into the steel billet, and is reflected off the back wall of the steel (pulse/echo). As an ultrasonic beam travels through a medium, it diverges. When the signal is received back at the probe, because of the distance the signal has travelled, (in this case about 300mm), the returning echo is over 4 times the diameter of the original probe. There is therefore potentially a substantial amount of information not being collected by the single probe.

2.6. Conclusion

This chapter explains the reasoning behind this project in context to the operation of the Bloom and Billet Mill process at Thrybergh Mill and the limitations of the existing non-destructive testing technology currently utilised.

2.7. References

1. Zhang, L. and B.G. Thomas. *Inclusions in Continuous Casting of Steel.* in *XXIV National Steelmaking Symposium.* 2003. Morelia, Mexico. p. 138-183

2. Kiessling, R., *Non-metallic inclusions in steel.* 1989, London: The Institute of Metals.

3. Dekkers, R., *Non-metallic inclusions in liquid steel.* 2002, PhD. Thesis. Leuven Universiteit:

4. Singh, B. and S.K. Kaushik, *Influence of steel-making processes on the quality of reinforcement.* The Indian Concrete Journal, 2002. **76**(7): p. 407-412.

5. Wolfram, A. *Automated ultrasonic inspection.* in *15th WCNDT conference.* 2000. Rome, Italy. www.ndt.net/article/wcndt00/papers/idn197/idn197.htm

6. Shin, B.-C. and J.-R. Kwon, *Ultrasonic transducers for continuous-cast billets.* Sensors and Actuators A: Physical, 1996. **51**: p. 173-177.

7. Krautkrämer, J. and H. Krautkrämer, *Ultrasonic Testing of Materials.* 4th ed. 1990, Berlin, Heidelberg, New York.: Springer-Verlag. p. 677.

8. Webb, P. and C. Wykes, *Suppression of second-time-around echoes in high firing rate ultrasonic transducers.* NDT & E International, 1995. **28**(2): p. 89-93.

9. Zhang, L., et al. *Evaluation and Control of Steel Cleanliness - Review.* in *85th Steelmaking Conference Proceeding.* 2002. Warrendale, PA, U.S.A. p. 431-452.

Chapter 3.

Review of Current Systems and Technologies

3.1. Introduction

This chapter gives an outline of the major methods of Non-Destructive Testing (NDT), technologies currently employed for industrial inspection, such that the method under investigation in this thesis can be compared to other methods. Since this method is a variant of two current ultrasonic techniques, the chapter starts by describing the constraints within which ultrasonic testing is of use. Different ultrasonic generating transducers are then presented detailing their advantages and disadvantages. Describing and comparing the different excitation configuration, analysis techniques and data representations commonly used in commercial systems complete the ultrasonic testing section.

The next part of the chapter outlines and assesses other competing technologies such as visual, radiography and magnetic particle inspection, and dye penetration. Finally, the project remit is put into context with respect to the technologies presented in this chapter.

3.2. Ultrasonic Methods

Ultrasonic testing of material properties is a commonly utilised technology that is readily available commercially. Systems range from basic pulse/echo systems to scanning phased array systems employing digital signal processing to improve signal to noise ratios and provide real-time data analysis. A typical ultrasonic system consists of a transducing system to transmit and receive ultrasonic waves, a coupling system to the sample under inspection, a sample and finally analysis software. The type of transducer required depends on factors such as the frequency of operation, the ambient conditions, the method of inspection, the mode of propagation and cost and availability. This section outlines both the different transducing and inspection methods currently available and contrasts and compares their performances.

3.2.1. Generating Ultrasound

The methods discussed in this section involve converting an electrical signal either directly or indirectly into an ultrasonic wave, which propagates through a material.

They are:

- Piezoelectric transducers
- Electromagnetic Acoustic Transducers (EMAT)
- Laser Generated Ultrasound

3.2.2. Piezoelectric Transducers

A transducer containing a piezoelectric element will convert electrical signals into mechanical vibrations in transmit mode, and mechanical vibrations into electrical signals in receive mode. The frequency of the mechanical vibration is determined by the resonant frequency of the element, which in turn is governed by the element thickness. Thus, a thin wafer element vibrates with a wavelength of twice its thickness and therefore, the piezoelectric elements are cut to a thickness of half the desired wavelength. Quartz was one of the materials originally used as a piezoelectric element. However, with the development of polycrystalline ceramics [1], which can be polarized and be cut in a variety of manners to produce wave mode required (Figures 3.2. and 3.3.) these have now been superseded.

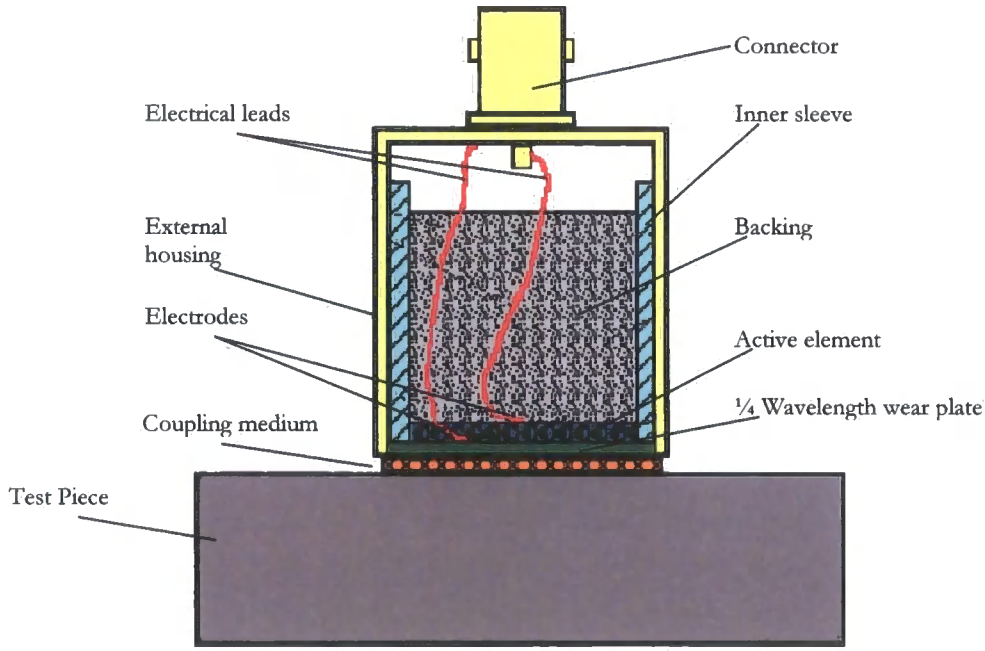

Figure 3.1. Diagram of typical Piezoelectric transducer

Figure 3.1. is a diagram of a typical piezoelectric transducer used in pulse/echo system and shows the electrical connections to the active element, the wear plate and backing material. This transducer was designed for excitation by an impulse voltage signal and thus damping has been introduced via the backing material to reduce the settling time of the resulting ultrasonic impulse response. This results in shorter bursts or pulses of ultrasonic energy enabling the time between consecutive pulses to be reduced.

The direction in which tension or compression develops electrical polarization parallel to the strain is called the piezoelectric axis. In quartz, this axis is knows as the "X-axis", and in poled ceramic materials such as PZT the piezoelectric axis is referred to as the "Z-axis". From different combinations of the direction of the applied field and orientation of the crystal it is possible to produce various stresses and strains in the crystal. The direction in which tension or compression develops is called the piezoelectric axis and is polarized parallel to the strain, indicated with a 'P' in the schematics.

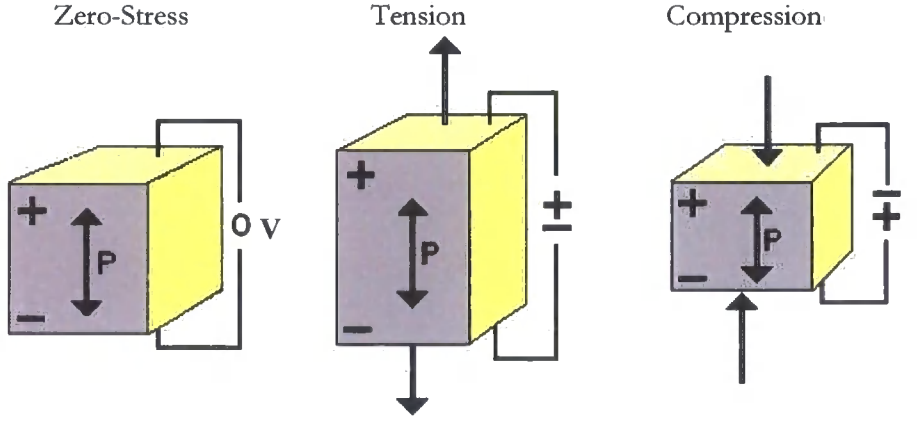

Figure 3.2. Longitudinal / compression wave generation

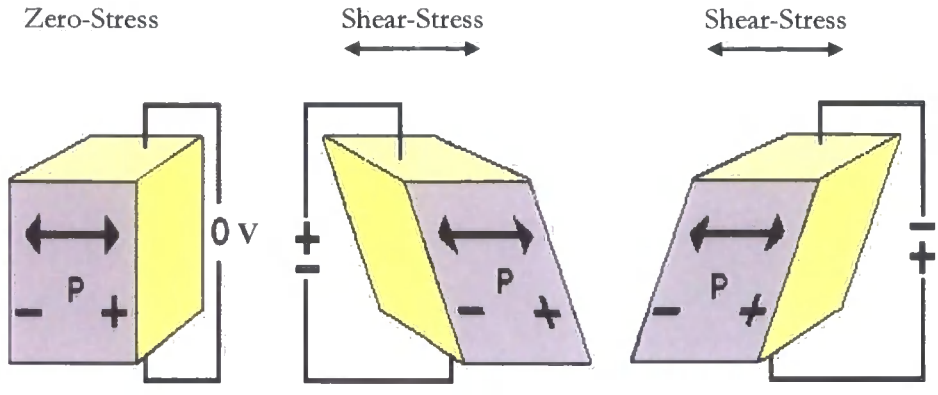

Figure 3.3. Transverse / shear wave generation

Schematic representations of the cross-section of typical piezoelectric crystals are presented in Figure 3.2. and 3.3. The figures indicate that with a positive applied voltage perpendicular to the piezoelectric axis, a longitudinal polarized crystal expands. If however the electric field is applied parallel to the piezoelectric axis, a shear motion is induced [2]. Under a negative applied voltage, the motion is opposite; the longitudinal crystal contracts, the shear crystal shifts in the opposite direction.

Piezoelectric transducers can be used to excite a variety of modes into the test sample. The four principle modes are longitudinal, shear, surface and in thin materials, plate waves. However, a major factor that determines the amount of energy transmitted in and out of the material are the acoustic impedances of the different components of the system. Thus, the coupling medium between the transducer and the sample requires consideration. The primary function of the coupling medium is to provide a high degree of mechanical coupling, and in contact testing, must be thin to have minimum effect of the acoustic wave [3]. The reflection coefficient of an air/steel boundary is 0.98, whereas using water as a couplant reduces this value to 0.94 (Section 5.6.) showing that water, as a couplant is more efficient [1].

Thus, these transducers are often used in automatic water immersion systems or a water-based gel is used for manual systems. Water couplant cannot support shear waves and thus only longitudinal waves will transmit into the material.

3.2.3. Electromagnetic Acoustic Transducers (EMAT)

An EMAT is a non-contact device that generates and detects ultrasound in electrically conducting or ferromagnetic materials [4]. Thus in this case, the ultrasound is generated directly within the material and the acoustic impedance of the medium between the transducer and sample is not relevant although the electromagnetic properties are.

There are two types of EMAT, one is based on the Lorentz force and can be used in non-ferromagnetic materials, and the other type is based on magnetostriction and can be used for magnetic materials and those that exhibit magnetostriction.

In the Lorentz type, a coil is used to create a radio frequency signal that induces an eddy current density directly into the conducting sample, which has components perpendicular to an applied dc magnetic field. A Lorentz force is thus produced as shown in equation. 3.1. resulting in small mechanical vibrations and hence an elastic wave propagates into the volume of the material, or along the surface. The use of an EMAT for the detection of ultrasound works via an inverse process, where motion of the surface induces current into the coil. The direction of the magnetic field also determines whether shear or compression waves will be detected at the receiver [5].

$$F = JXB \qquad [3.1]$$

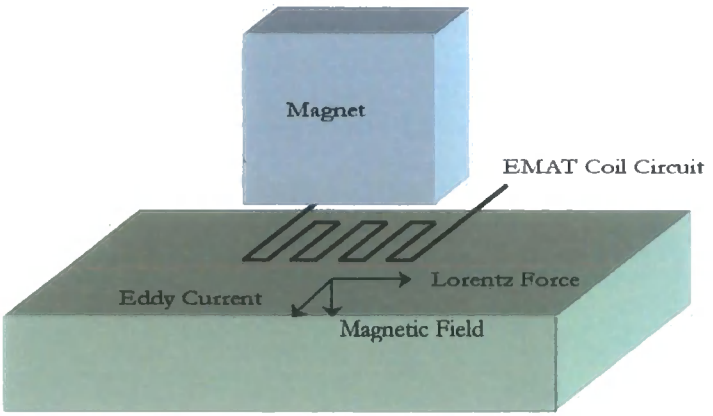

Figure 3.4. Diagram of EMAT showing relevant forces

The second type of EMAT is based on magnetostriction in ferromagnetic materials. As with the Lorentz type, a coil is used to create a radio frequency (RF) field, which produces magnetic flux changes in the material. If a dc magnetic field is applied parallel to the surface of the sample, then the RF field generated causes the magnetic domains to align. This effect gives rise to a change on dimensions known as magnetostriction [6]. These produce a series of tensile and compressive strains hence producing an elastic wave. Regardless of the generation method the RF coupling is dependent upon the lift-off distance between the EMAT and the part. It is therefore important to keep the EMAT within close proximity to the object being tested (~ 1 mm) limiting the use of an EMAT to flat or mildly curving surfaces [7]. When an EMAT transmitter is placed near an electrically conducting material, not necessarily in contact with, ultrasonic waves are launched in the material through the reaction of induced eddy currents (see Chapter 4.) and static magnetic fields (Lorentz forces). This eliminates the problems associated with acoustic coupling to the metal part under examination as the electro-mechanical conversion takes place directly within the electromagnetic skin depth of the material surface. Therefore, an EMAT facilitates non-contact operation

and enable inspection at elevated temperatures [8], on moving objects, in vacuum or oily or rough surfaces and also in remote and hazardous locations.

3.2.4. Laser Generated Ultrasound

Laser ultrasonic testing combines the sensitivity of ultrasonic inspection with the flexibility of optical systems in dealing with complex inspection problems [9]. It can interrogate parts in hostile environments or at temperatures well above those that can be tolerated using other techniques [10], and operate at a considerable standoff of up to several meters from the probed part.

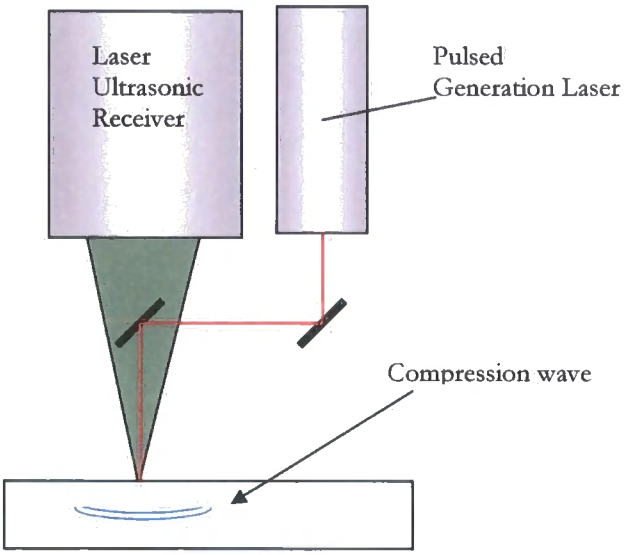

Figure 3.5. Diagram of laser generated ultrasound

Laser ultrasonics involves laser-in, laser-out excitation and detection without the requirement of a couplant medium (Figure 3.5.) [3]. When the laser pulse strikes the sample, ultrasonic waves are generated. The impact generation method may be classed in two main categories: thermoelastic regime and ablative regime. The regime is determined by the energy density, the wavelength, pulse width and the properties of the

material under examination. In the case of ablation, a laser source is chosen with a wavelength that will have sufficient energy density to cause vaporization or ablation of the surface of the material [11]. The recoil that follows the material ejection off the surface predominantly produces longitudinal force at normal incidence to the material surface; but also produces shear waves, and surface following waves. Laser ultrasound generated in the thermoelastic regime produces a buried ultrasonic source with a constraining effect of the material above it, which induces longitudinal ultrasonic wave at normal incidence (Figure 3.5.) When the reflected ultrasonic wave reaches the surface of the sample, a separate laser ultrasonic receiver (interferometer) is used for detection of the ultrasonic wave. The resulting surface displacement is measured with the laser ultrasonic receiver based upon an adaptive interferometer.

3.2.5. Inspection Techniques

In ultrasonic testing, high-frequency sound waves are transmitted into a material to detect imperfections or to locate discontinuities in material properties. The frequency utilised depends on factors such as the attenuation as the wave travels through the material under test, dispersion and resolution of the discontinuity. Ultrasonic inspection can be utilised for several purposes including flaw detection, material evaluation, and dimensional measurements. When an ultrasonic wave is introduced into a material it has four principle modes of propagation, longitudinal, shear, surface, and in thin materials, plate waves. The first two modes can exist in the bulk materials and are therefore best suited to the internal investigation of a material. To reduce the number of modes further some systems employ water coupling since water does not support shear waves [12], leaving only longitudinal waves. The way, in which sound waves propagate through materials, and the orientation of the area under inspection,

dictate the ultrasonic technique employed. These techniques fall into two main categories, and are pulse/echo and through transmission, all other methods of ultrasonic defect detection are adaptations and elaborations of these two main categories.

3.2.6. Pulse/Echo

This is the most commonly used ultrasonic testing technique, whereby sound is introduced into a test object via a dual-purpose transmitter/receiver probe. The signal is then reflected from any suitably orientated internal imperfections or the geometrical surfaces of the test object, and returns to the same transmitter/receiver probe. The two-way transit time measured is divided by two to account for the return transit path and multiplied by the velocity of sound in the test material. The result is expressed in the relationship:

$$d = vt/2 \qquad [3.2.]$$

where

d = the distance from the surface to the discontinuity in the test piece

v = the velocity of sound waves in the material

t = the measured round-trip transit time

When a suitably orientated discontinuity is in the path of an ultrasonic pulse, a percentage of the pulses energy will reflect back to the probe from the surface of the flaw. The reflected signal is then transformed via the receiving probe back into electrical signal to the ultrasonic flaw detector where it can be then displayed on a

screen. Signal transit time can be directly related to the distance that the signal travelled. This echo signal can then be processed and information about the reflecting discontinuity, such as its location, size, and orientation, can be determined [13]. There are several methods of displaying the ultrasonic signal, however the three most widely employed methods are A-scan, B-scan and C-can, the most commonly used of which is the A-scan. An A-scan plots signal amplitude against signal transit time through the medium (Figures 3.6. and 3.7.) and is then displayed as a single signal path. Because of this use of transit time, an A-scan can also be employed for material thickness measurements.

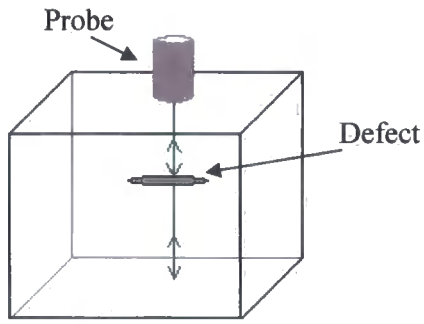

Figure 3.6. Diagram of A-scan showing defect in the core of the material

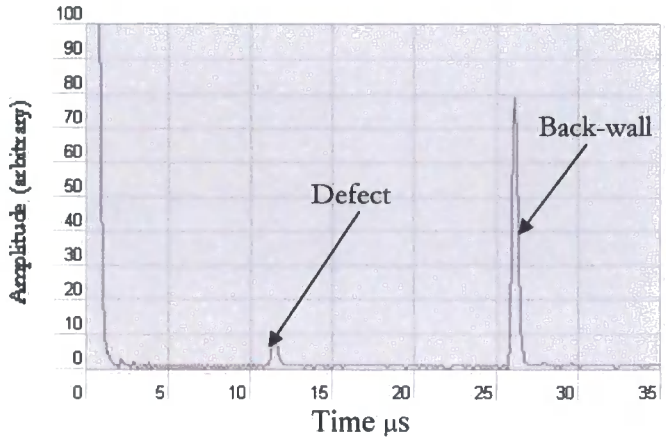

Figure 3.7. Representation of an A-scan showing initial pulse, defect in core of the material and back-wall echo.

The B-Scan is a multi-signal path display, and can be visualized as a transverse cross-sectional view from the top to the bottom of the component. As the probe is moved, the A-Scan signals are recorded and plotted according to probe position. The response from a defect will be plotted along the beam axis even when it does not lie on it, causing arc shaped indications on the B-Scan image, owing to the beam divergence.

These characteristic arcs vary in shape and size according to the width of the ultrasonic beam at different depths within the material and the defect encountered. B-scans are generally displayed in greyscale; where intensity is proportional to the amplitude of the signal see Figure 3.8. and 3.9. The B-scan is less practical for non-destructive testing where large volumes are to be examined, as they require a comparatively long scanning time when compared to an A-scan [3].

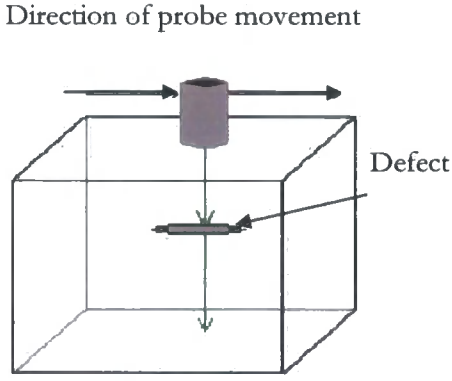

Figure 3.8. Diagram of B-scan test showing probe movement and defect

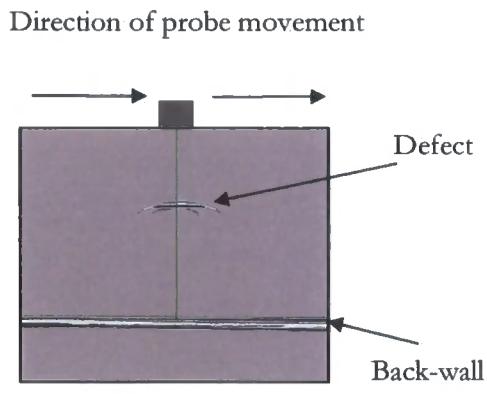

Figure 3.9. Representation of B-scan display showing probe and defect position

The C-scan is essentially a plan view of the scanned material. The display is similar to that of a B-scan, in that the intensity displayed is proportional to the amplitude of the reflected signal. In sophisticated systems, digital signal processing (DSP) can be applied to the signal facilitating filtering and signal manipulation to givie clearer and more readily identifiable results (Figures 3.10. and 3.11.)

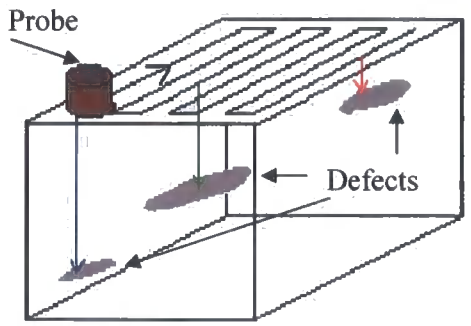

Figure 3.10. Representation of C-scan probe path and defects.

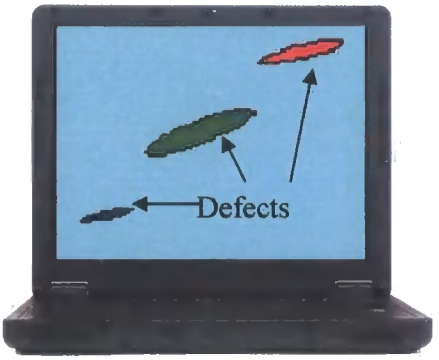

Figure 3.11. The C-scan display with defect reconstruction.

3.2.7. Through Transmission

In this method ultrasonic energy is introduced into a test object by one probe, propagates through the test object and received by a second transducer, usually on the opposite side of the test object. This method requires considered calibration prior to any investigation as it relies on the changes in received signal amplitude as indications of variations in material continuity.

3.2.8. Phased Array

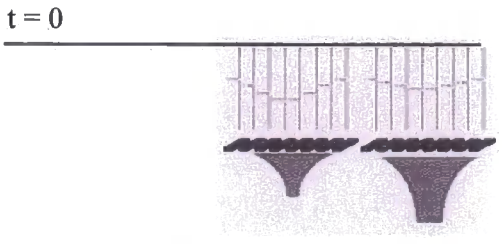

Figure 3.12. Diagram of electronic focusing, showing how electronic delay is used to focus the beam [14].

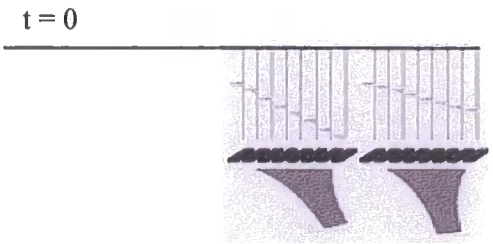

Figure 3.13. Diagram electronic beam steering by applying electronic delay [14].

The Phased Array concept is based on the use of transducers made up of individual elements that can each be independently driven. Each probe is made up of a large number of simple probes, between 10 and several hundred [5], organized in linear, annular, circular or matrix arrays, used as transmitters and/or receivers of ultrasonic waves[14]. Excitation of each the transducer elements can be individually controlled and exited with different timing delays, facilitating electronic sound-field steering, this permits electronic scanning (beam sweeping), focusing and deflection (beam steering) to be carried out (Figures 3.12. and 3.13.).

These phased array probes are connected to specially adapted pulser/receiver drive units enabling independent or simultaneous pulse emission and reception along each channel. Initial costs for the electronics and the development of the software required for the implementation of a phased array systems, are more expensive than that of conventional ultrasonic counterparts. Also, phased array probes are more expensive than standard ultrasonic transducers and each probe is generally application specific [15].

However as more applications become commonplace, it is expected that demand for phased array systems and certain array probes will rise. The use of phased array systems in industry is expected to increase over time. This is to facilitate a reduction of inspection times and to address the inspection problems associated with complex component geometries that are not feasible with conventional methods [16, 17].

3.2.9. Time of Flight Diffraction (TOFD)

Time-of-flight diffraction (TOFD) technique is based on forward-scattered diffraction of an ultrasonic wave at the tips of discontinuities. This is in contrast to conventional pulse echo techniques that rely on directly reflected signals from internal structures [18]. The TOFD technique as an ultrasonic NDT technique was first described and put into practical use by Dr. Maurice G. Silk in 1977 [19]. The TOFD technique was refined and developed over a period of years by Silk and his co-workers at the Atomic Energy Authority's Harwell Laboratory.

The technique uses two probes in a transmitter-receiver arrangement, the probes having a small active element to give wide beam spread angle. Broad beam probes are used so that the entire crack area is flooded with ultrasound and, consequently, the entire volume is inspected using a single scan pass [20]. The technique requires the two probes to be placed facing each other and approximately equidistant from the flaw. With the location of the discontinuity being determined by the variation in propagation times of the ultrasonic waves at the receiver probe. Mondal et.al. (2000) state that the probe frequency should be 10 MHz or higher [20], because as Charlesworth et.al (2000) state the accuracy of the measurement increases with that of the frequency [21], and angled at between 45 to 70 degrees [22].

When ultrasound is introduced into the material, each defect edge works as a point source of diffracted waves. The received signals can be displayed in an A-scan presentation (Figure 3.17.) however it is more often, stacked together to give a 2-dimensional B-scan image (Figure 3.14.) for greater image clarity.

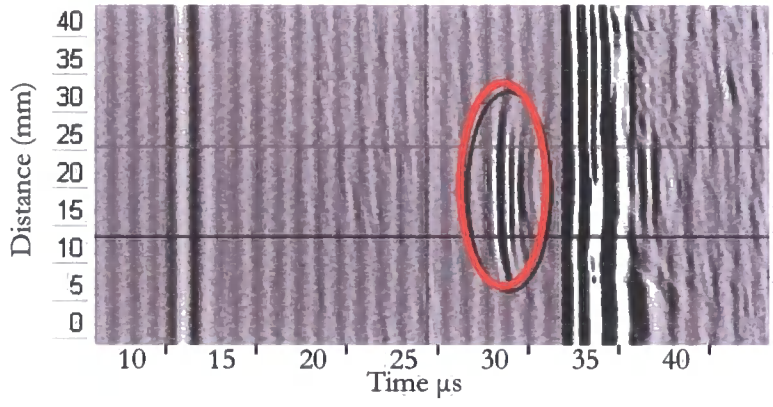

Figure 3.14. Illustration of a typical TOFD B-scan, with the diffraction arcs circled (from www.ultrasonic.de/article/tofd/browne/browne)

Four types of ultrasonic wave are involved in the formation of a TOFD image [18]:

1. A longitudinal wave generated by the transmitting probe then partially transformed into spherical wave when the beam encounter the tip or tips of a flaw.
2. A lateral ultrasonic wave that propagates on the surface of the material between the two transducers.
3. A longitudinal wave reflected from the back-wall.
4. A shear wave generated by the mode conversion of the longitudinal wave at the interface of discontinuities.

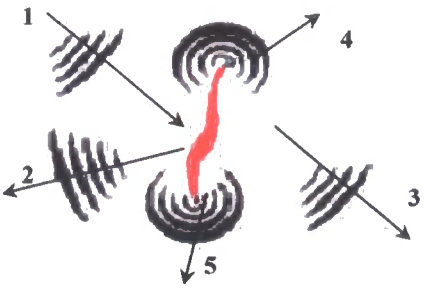

1. Transmitted Wave
2. Reflected Wave
3. Through Transmitted Wave
4. Diffracted Wave at Upper Crack Tip
5. Diffracted Wave at Lower Crack Tip

Figure 3.15. Diagram showing ultrasound and crack interaction
(www.ndt.net/ndtaz/ndtaz.php)

The theory of the spherical wave is that of a wave front propagating from a relatively small source, like that of the surface of an expanding soap bubble, i.e. a wave in which points of the same phase lie on the surfaces of concentric spheres.

Charlsworth et.al (2002) state that it is preferable to use compression waves, because of their earlier arrival time. However as shear waves travel at approximately half the velocity of a compression wave, they can offer enhanced resolution [21]. The slower speed also means that the signal of interest could arrive amongst other spurious signals, including mode-converted compression waves, and compression waves that have travelled greater distance. The locations of the tips of the crack are determined from the time differences between the lateral wave, and the pulses following the paths, P1 + P2 (t_1) and P3 + P4 (t_2) From the detected positions and times the dimensions of the discontinuity can be determined. The following equations are for the arrival times of the various signals from Figures 3.16. and 3.17.

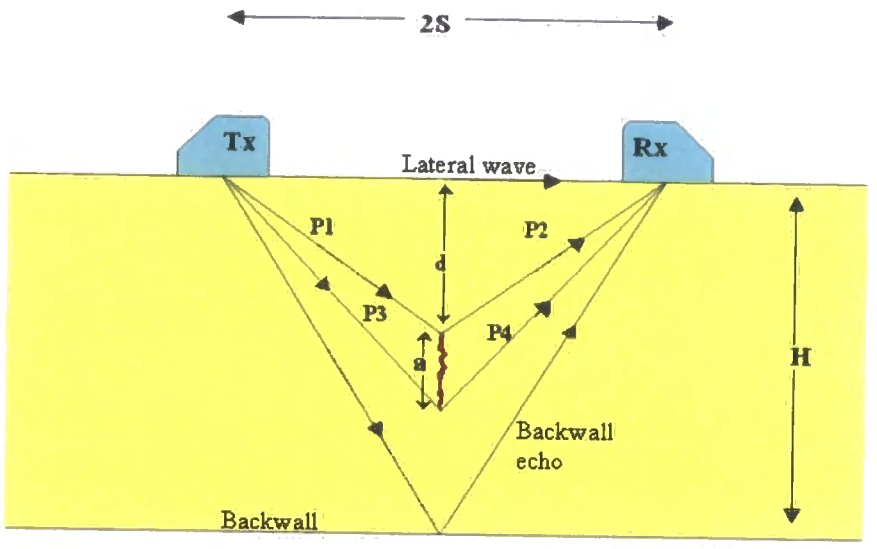

Figure 3.16. Diagram showing twin probes and signal paths of a typical TOFD scan

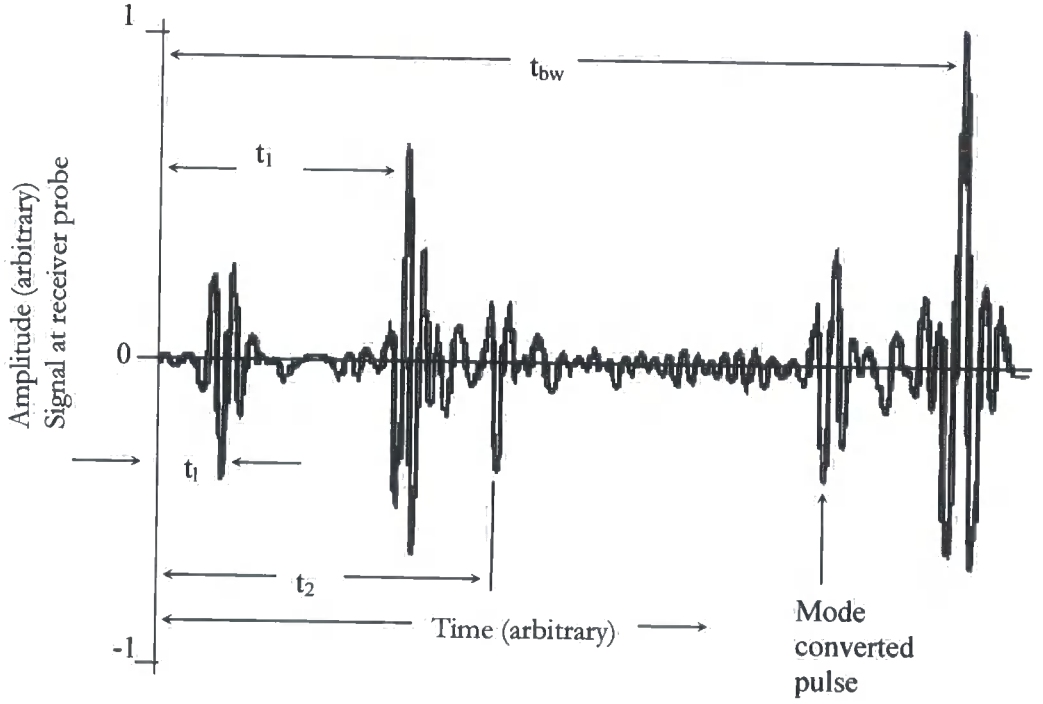

Figure 3.17. A-scan from Figure 3.16.

When the defect is at normal incident to the surface and the defect is centrally positioned between the probes, as in Figure 3.16. the following equations apply:

Time of surface (lateral) wave

$$t_L = \frac{2S}{C} \qquad [3.3.]$$

Time to top of defect (P1 + P2)

$$t_1 = \frac{2\sqrt{S^2 + d^2}}{C} \qquad [3.4.]$$

Time to bottom of defect (P2 + P4)

$$t_2 = \frac{2\sqrt{S^2 + (d+a)^2}}{C} \qquad [3.5.]$$

Time of Backwall echo

$$t_{bw} = \frac{2\sqrt{S^2 + H^2}}{C} \qquad [3.6.]$$

Where

a = defect size

d = defect depth below surface

H = material thickness

C = velocity of relevant wave mode (Longitudinal or Transverse)

S = ½ probe separation distance

The following equations refer to Figures 3.16. and 3.17. and give the depth of defect below the surface and the defect size respectively:

Defect depth below surface

$$d = \tfrac{1}{2}\sqrt{C^2 t_1^2 - 4S^2} \qquad [3.7.]$$

Defect size

$$a = \tfrac{1}{2}\sqrt{C^2 t_2^2 - 4S^2} - d \qquad [3.8.]$$

TOFD has several advantages over other ultrasonic techniques, in that, depth sizing is very accurate and the defect height can be exactly determined. An exception to this is that the technique is not effective at detecting or sizing defect lying parallel to the inspection surface [23]. A disadvantage of TOFD is that diffraction waves are low in amplitude than direct reflection waves and therefore the sensitivity to flaw detection is correspondingly lower in amplitude. Also the defects can only be realized if the amplitude and phase of the diffracted ultrasound can be reliably interpreted [24].

TOFD has been successfully applied for testing a wide range of steel plates and pipelines thicknesses. However according to Charlesworth et.al (2002) crack sizing results performed with ultrasonic methods on a thick-walled pressure vessel weld, demonstrated that it is uncertain if TOFD is a reliable method for the detection of cracks or sharp grooves at the inner walls of pipe work or vessels [21]. There is however no doubt of the potential for Time-of-flight diffraction used as an adjunct to other techniques to assist with defect characterisation, location and sizing.

3.2.10. Synthetic Aperture Focusing Technique (SAFT)

The Synthetic aperture focusing technique (SAFT) is based on geometrical reflection [25] of the ultrasound, and is essentially a digital signal processing technique (DSP) employed for ultrasonic testing. It provides an accurate measurement of the spatial location and extent of flaws contained within components [26]. SAFT can be split into two sub-categories that of Conventional SAFT and Multi-SAFT.

In conventional SAFT the pulse echo method is used, which is defined as the use of a single transducers for both source and receiver scanning [27], however Multi-SAFT is a technique in which separate transducer is used for transmitting and receiving.

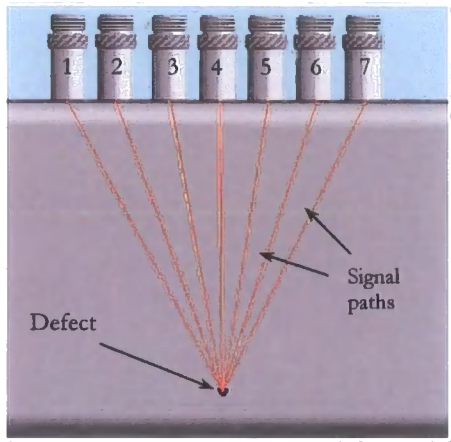

Figure 3.18. Signal paths from probes to defect

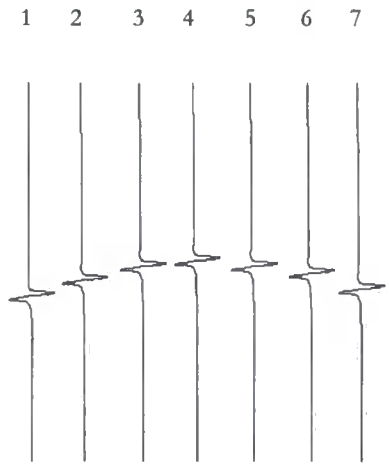

Figure 3.19. Hyperbola formed by signal time differences to defect

The use of these SAFT techniques improves the image resolution that can be obtained, without the use of the traditional ultrasonic lenses. However Osetrov (2000) states that some flaws can be incorrectly reconstructed using an inappropriate SAFT algorithm [28]. Among the most significant features are hyperbolae (Figure 3.19.) indicating localised scattering from embedded defects [29].

The signal-processing behind SAFT is essentially a time shifted B-scan, in which the transit-time for the ultrasonic beam to travel to and from a point is a hyperbolic function of the probe position and the defect depth (Figure 3.19). When the equation of this hyperbola is known, A-scan signals can be shifted in time (Figure 3.20) and added together (Figure 3.21.) for a pseudo B-scan.

This compensation corresponds to time domain delaying of the different channels in a typical real-time SAFT with delay and sum approach [30].

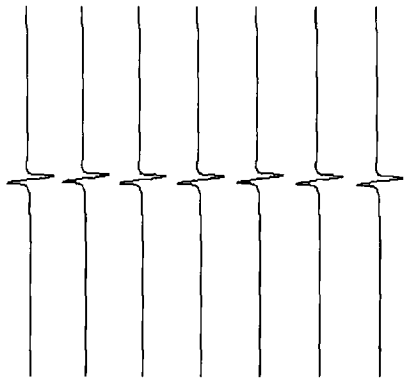

Figure 3.20. Time shifted defect signals

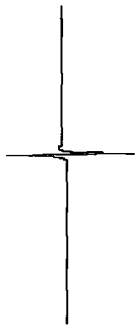

Figure 3.21. Signal after summation

Where no defect is present the signal interference with the material is haphazard and the signal is small and lost within the random signal noise. However where a material defect is present, the constructive interference of the waveforms, form a large cohesive signal, facilitating signal thresholding. A comparison was made by Boomsang et.al. (2004) of conventional B-scan images, with SAFT images. These results showed that synthetic focusing apertures, offer better signal-to-noise ratios with improved capabilities in lateral resolution [31]. A variation of SAFT called ALOK which is German for Amplitude Laufzeit OrtsKurven and is where the expected travel times of hyperbolic curves are used to improve signal-to-noise ratio (SNR) of defects, however, no synthetic focusing occurs with this method.

3.3. Visual and Optical Testing (VT)

Visual and optical testing is the most basic NDT method of material examination. The instrument being used for testing is the human eye and therefore the visual inspector requires regular vision tests to ensure the eyes are capable of their job [32].

The visual examiners follow various procedures that range from simply looking at a part with the naked eye, to see if surface defects are visible, to using a Borescope (Endoscope) to gain an image from an inaccessible location (Figure 3.22.) as the main point of visual testing is that the inspector must be able to see the surface being tested.

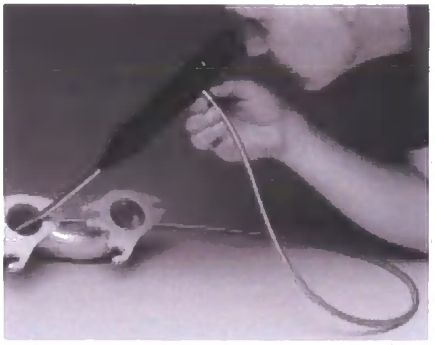

Figure 3.22. Simple magnifying Borescope

Figure 3.23. Camera Borescope with image rectifier

There are several problems associated with the use of this equipment, including eyestrain and image distortion, due to the wide angled objective lens as in Figure 3.22. However, the use of computer controlled camera systems can be programmed to automatically correct this distortion [33] (Figure 3.23). These systems can also be automated and programmed to locate, identify and measure the features of an inspected component.

3.4. Radiography Testing (RT)

Volumetric nondestructive testing (NDT) is typically performed in industry using either radiography or ultrasonics. Radiography having the disadvantages that it can be a safety hazard and is poor at detecting the more critical planar discontinuities [15].

Radiographic testing involves the use of penetrating gamma or X-rays to examine material internal features for discontinuities. X-rays are produced by high voltage X-ray machines whereas gamma rays are produced from disintegrating radioactive isotopes, such as Iridium 192 or Cobalt 60 [34].

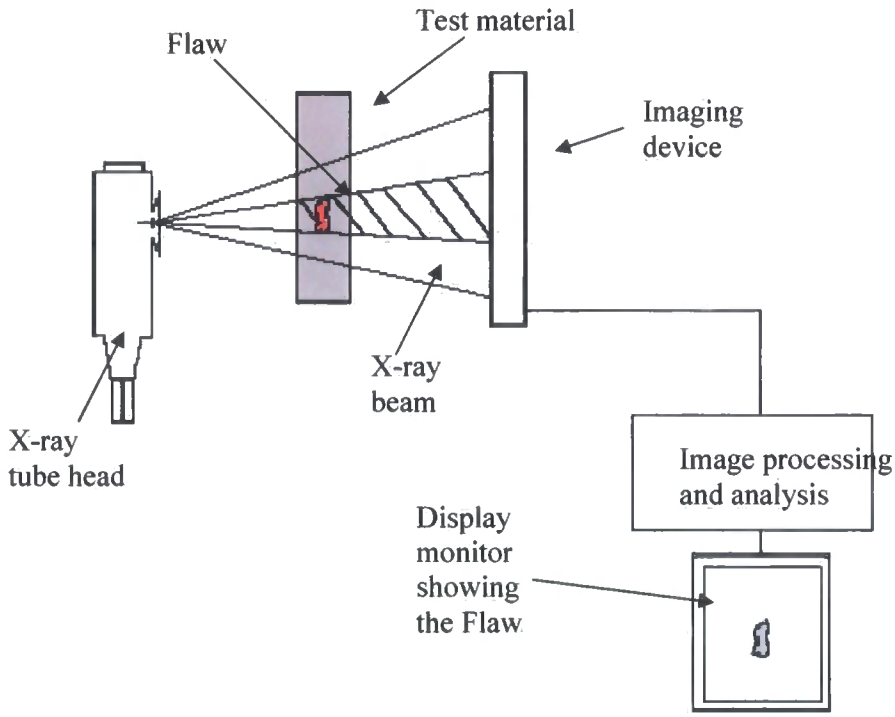

Figure 3.24. Typical X-ray inspection set-up

The electromagnetic radiation has a short wavelength, and can pass directly through the material, being partially absorbed during transmission, and onto monitor (Figure 3.24.), film or digital media that is becoming increasingly reliable and cost effective [35]. The choice of radiation source is partially dictated by the properties of the material to be examined and the materials thickness.

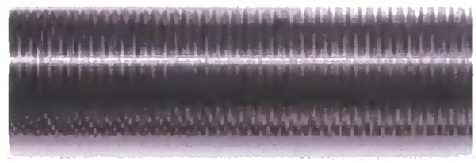

Figure 3.25. Photograph of threaded pipe

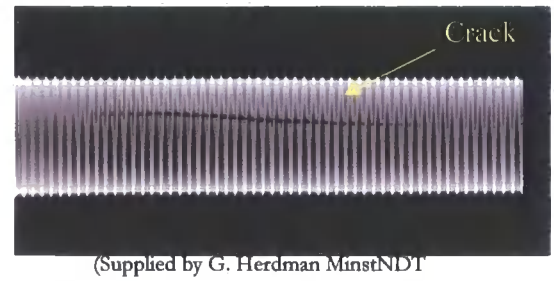

(Supplied by G. Herdman MinstNDT

Figure 3.26. Radiograph of threaded pipe showing defect

Also gamma radiation sources have the advantage of portability, which makes them ideal for use in site working. The resulting shadowgraphs display the internal features of the inspected part. Material thickness and density changes are displayed as lighter or darker areas on the film, with the darker areas of the radiograph representing internal voids in the component (Figure 3.26.).

As Griffiths (2001) states [36], radiography on an industrial site poses a number of safety challenges that are frequently not adequately addressed. X-rays and gamma rays are very hazardous and can damage living tissue. To ensure there are no hazards to personnel, precautions must be taken, and a radiography inspection should be performed inside a protective enclosure or with appropriate barriers and warning signals.

3.5. Magnetic Particle Inspection (MPI)

The Magnetic Particle Inspection NDT method is achieved by inducing a magnetic field, within a ferromagnetic material. MPI can be used for detection of surface-breaking or near-surface cracks, blowholes, and non-metallic inclusions etc. However, if the crack runs parallel to the magnetic field, there is little disturbance to the magnetic field and it is unlikely that the crack will be detected.

For this reason the component is magnetised in more than one direction and at 90° to each other. Under optimal conditions, and with good surfaces, detection of defects of about 0.5mm long can be achieved. The sensitivity of MPI depends on the magnetisation method and on the electromagnetic properties of the material tested as well as on the size, shape and orientation of the defect [37].

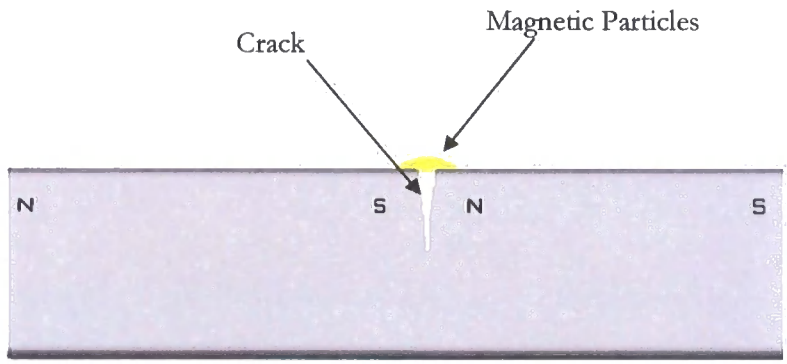

Figure 3.27. Billet with crack showing the flux leakage field and effective poles

The surface is dusted with iron particles that can be either dry or be suspended in liquid and are generally brightly coloured. If the material has no flaws, most of the magnetic flux is concentrated below the material's surface. However, if a flaw is present, such that it interacts with the magnetic field, the flux is distorted locally and the flux appears to leak from the surface of the specimen in the region of the flaw as shown in Figure 3.27.

Surface and near-surface flaws produce magnetic poles or distort the magnetic field in such a way that the iron particles are attracted and concentrated in these areas. This produces a visible indication of a defect on the surface of the material and is much easier to detect than the actual crack and this is the basis for magnetic particle inspection.

The demagnetisation of the component is often specified after MPI to avoid the build up of particles. This demagnetisation is achieved by subjecting the component to a continuously alternating and reducing magnetic field, with the start point of the cyclic demagnetisation being, as high, or higher than that of the magnetizing field.

3.6. Eddy Current Testing (EC)

Eddy currents are created through electromagnetic induction and take their name from the "eddies" that are formed when a liquid or gas flows in a circular path around obstacles. As an alternating current flows through a coil a dynamic expanding and collapsing magnetic field forms, and when a conductive material is placed within close proximity electromagnetic induction occurs and eddy currents are induced in the material. A secondary magnetic field is generated by the eddy current, which opposes the coil's magnetic field as shown in Figure 3.28.

Concentrated mainly at the surface of a material, eddy currents can therefore only be used to detect surface and near surface defects, due to the skin effect [38]. Skin depth is a term used for the depth at which the amplitude of an electromagnetic wave attenuates to 1/e of its original value or 37% of it value at the surface [39]. The skin depth for plane waves δ can be calculated using equation 3.9.

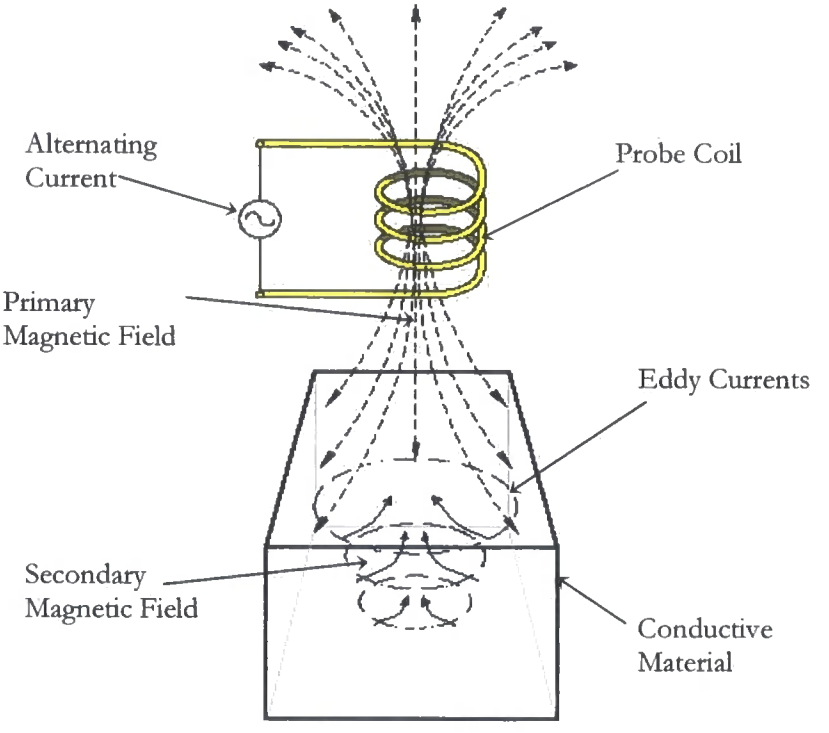

Figure 3.28. Diagram of the generation of eddy currents

$$\delta = \sqrt{\frac{2\rho}{\omega\mu}} \qquad [3.9]$$

where

ρ = resistivity of conductor

ω = angular frequency of current = $2\pi \times$ frequency

μ = absolute magnetic permeability of conductor

The skin effect is a fundamental electromagnetic phenomenon and is dependent upon specimen conductivity permeability and the operating frequency. This is explained by Lenz's Law, which states "when an EMF is induced in a conductor by any change in the relation between the conductor and the magnetic field, the direction of the EMF is such as to produce a current whose magnetic field will oppose the change"[40]. The skin effect has been widely used for non-destructive testing using inductance coils and magnetic/eddy current techniques for both sub-surface inspection [41] and for crack detection [42].

For most NDT inspection applications, eddy current probe frequencies are in the range 1kHz to 3MHz are used with the lower frequencies giving deeper penetration, typically between 5 μm and 1 mm. The presence of any discontinuity will cause a change in eddy current flow and a corresponding change in the phase and amplitude of the measured eddy current [43]. Eddy currents are also affected by the electrical conductivity and magnetic permeability of a material, which makes it possible to distinguish between various conductive materials based on these properties.

3.7. Dye Penetrant Inspection (DPI)

The purpose of the dye penetrant inspection is to increase the visible contrast between a discontinuity and the background material. This is achieved by applying a penetrating liquid that contains a visible or fluorescent dye, as shown in Figure 3.29. Excess solution is then removed from the surface of the object but leaving it in surface breaking defects.

A developer is then applied to draw the penetrant out of the defects. With fluorescent dyes, ultraviolet light is used to make the bleed-out fluoresce brightly, thus allowing imperfections to be readily seen. With visible dyes, vivid colour contrasts between the penetrant and developer make bleed-out easy to see. Dye penetrant inspections are suitable for both ferrous and non-ferrous materials, but the detection is limited to the detection of surface breaking discontinuities in non-porous materials.

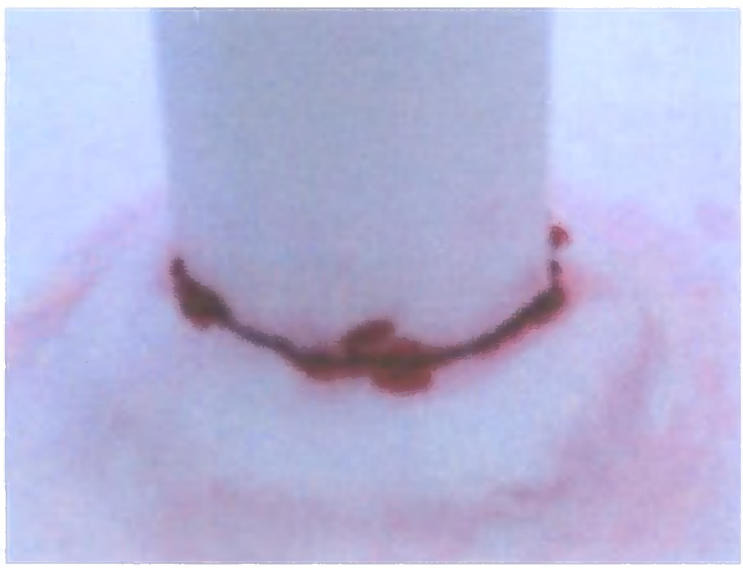

Figure 3.29. Example of DPI used to inspect weld condition

3.8. Conclusion

This chapter contained an overview of the various NDT technologies and as such covered all the methods relevant to the project. As the project remit was an immersion ultrasonic system using piezoelectric transducers, those were discussed in greater depth. Several of the methods described were totally unsuitable for the interrogation of the core of the billet, including Dye Penetrant Inspection, Magnetic Particle Inspection, Eddy Current, and Visual Testing. As all of these methods are suitable for only surface, surface breaking, or in the case of Eddy Current near surface defects.

The use of Radiography for billet inspection has problems with the radiation containment, as inspection should be performed inside a protective enclosure. This would necessitate the protective enclosure allowing for the billet to traverse through and to the next station without interruption, and have an automated defect detection and marking system, instead of producing radiographic images. According to Hanke et.al. (2004) the current methods for high-speed volume data evaluation have cycle times of about one minute, for a defect detection size of circa 15 cm [44], and this is an impractical throughput and defect detection size for economic and competitive production of steel.

The use of an EMAT for automated billet inspection would eliminate the need for an immersion system and the potential problems that they entail, predominantly air entrapment. However as an EMAT is required to be in close proximity (~ 1 mm) [7] with the material they a inspecting, this would be problem with a moving billet where the stand off distance is constantly changing due to material 'snaking'.

Also they are less efficient at converting electrical energy into sound, which would prove problematic when testing a large cross-sectional material or a highly attenuating material as performance decreases with distance [3].

The expenditure on a laser ultrasonic system capable of scanning a 75mm square section billet, moving at 1 m/s, in a steel mill would be excessive. That a laser system could complete the examination is not in question, however the required financial outlay would necessitate a marked increase in material throughput. Also because of the use of lasers, the inspection area may require being in an enclosure or be in a limited access area. However according to Kline (1996) laser-based ultrasound is definitely not a solution to all problems, but it can be very powerful in the right application, especially if surface ablation is allowed [10].

3.9. References

1. Hellier, C.J., *Handbook of Nondestructive Evaluation.* 2001, New York, U.S.A.: McGraw-Hill.

2. Johnston, P.H. *Free Response of Piezoelectric Crystals in Series and in Parallel.* in *Review of Progress in Quantitative Nondestructive Evaluation.* 2003, p. 729-736.

3. Birks, A.S. and R.E. Green Jr., *Ultrasonic Testing.* 2nd ed. Nondestructive Testing Handbook, ed. P. McIntire. Vol. 7. 1991, Baltimore, Maryland, U.S.A.: American Society for Nondestructive Testing. 893.

4. Dixon, S., et al., *A Laser - EMAT System for Ultrasonic Weld Inspection.* Ultrasonics, 1999. **37**(4): p. 273-281.

5. Krautkrämer, J. and H. Krautkrämer, *Ultrasonic Testing of Materials.* 1990, New York: Springer-Verlag. 677.

6. Marton, L. and C. Marton, *Ultrasonics.* Methods of Experimental Physics, ed. P.D. Edmonds. Vol. 19. 1981, London: Academic Press Inc. 619.

7. Klein, M.B. and T. Bodenhamer, *Laser ultrasonics*, in *Industrial Laser Solutions.* 2004, **19**(12). http://ils.pennnet.com/home.cfm.

8. Light, G.M. and J. Demo, *An Evaluation of EMAT Technology for High-Temperature NDE.* 1998, www.ndt.net/article/0398/light/light.htm.

9. Cho, H., et al., *Non-contact Laser Ultrasonics for Detecting Subsurface Lateral Defects.* NDT & E International, 1996. **30**: p. 301-306.

10. Klein, M.B., *Laser generated ultrasound.* 1996, www.ndt.net/article/az/ut_idx.htm.

11. Wang, X.D., et al., *Laser-generated ultrasound with an array of melting sources.* Applied Physics A. Materials Science and Processing, 2000. **70**(2): p. 203-209.

12. Lynnworth, L.C. and E.P. Papadakis, *Ultrasonic Measurements for Process Control: Theory, Techniques, Applications.* 1989, Boston: Academic Press.

13. Corneloup, G., et al., *Ultrasonic image data processing for the detection of defects.* Ultrasonics, 1994. **32**(5): p. 367-374.

14. Poguet, J., et al., *Phased Array Technology: Concepts, Probes and Applications.* 2002, www.ndt.net/article/az/ut_idx.htm.

15. Granillo, J. and M. Moles, *Portable Phased Array Applications.* The NDT Technician, 2005. **4**(2).

16. Anderson, M.T., *Ultrasonic Phased Array.* The NDT Technician, 2003. **2**(2).

17. Mahaut, S., et al., *Development of phased array techniques to improve characterization of defect located in a component of complex geometry.* Ultrasonics, 2002. **40**: p. 165-169.

18. Betti, F., et al. *Accuracy Capability of TOFD Technique in Ultrasonic Examination of Welds.* in *ASNT Spring Conference and 8th Annual Research Symposium.* 1998. Orlando, U.S.A.: www.nardoni.it/Serv02link.htm.

19. Silk, M.G., *Ultarsonic Testing - Special Techniques.* The Capabilities and Limitations of NDT, ed. P.D. Hanstead. Vol. 5. 1988, Northampton: British Institute of Non-Destructive Testing. 31.

20. Mondal, S. and T. Sattar, *An overview TOFD method and its Mathematical Model.* www.ultrasonic.de/article/v05n04/mondal/mondal.htm, 2000. **5**(4).

21. Charlesworth, J.P. and J.A.G. Temple, *Engineering Applications of Ultrasonic Time-of-Flight Diffraction.* Second Edition ed. Ultrasonic Inspection in Engineering, ed. M.J. Whittle. 2002, Baldock: Research Studies Press Ltd. 254.

22. Ginzel, E., et al., *TOFD Enhancement to Pipeline Girth Weld Inspection.* NDT. Net, 1998. **3**(4).

23. Baby, S., et al., *Defect detection study in austenitic steel welds and the performances of different ultrasonic transducers.* Insight, 2001. **43**(11): p. 735-741.

24. Ravenscroft, F.A., et al., *Diffraction of ultrasound by cracks: comparison of experiment with theory.* Ultrasonics, 1990. **29**(1): p. 29-37.

25. Frederick, J.R., *Ultrasonic Engineering.* 1965, London: John Wiley & Son.

26. Elbern, A.W. and L. Guimarães. *Synthetic Aperture Focusing Technique for Image Restauration.* in *International Symposium on NDT Contribution to the Infrastructure Safety Systems.* 1999. Torres, RS Brazil.

27. Doctor, S.R., et al., *SAFT the Evolution of a Signal Processing Technology for Ultrasonic Testing.* NDT International, 1986. **19**(3): p. 163-167.

28. Osetrov, A.V., *Non-linear algorithms based on SAFT ideas for reconstruction of flaws.* Ultrasonics, 2000. **38**: p. 739-744.

29. Schickert, M., et al., *Ultrasonic Imaging of Concrete Elements Using Reconstruction by Synthetic Aperture Focusing Technique.* Journal of Materials in Civil Engineering, 2003. **15**(3): p. 235-246.

30. Ylitalo, J., *A fast ultrasonic synthetic aperture imaging method: application to NDT.* Ultrasonics, 1996. **34**: p. 331-333.

31. Boonsang, S., et al., *Synthetic aperture focusing techniques in time and frequency domains for photoacoustic imaging.* Insight, 2004. **46**(4): p. 196-199.

32. Iddings, F.A., *The Basics of Visual Testing.* The NDT Technician, 2004. **3**(3).

33. Smith, W.E., et al., *Correction of distortion in endoscope images.* Medical Imaging, 1992. **11**(1): p. 117-122.

34. Gilbert, D.J., *BINDT Yearbook 2005.* 2005, Northampton: The British Institute of Non-Destructive Testing. p. 74-75.

35. Deprins, E. *Computed Radiography in NDT Applications.* in *World Conference on NDT.* 2004. Montreal, Canada: www.ndt.net/article/wcndt2004/pdf/radiography/367_deprins.pdf.

36. Griffiths, R. *Safety Issues in the Management of Industrial Radiography.* in *10th APCNDT.* 2001. Brisbane, Austrailia: www.ndt.net/article/apcndt01/papers/505/505.htm.

37. Lovejoy, D.J., *Magnetic Particle Inspection: A practical guide.* 1st ed. 1993, Norwell, U.S.A.: Kluwer Academic Publishers. 459.

38. Takagi, T., et al., *Benchmark models of eddy current testing for steam generator tube: experiment and numerical analysis.* International Journal of Applied Electromagnetics in Materials., 1994. **7**(3): p. 149-162.

39. Halmshaw, R., *Mathematics and Formulae in NDT.* 2nd ed. 1993, Northampton: The British Institute of Non-Destructive Testing.

40. Kingsbury, R.F., *Elements of Physics.* 1965, Princeton, New Jersey, U.S.A.: D. Van Nostrand Co. Inc.

41. Uzal, E. and J.H. Rose, *The impedance of eddy current probes above layered metals whose conductivity and permeability vary continuously.* Magnetics, 1993. **29**(2): p. 1869-1873.

42. Bowler, J.R., *Review of eddy current inversion with application to non destructive evaluation.* International Journal of Applied Electromagnetics & Mechanics, 1997. **8**: p. 3-16.

43. Bowler, J.R., *Eddy-current interaction with an ideal crack.* Journal of Applied Physics, 1994. **75**(12): p. 8128-8137.

44. Hanke, R., et al. *Automated High Speed Volume Computed Tomography for Inline Quality Control.* in *World Conference on NDT.* 2004. Montreal, Canada.

Chapter 4.

Review of Basic Theory

4.1. Introduction

The system under investigation in this thesis, involves the generation, propagation, reflection and transmission of bulk ultrasonic waves in test samples. This chapter has been included to provide the reader with an overview of the basic theory underlying these phenomena

4.2. Propagation and Velocity

This section describes the propagation of bulk ultrasonic waves in an unbounded, lossy medium. If the displacement, u, of a small section of the medium in the elastic region is represented in terms of scalar and vector potentials [1] as shown in equation 4.1.

$$\mathbf{u} = \nabla\Phi + \nabla X \mathbf{H} \qquad [4.1]$$

and is then substituted into the equation of motion, two independent wave equations result.

$$\nabla^2 \mathbf{u} = \frac{1}{c_L^2}\frac{\partial^2 \mathbf{u}}{\partial t^2} \quad given\ \mathbf{u} = \nabla\Phi \tag{4.2}$$

$$\nabla^2 \mathbf{H} = \frac{1}{c_T^2}\frac{\partial^2 \mathbf{H}}{\partial t^2} \quad given \quad \mathbf{u} = \nabla x \mathbf{H}\ and\ \nabla \cdot \mathbf{H} = 0 \tag{4.3}$$

where equation 4.2 represents longitudinal or dilatational waves and equation 4.3 shear or rotational waves. These two waves can only be coupled on the boundary of the elastic body. The parameters c_L and c_T represent the phase velocity of each type of wave.

The general solution to these equations are:

$$\begin{aligned} \mathbf{u} &= Ae^{-\alpha_L x} * e^{j(k_L x - \omega t)}, \quad \mathbf{u} = \nabla\Phi \\ \mathbf{u} &= Be^{-\alpha_T x} * e^{j(k_T x - \omega t)}, \quad u = \nabla x \mathbf{H},\ \nabla \cdot \mathbf{H} = 0 \end{aligned} \tag{4.4}$$

where α_L and α_T are the attenuations of the waves as a function of distance. For a wave of frequency, ω, with a wave number, k, the velocity is given by,

$$c_p = \frac{\omega}{k} \tag{4.5}$$

where c_p is known as the phase velocity and is frequency dependent. If the ultrasonic signal consists of more than one frequency, then the group velocity gives the overall velocity of the group of waves;

$$c_g = \frac{d\omega}{dk} = c_p + k\frac{dc_p}{dk}. \qquad [4.6]$$

This is the velocity of constant phase of the modulation envelope as shown in Figure 4.1. It is also the velocity of energy transportation. Equations for the longitudinal and shear waves are given in equations 4.7 and 4.8. The individual harmonic components will each still have their own phase velocity given by

$$c_L = \sqrt{\frac{E}{\rho}\frac{1-u}{(1+u)(1-2u)}} \qquad [4.7]$$

$$c_T = \sqrt{\frac{E}{\rho}\frac{1}{2(1+u)}} \qquad [4.8]$$

where E is the Modulus of elasticity, ρ the density and u is Poisson's ratio.

Figure 4.2a shows that if there are no energy loss mechanisms or anisotropic effects in a material, i.e. it is non-dispersive, and all the frequency components have the same phase velocity, then there will be no distortion of the signal envelope. Figure 4.2b shows that distortion of the signal envelope will occur in a dispersive medium.

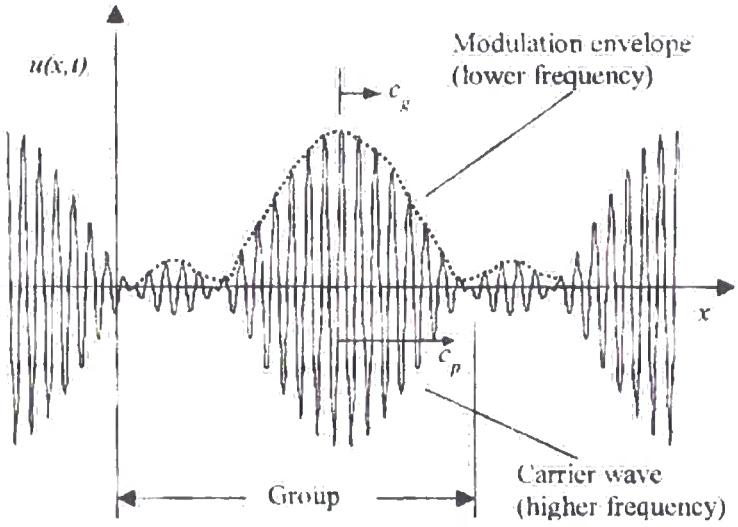

Figure 4.1. **Diagram showing group velocity** [2]

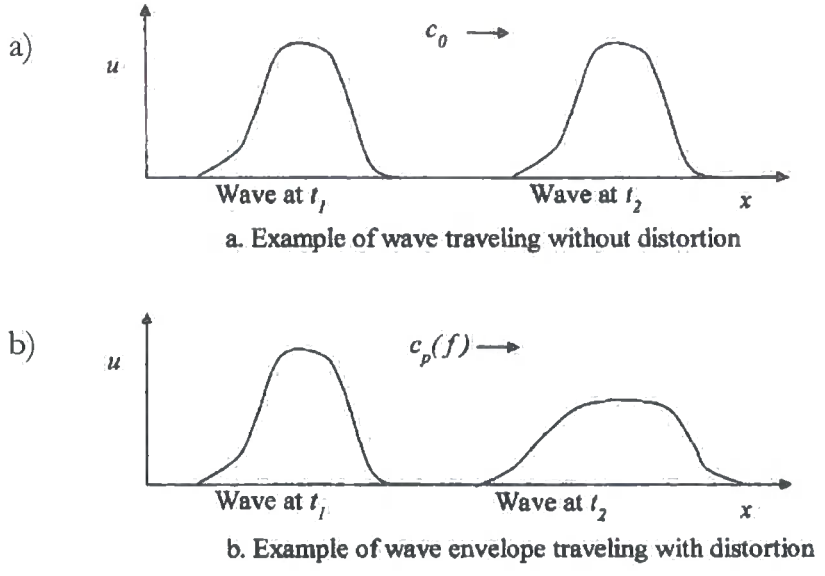

Figure 4.2. **Examples of signals in non-dispersive and dispersive media** [2]

4.3. Wave Propagation at Boundaries

Consider a plane stress wave p_i travelling in medium 1 approaching the boundary to medium 2 at normal incidence. Some of wave will be transmitted to medium 2 and the rest reflected back into medium 1. The degree to which this occurs is dependent in the ratio of the acoustic impedances of the two media, Z_1 and Z_2 and is defined by reflection coefficient, R and the transmission coefficient, T.

These are shown in equations 4.9 and 4.10.

$$R = \frac{p_r}{p_i} = \frac{Z_2 - Z_1}{Z_2 + Z_1} \qquad [4.9]$$

$$T = \frac{p_d}{p_i} = \frac{2Z_2}{Z_2 + Z_1} \qquad [4.10]$$

Where the acoustic impedance Z_i is given by

$$Z_i = \rho_i c_i \qquad [4.11]$$

where ρ_i is the density of the medium and c_i the velocity.

Thus, it can be seen that the larger the ratio between the two impedances, the more of the wave energy is reflected and less is transmitted [14]. For example, consider the boundaries between water and steel and air and steel. Their nominal properties are shown in Table 4.1.

Table 4.1 Material properties

Material	c in ms^{-1}	ρ in kg m^{-3}	Z in kPa s m^{-3}
Water at 20°C	1480	998.2	1.483
Air	343	1.168	0.413
Steel mild	5900	7830	46.000

(from www.edboyden.org/constants)

These values show that water provides a high degree of mechanical coupling hence more wave energy is transmitted at the water-steel interface (R=0.94), than at an air-steel interface and, water or water-based compounds are commonly used for ultrasonic coupling [3].

Now, consider the plane wave incident upon a boundary at an angle a_e. as shown in Figure 4.4. The angle of the reflected wave will be equal to the angle of incidence and the transmitted wave will be refracted according to Snell's law as shown in equation 4.12.

$$\frac{\sin a_i}{\sin a_d} = \frac{c_1}{c_2} \qquad [4.12.]$$

where c_1 is the velocity in material 1, c_2 is the velocity in material 2, a_i is the angle of incidence, a_r is the angle of reflection and a_d is the angle of refraction.

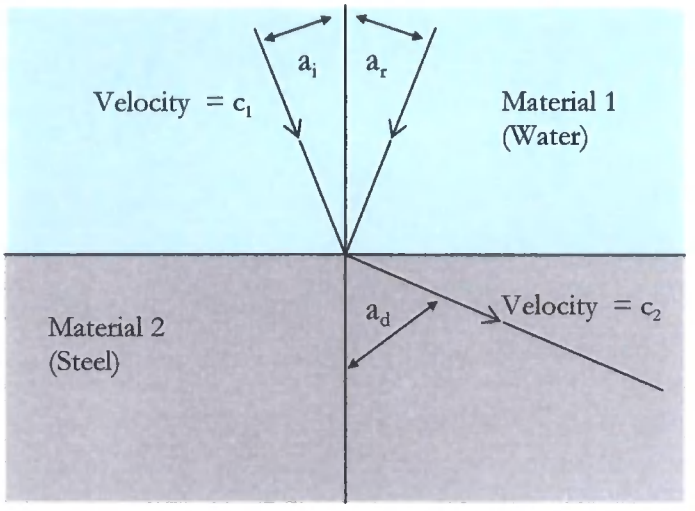

Figure 4.3. Diagram of Snell's law for refracted angles

When a longitudinal wave propagates through a boundary, part of the energy can convert to a shear wave. Since shear waves have a different velocity, the angle of refraction will be different. If the longitudinal wave moves from a slower to a faster material as in the immersion testing of steel, there is an angle of incidence that creates a 90 degrees angle of refraction for the wave. This angle is known as the first critical angle and can be found from Snell's law by putting in an angle of 90 degrees. The resulting wave is referred to as a creep wave. However, it has the same velocity as the longitudinal wave. Rearranging equation 4.12. and using velocities of 1480 ms^{-1} for water and 5900 ms^{-1} for steel, the critical angle is:

$$\frac{1480}{5900} \text{ x } \sin 90^0 = 14.53^0 \qquad [4.12.]$$

For this reason, most angle beam transducers generate a shear wave in the test specimen. However, there is also a critical angle for shear waves. At this point, known as the second critical angle, all of the ultrasonic wave energy is either reflected away from the boundary or refracted into a surface shear wave or shear creep wave.

4.4. Loss mechanisms

There are three main loss mechanisms in solid media, scattering, diffraction and absorption due to internal frictional losses. These can be detected primarily by measuring the attenuation of a reflected signal from a known boundary and can be represented mathematically by the attenuation coefficient a described in section 4.1. Evidence of scattering can also be obtained by looking at the background noise known as grass.

The effective diffraction loss and phase change in the field of broadband transducers is computed in terms of the normalized distance travelled at the centre frequency of the pulse, it this instance, 5MHz. The diffraction loss fluctuates in the nearfield with S before becoming monotonic in the far field, and increasing as the logarithm of S (Equation 4.13) Where, z is the distance to the crystal, λ, is the wavelength, and a is the transducer radius [4].

$$S = z\lambda/a^2 \qquad [4.13]$$

However the most dominant mechanism is scattering and this occurs from the fact that the material is not strictly homogeneous. It contains boundaries at which the acoustic impedance changes abruptly. In a material with a very course grain structure of a size comparable to the wavelength of the signal, the scatter can be visualised geometrically [5]. At an oblique boundary the wave is split into various reflected wave types. This process repeats itself for each grain boundary encountered and Birks (1991) states, it is one of the main sources of loss in commercial alloys [6]. Thus, the original sound beam is constantly sub-divided into partial waves and throughout its complex pathway and frictional losses its energy converted into heat.

If P_T is the signal power at the transmitting probe, and P_R is the signal power at the receiving end then the power attenuation A_p in decibels is given by the formula,

$$A_p = 10 \log_{10}(P_T/P_R). \quad [4.14]$$

The sound attenuation increases with an increase in the frequency, and as the distance increases from the source. For the case of Rayleigh scattering with , $\lambda > 2\pi\overline{D}$ [7]

$$\alpha_L = \frac{8\pi^3\mu^2 T f^4}{375\rho^2 v_l^3}\left[\frac{2}{v_l^5} + \frac{3}{v_t^5}\right] \quad [4.15]$$

$$\alpha_T = \frac{2\pi^3\mu^2 T f^4}{125\rho^2 v_t^3}\left[\frac{2}{v_l^5} + \frac{3}{v_t^5}\right] \quad [4.16]$$

and for Rayleigh scattering with $\lambda < 2\pi\overline{D}$ [3] [7]

$$\alpha_l = \frac{16\pi^2\mu^2\overline{D}f^4}{525 v_l^6 \rho^2} \quad [4.17]$$

$$\alpha_t = \frac{4\pi^2\mu^2\overline{D}f^4}{210 v_t^6 \rho^2} \quad [4.18]$$

where $\overline{D}$ is the average grain diameter

In immersion testing the ultrasonic attenuation coefficient of a specimen can be calculated using the equation 4.19. [8], [9]. The ratio of received amplitudes (R) is determined experimentally, taking amplitude readings with and without the test specimen in position.

$$\exp(-2\alpha_2 L) = R\exp(-2\alpha_1 L)\left[\left(\frac{\rho_1 V_1}{4\rho_2 V_2}\right)+\left(\frac{\rho_2 V_2}{4\rho_1 V_1}\right)+\frac{1}{2}\right] \qquad [4.19]$$

Where the subscripts 1 & 2 are the immersion liquid and the specimen respectively. V is the velocity of the ultrasound; L is the specimen thickness, α is the attenuation coefficient and ρ is the density. R is ratio of received amplitudes when the specimen has been removed and can be determined experimentally.

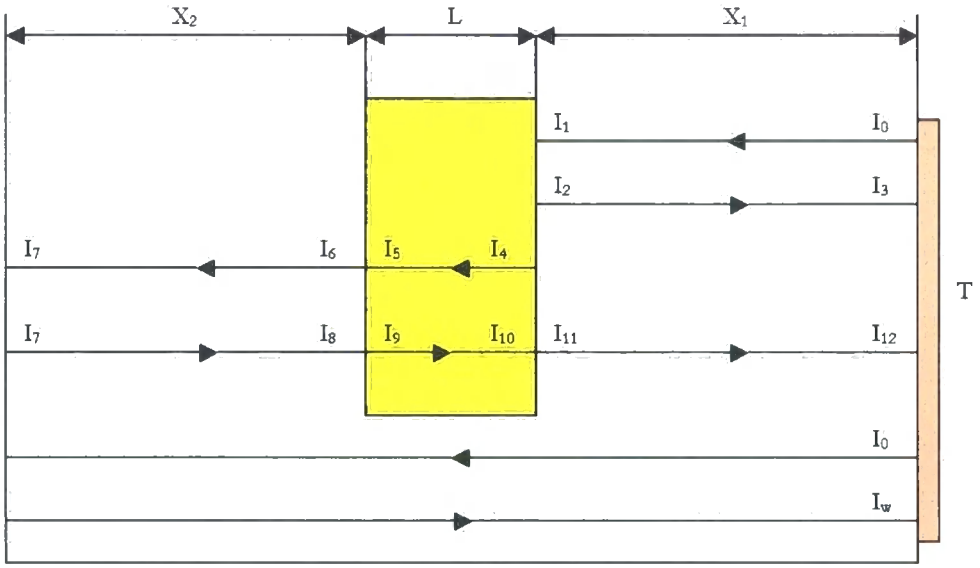

Figure 4.4. Diagram of immersion technique with nomenclature of signal intensities

Figure 4.4. shows a schematic diagram of the experimental immersion technique employed by Youssef, M.H. and N.K. Gobran [9] to evaluate the attenuation coefficient of a specimen material of thickness L. A transducer (T) was positioned at

distance X_1 from the specimen on one side of the immersion tank, with the specimen being a distance of X_2 from the opposite tank wall. I_0 is the intensity of the signal leaving the ultrasonic transducer, with I_1 representing the intensity of the signal reaching the specimen, after travelling a distance of X_1. I_3 represents the intensity of the signal reaching the transducer, after travelling a distance of $2X_1$ with I_{12} representing the intensity of the signal arriving at the transducer, after travelling a distance of $2X_1+2L+2X_2$.

4.5. Diffraction of Waves

Diffraction can be generalised as the spreading of a plane sound wave as it passes through an aperture or the edge of an obstacle. Therefore, when an ultrasonic wave impinges on a discontinuity the wave is scattered by the discontinuity, and at the edge of the discontinuity the wave will be diffracted [10]. In this way, the wave energy that was travelling in one direction can be radiated and distributed into a wide range of angles, with a consequent reduction in the energy travelling in the original direction of propagation.

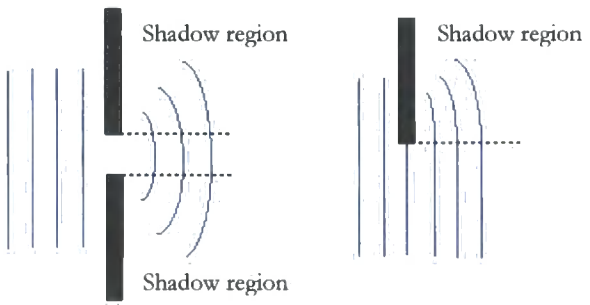

Figure 4.5. Drawing showing waves diffracting around objects

This can be explained using the Huygens-Fresnel principle; an impermeable wall does not produce a sharp shadow within the sound field because its edge can be regarded as the origin of new elementary wave (Figure 4.5.) [5].

4.6. Sound Pressure and Beam Profile

Ultrasonic transducers can be considered to be cylindrical apertures and hence the ultrasonic wave will diffract to produce a beam profile, the parameters of which are dependent of the aperture radius and wavelength. Figure 4.6. and 4.7. shows a simulation of the beam profile along its axis for 5MHz immersion transducer in water. Figure 4.6. shows the areas of the high pressure (lighter) and low pressure (darker) within the sound field.

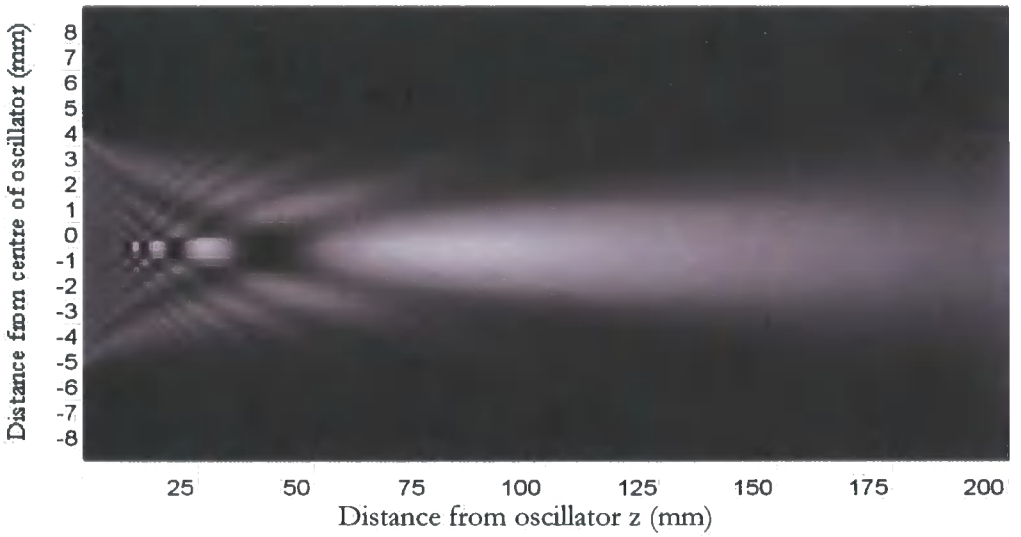

Figure 4.6. Areas of the high (lighter) and low pressure (darker) within the sound field

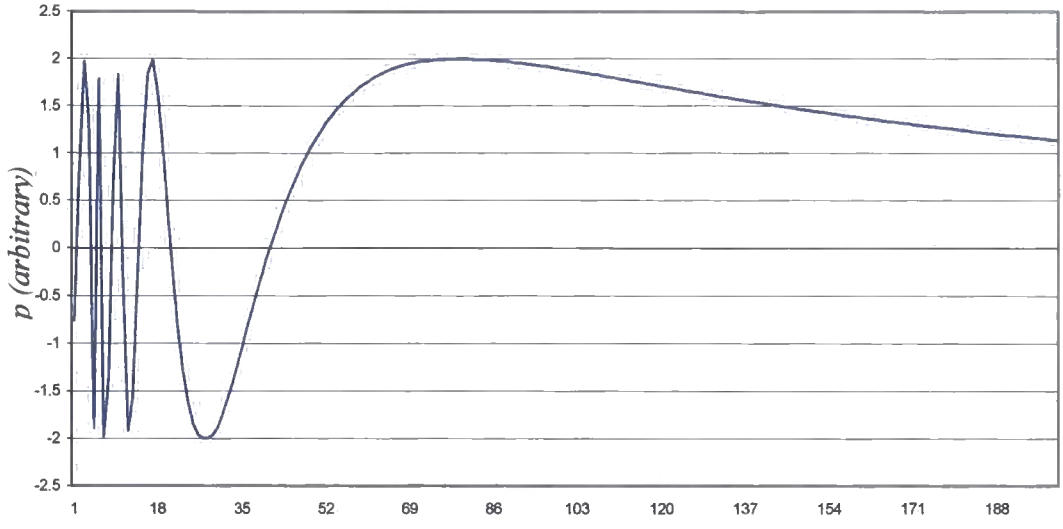

Figure 4.7. Plot of the sound pressure

According to Krautkrämer et al [5] the sound pressure on the axis (Figure 4.7.) is given by the formula (Equation 4.20.) where z is the distance on the axis from the centre point of the oscillator and D is its diameter shown in Figure 4.7.

$$p = p_o 2\sin\left(\frac{\pi}{\lambda}\left[\sqrt{\left(\frac{D}{2}\right)^2 + z^2} - z\right]\right) \qquad [4.20.]$$

4.6.1. The Near and Far fields

The Nearfield (N) has areas of differing sound pressure and it extends from the source of radiation to a point just short of the far field or Fraunhofer zone (Figure 4.8.) defined by the location of the last pressure maximum as shown in Figure 4.7.

This transition point also depends upon the diameter of the transducer, D and wavelength λ (Figure 4.8.) in accordance with the relationship the near field equation for a cylindrical transducer (Equation 4.21.). These fluctuations in the sound intensity are caused by waves that originate from one part of the emitter interfering constructively or destructively with waves from another area of the emitter. Because of intensity variations within the near field, it can be difficult to evaluate flaws accurately in materials if they are positioned within this zone. At the far field however, the beam strength is always greatest at the centreline of the beam and diminishes as it spreads outward.

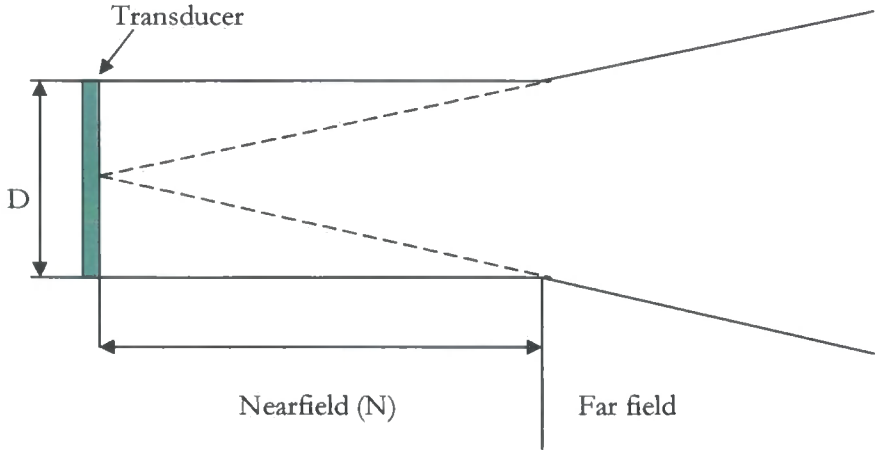

Figure 4.8. Diagram of the Nearfield

$$N = \frac{D^2 - \lambda^2}{4\lambda} \qquad [4.21.]$$

In most practical cases the diameter of the oscillator is much greater than the wavelength and the equation is simplified to,

$$N = \frac{D^2}{4\lambda} \qquad [4.22.]$$

4.6.2 Beam Profile

This section will look at the beam profile from a cylindrical transducer so that it can be related to the transducer array researched in this thesis. Standard ultrasonic theory shows that the central beam in the near field diverges slowly [2]. In the far field this beam divergence is more pronounced and is a measure of the angle from one side of the sound beam to the central axis of the beam, and the beam spread angle is twice the angle of beam divergence. The maximum sound pressure is always found along the acoustic axis or centreline of the transducer. Therefore, the strongest reflections come from the region immediately in front of the transducer [6]. The sound intensity attenuates according to an inverse square law, that is, the intensity is inversely proportional to the square of the distance. In the far field the Equation 4.23 determines the angle of divergence for the extreme width of the beam [11].

$$\sin\frac{\theta}{2} = \frac{1.22\lambda}{D} \qquad [4.23.]$$

where λ is the wavelength, D is the diameter of the oscillator, and 1.22 is a given constant for the extreme beam width. The constant 1.22 can be replaced by 1.08 to calculate the angle of divergence for the edge of the beam, 20dB below the intensity of the centre of the beam [12].

4.7. Signal to Noise Ratio

The signal to noise ratio is defined as the ratio of the amplitude of an ultrasonic echo arising from the discontinuity in a material (signal V^s), to the r.m.s amplitude of the background noise signal or grass (V^n).

The signal-to-noise ratio (SNR) in decibels is given by:

$$SNR = 20 \log_{10}(V^s/V^n) \qquad [4.24.]$$

This noise can arise from the material characteristics, un-required ultrasonic modes and equipment noise. Ambient noise is very often the real source, and is especially likely to occur in automated testing installations. Several opinions arise when discussing signal processing for enhancing the required part or suppressing the unwanted part of the signal, all claiming to have positive results. Enhancing the reliability of flaw detection, through the use of digital signal processing [13], using contact and immersion techniques, showed that the immersion techniques provided a greater level of reliability.

The use of a wavelet transform process and is stated by Chen and Shi [14], to be more powerful than frequency filtering as a method of enhancing reliability. However negligible improvements were made from immersion tests. There have been many applications of wavelet transforms in ultrasonic non-destructive testing [15, 16]. Li and Ma [17] used a wavelet transform to identify signals of localised defects in bearings, while Cho et. al. [18] applied the wavelet transform of the digital data in deducing the scattering of subsurface lateral defects.

4.8. Inspection Dead Zone

The inspection dead zone is defined as the distance just below the surface of a test object that cannot be inspected because of the finite length of the excitation pulse. During this time the piezoelectric crystal cannot act as a receiver for the reflected echo, as the transmitted pulse may saturate the receiver (Figure 4.9.).

The distance which depends on the pulse frequency and width may extend to several millimetres within a material [6]. Therefore as the pulse width increases or the frequency decreases, the dead zone increases correspondingly [19], with the actual value dependent on the material under examination [12].

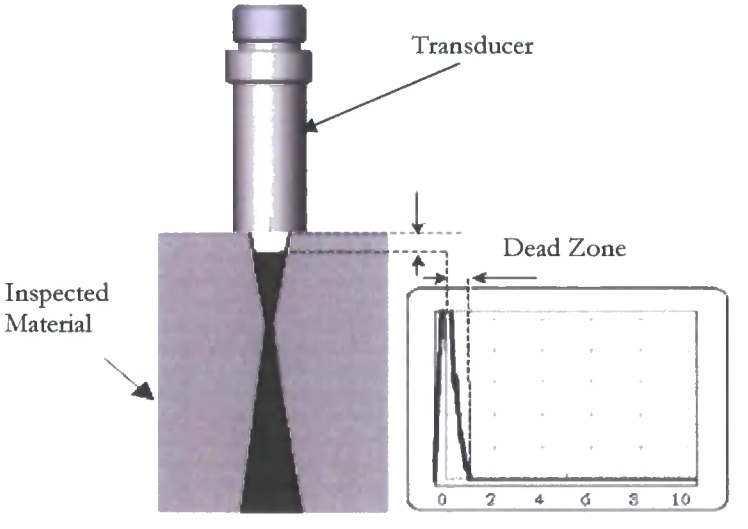

Figure 4.9. Diagram of Dead Zone with representative A-scan

4.9. Summary

This chapter has given an overview of the basic theory used in the implementation of the research project described in this thesis. A particular emphasis has been given to unbounded bulk wave propagation using cylindrical transducers and the relationship between theory and inspection terminology.

4.10. References

1. Morse, P.M. and H. Feshbach, *Methods of theoretical physics.* International Series in Pure and Applied Physics. 1953, New York: McGraw-Hill. 1008.

2. Rose, J.L., *Ultrasonic Waves in Solid Media.* 1999, Cambridge: Cambridge University Press.

3. Wolfram, A. *Automated ultrasonic inspection.* in *15th WCNDT conference.* 2000. Rome, Italy: www.karldeutsch.de/PDF/Automated_UT_inspection_May00.PDF.

4. Papadakis, E.P., *Ultrasonic Diffraction Loss and Phase Change for Broad-Band Pulses.* The Journal of the Acoustical Society of America, 1972. **52**(38): p. 847-849.

5. Krautkrämer, J. and H. Krautkrämer, *Ultrasonic Testing of Materials.* 1990, New York: Springer-Verlag. 677.

6. Birks, A.S. and R.E. Green Jr., *Ultrasonic Testing.* 2nd ed. Nondestructive Testing Handbook, ed. P. McIntire. Vol. 7. 1991, Baltimore, Maryland, U.S.A.: American Society for Nondestructive Testing. 893.

7. Marton, L. and C. Marton, *Ultrasonics.* Methods of Experimental Physics, ed. P.D. Edmonds. Vol. 19. 1981, London: Academic Press Inc. 619.

8. McSkimin, H.J., *Physical Acoustics, Principles and Methods.* Vol. 1. 1964, New York: Academic Press.

9. Youssef, M.H. and N.K. Gobran, *Modified treatment of ultrasonic pulse-echo immersion technique.* Ultrasonics, 2002. **39**: p. 473-477.

10. Charlesworth, J.P. and J.A.G. Temple, *Engineering Applications of Ultrasonic Time-of-Flight Diffraction.* Second Edition ed. Ultrasonic Inspection in Engineering, ed. M.J. Whittle. 2002, Baldock: Research Studies Press Ltd. 254.

11. Halmshaw, R., *Mathematics and Formulae in NDT.* 2nd ed. 1993, Northampton: The British Institute of Non-Destructive Testing.

12. Hellier, C.J., *Handbook of Nondestructive Evaluation.* 2001, New York, U.S.A.: McGraw-Hill.

13. Chen, J. and Y. Shi, *Enhancing the reliability of ultasonic testing by digital signal processing.* Insight, 2002. **44**(4): p. 237-245.

14. Chen, J.Z., et al., *Ringing Noise Estimation and Suppressionby High Pass Filtering and Wavelet Packet Transform.* Materials Evaluation, 2000(58): p. 979-984.

15. Murthy, R., et al., *Detection of Ultrasonic Anomaly Signals using Wavelet Decomposition.* Materials Evaluation, 1997. **55**: p. 1274-1279.

16. Chen, J., et al., *Noise analysis of digital ultrasonic nondestructive evaluation system.* International Journal of Pressure Vessels and Piping, 1999. **76**(9): p. 619-630.

17. Li, C.J. and J. Ma, *Wavelet Decomposition of Vibrations for Detection of Bearing Localised Defects.* NDT & E International, 1997. **30**: p. 143-149.

18. Cho, H., et al., *Non-contact Laser Ultrasonics for Detecting Subsurface Lateral Defects.* NDT & E International, 1996. **30**: p. 301-306.

19. Filipczynski, L., et al., *Ultrasonic Methods of Testing Materials.* 1966, London: Butterworth & Co. Ltd.

Chapter 5.

System and Initial Experimental Work

5.1. Introduction

This project involves investigating a single transmitter, multi-receiver system in the context of defect detection. A room temperature laboratory based system was developed to examine the underlying principles. Thus, this chapter firstly describes the basic system. The system was then characterised to understand the effect of the system components on any experimental results and to optimise the set-up conditions. These tests and results are presented.

The first contact experiments on a steel billet are then described and analysed. The final part of this chapter presents experiments carried out on a V1 calibration block to understand and verify the base theories underlying this work. The advantages and limitations of this approach are then examined.

5.2. Experimental Apparatus

A block diagram of the basic experimental set up is shown in Figure 5.1. The equipment used was

- Hewlett Packard "Infinium" oscilloscope
- Socomate USPC 3100 PC based ultrasonic flaw detector
- Three, 3/8 inch diameter, 5MHz transducers.
- Immersion tank, with linear material transportation facility.
- Ultrasonic couplant Gel (Ultragel II from Diagnostic Sonar Ltd.)

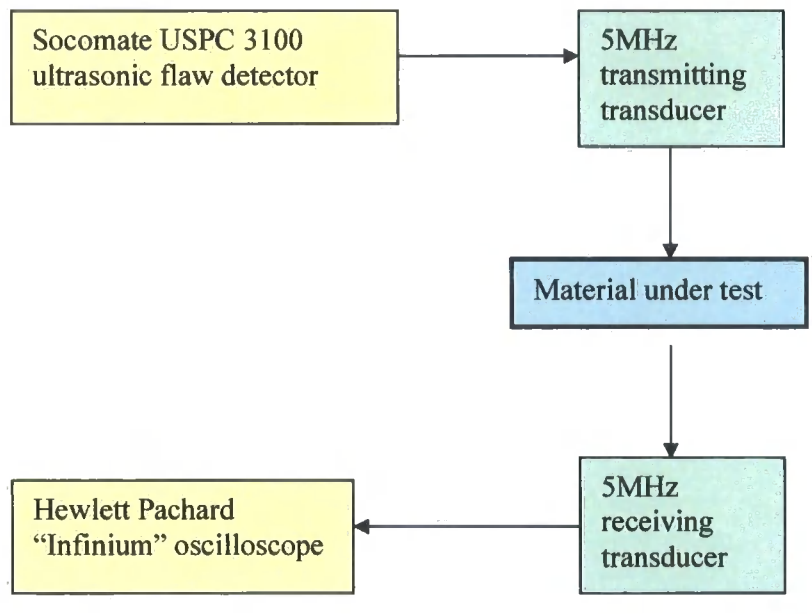

Figure 5.1. Block diagram of experimental set-up

5.2.1. Hewlett Packard "Infinium" Oscilloscope

The 54820A Infinium is a 2-channel oscilloscope (Figure 5.2.), with a Windows-based graphical interface, and an integrated 3.5"floppy disc drive for data transfer. The oscilloscope has a bandwidth of 500 MHz, and the capability of simultaneously sampling, on both channels, at a rate of 2 x 10^9 sample/seconds. For consistency, signal stability and to improve the signal to noise ratio the acquisition filter was set to average the signal over 16 samples. The averaging stabilised the received signal on the display screen, which facilitates accurate interpretation of the signal. The 16 averages was the optimum setting for the signal acquisition on the oscilloscope, as a greater numerical average would affect the refresh rate and sample length at the chosen sampling frequency of 50MHz. The sampling frequency of 50MHz is outside the Nyquist sampling frequency avoiding signal aliasing problems [1].

The pulse repetition frequency of 5kHz, the systems slowest repeat rate, was applied to facilitate signal decay and reduce spurious echoes. These parameters are applicable for the duration of the project unless otherwise stated.

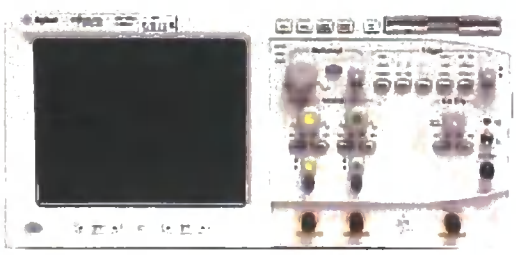

Figure 5.2. HP Infinium oscilloscope.

Figure 5.3. Socomate USPC3100.

5.2.2. Socomate USPC 3100

The priority of the ultrasonic equipment was to be adaptable to the potential changes within the scope of the project. Various stand-alone pulser/receivers and flaw detectors were considered from various manufacturers. The Socomate USPC 3100 had the required specifications with the additional flexibility that the software can be modified if required, and additional channels can be added, both of which could be advantageous to the project.

The Socomate USPC 3100 is a "Plug & Play" Windows based PC Card flaw detector with two transmit/receive channels (Figure 5.3.). The frequency ranges from 0.5 MHz to 20 MHz at a dynamic range of 70dB, with a Pulse Repetition Frequency (PRF) of up to 20kHz.

5.2.3. Transducers

The nature of the project dictated that the transducers employed were capable of operating in a liquid environment, and for this reason immersion transducers were used. Immersion inspection gives uniform coupling, and facilitates operation in situations where the part to be tested is either partially or fully submerged in water (Figure 5.4.). The active piezoelectric elements of the transducers have an impedance matched protective cover. This layer is to prevent damage to the crystal and facilitates the sound energy transfer into the water and therefore into the component being inspected [2]. The thickness of this layer will need to be considered when taking any time/distance measurements. This is accomplished by selecting a matching layer that is 1/4 wavelength thick ($\lambda/4$) and of the desired acoustic impedance with the active element ½ the nominal wavelength ($\lambda/2$) thick [3] (Figure 5.4).

The choice of the wear surface thickness is based upon the idea of superposition that allows waves generated by the active element to be in phase with the wave reverberating in the matching layer (Figure 5.4.) Because the transducers used for this project are immersion probes the matched layer is 1/4 of the wavelength of the propagating wave through water. Using equation 2.1. the matched layer is 0.075mm and the piezoelectric element is 0.150mm thick.

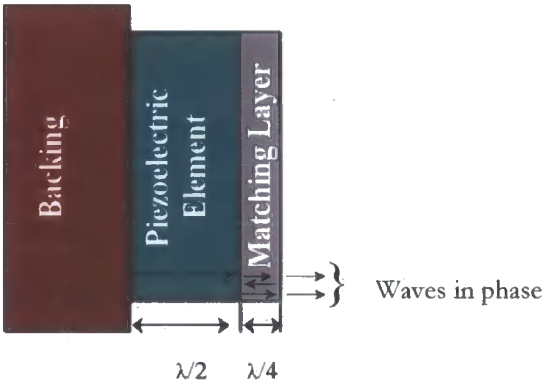

Figure 5.4. Diagram showing the piezoelectric element and matching layer with signal paths

The wavelength of the ultrasound is dependent upon both the material through which it is propagating and the frequency (Section 4.1.). This also has a significant affect on the probability of detecting a discontinuity within the material. In industrial automated pulse echo inspections, discontinuities that are larger than one-half the size of wavelength ($\lambda/2$) can be detected [4]. Transducer choice is therefore a balance between signal attenuation and resolution. Because as the frequency increases and the wavelength shortens, the attenuation also increases, as rapid oscillation looses more energy that slower oscillations due to energy conversion into heat [5]. Lower frequencies transducers of between 0.5MHz-2.25MHz provide greater energy and penetration in a material, while high frequency crystals of between (15.0MHz-25.0MHz) provide reduced penetration but greater sensitivity to small discontinuities [5].

The 5MHz piezoelectric transducers were chosen as the optimum frequency for this project [6]. The transducers used during all these experiments were manufactured by NDT Systems and are 5MHz, immersion transducers, with a 0.375inch (9.525mm) diameter piezoelectric crystal (Figure 5.5.)

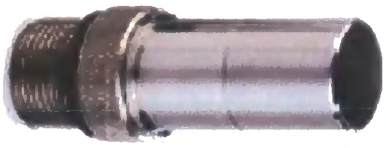

Figure 5.5. A typical ultrasonic immersion transducer

5.2.4. Transducer/Sample Coupling

Because of the large impedance mismatch between air and in the case of this project, steel, water is commonly used for ultrasonic coupling [7]. Acoustic impedance is discussed in section 4.11 of this thesis. Water as a coupling medium is predominantly used in automatic testing similar to the system under evaluation. The advantages of using this type of testing are that the surface of the material does not have to be smooth as is required by contact testing. Water coupling also alleviates the possibility that the transducers will be struck by moving bar, and remove the complications involved with the near field of the probe. Ultrasonic sound waves travel at a much lower velocity in water than in steel.

The longitudinal wave velocity is approximately four times greater in steel than in water. Because of the difference in the wave velocity, the length of the near field is proportionately greater in water [5].

The beam divergence is also proportionately greater in water, causing significant energy dispersion over modest water path lengths between the transducer and the material being tested. In this project the divergence of the signal is seen as an advantage as it required to be detected by the passive probes. It is also necessary to take into account the length of the signal path and its velocity through the different media. The second signal is required to occur after the back-wall echo from the first signal is received. The Thrybergh Bar Mill system therefore requires recalibrating at every material size change over. Figure 5.6. illustrates how the transit time of the signal can be calculated using the equation 5.1.

$$ToF = 2\left(\frac{c_w}{l_w}\right) + 2\left(\frac{c_s}{l_s}\right) \qquad [5.1.]$$

Where

c_w = Velocity in water

l_w = Path length in water

c_w = Velocity in steel

l_s = Path length in steel

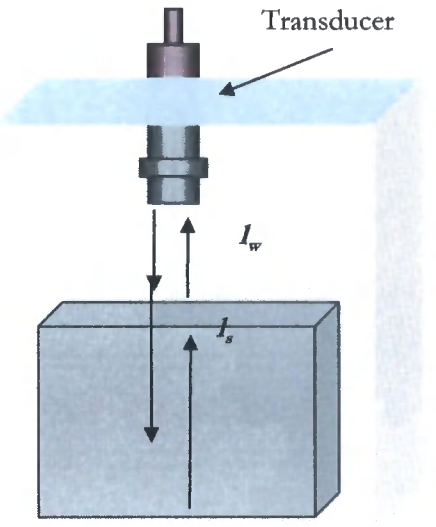

Figure 5.6. Diagram showing the signal path through the water coupling & steel.

An ultrasonic couplant is used in virtually all contact testing applications, facilitating the transmission of ultrasonic sound energy between the transducer and the test piece. Where contact to the test piece is required a contact couplant, typically a viscous, non-toxic liquids, gels, or pastes will be used. Their use is necessary because sound energy, at the ultrasonic frequencies typically used for non-destructive testing, is not effectively transmitted through air because of the impedance mismatch [6]. Even extremely thin air gaps between the transducer and the test piece affect the efficiency of sound energy transmission and render testing impossible. Air interfaces represent a severe acoustic impedance mismatch with respect to both transducer and the material undergoing examination (Chapter 4.11.) The general purpose propylene glycol ($C_3H_8O_2$) based couplant used in these experiments was chosen because it has good surface wetting properties, it will not corrode or otherwise attack materials, and it is easily washed off with water. It is also chemically non-reactive and does not evaporate quickly at room temperature. Propylene glycol has an acoustic impedance of 1.61×10^5 $kgm^{-2}s^{-1}$ and is similar to that of water of1.48×10^5 $kgm^{-2}s^{-1}$.

5.3. Characterisation of the System

This section describes tests, which were carried out to characterise the response of the measurement system to assist with the interpretation of experiments on different sample materials. The output voltage from the USPC 3100 flaw detector is a short voltage pulse whose width can be modified to match half the wavelength of the piezoelectric transducer to be excited and has been designed to drive transducers in the 0.5MHz to 20MHz range. Two tests were carried out, the first being to assess the excitation voltage as a function of pulse width and the second to assess the received voltage of a through transmission transmitter/receiver system coupled by water with no sample present with respect to pulse width.

5.3.1. Transmitter Voltage

This experiment was set up to determine the variability in the transmitter voltage as a function of pulse width. The test circuit was set up as shown in Figure 5.7. The pulse width was swept through settings used to drive transducers from 0.5MHz to 20MHz. The open circuit voltage was recorded through a 50Ω impedance matched, 100 times voltage attenuator, by the 500MHz bandwidth oscilloscope. The attenuator was necessary as the voltage pulse was outside the safe operating range of the oscilloscope. For each pulse width, the outputs from several pulses were taken and the average maximum and minimum values were recorded, with the results are shown in Figure 5.8.

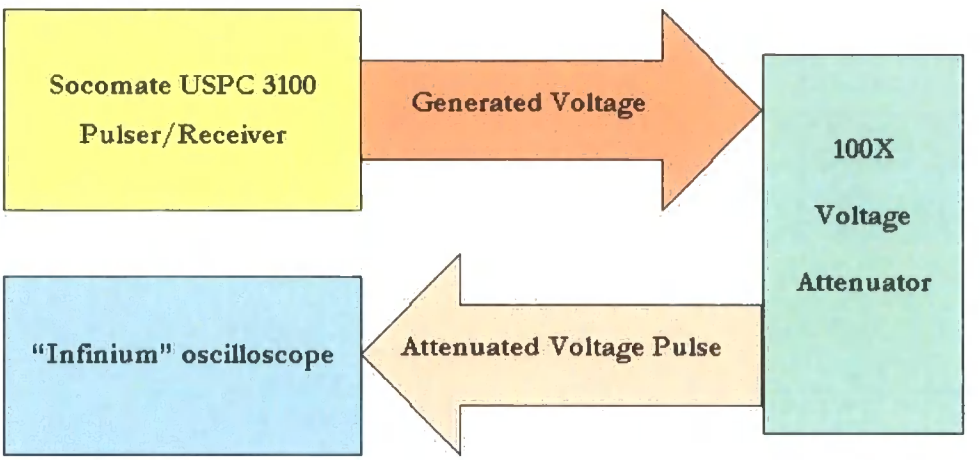

Figure 5.7. Block diagram showing flaw detector connected to the oscilloscope via the inline 100x signal attenuator

Since the transducer geometry determines the ultrasonic frequency, the ultrasonic amplitude is dependent on the amount of excitation power present at that frequency. The spectrum of a pulse is a sine cardinal (sinc) function whose zeros are determined by the pulse width. Figure. 5.8. shows the sinc function characteristic effectively traversing the ultrasonic frequency as the pulse width increases.

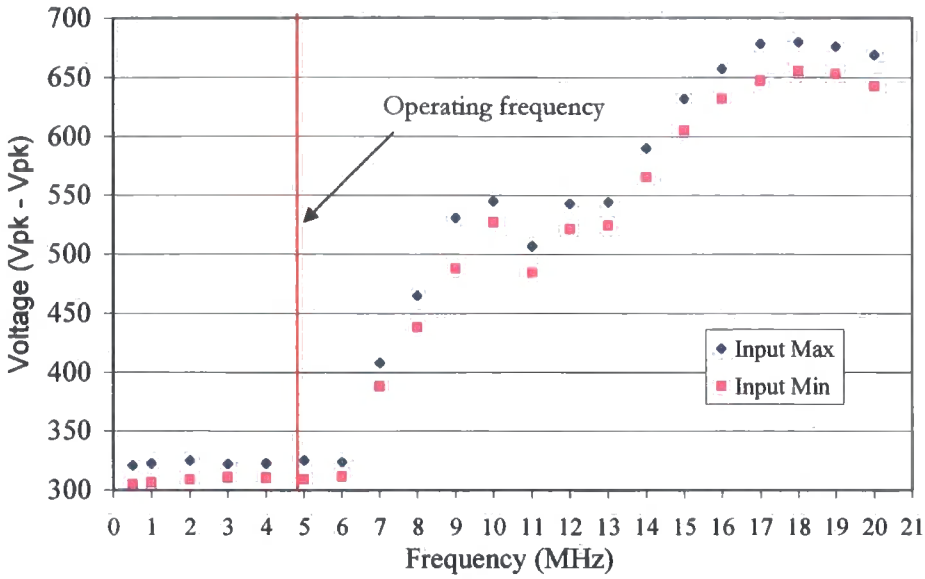

Figure 5.8. Graph showing input voltage plotted against frequency

The results of these experiments showed that the excitation voltage is constant for settings used to drive transducers up to 6.5MHz where the voltage rapidly increased (Figure5.8.). The area, at which the voltage started to increase, is above the designated 5MHz operating point for this project and was not investigated further. At any one pulse width, the voltage was stable to within 6.7% as defined by three standard deviations.

5.3.2. Receiver Characteristics

The aim of this experiment was to characterise a transmitter receiver system without a sample present using water coupling to give a base measurement for comparison. This was carried out in a temperature controlled immersion tank. The temperature of the water was set at 24 $^{+}$/- 1 degrees Celsius.

This is above that of the ambient room temperature, and was chosen to give consistent readings regardless of the surrounding environmental conditions.

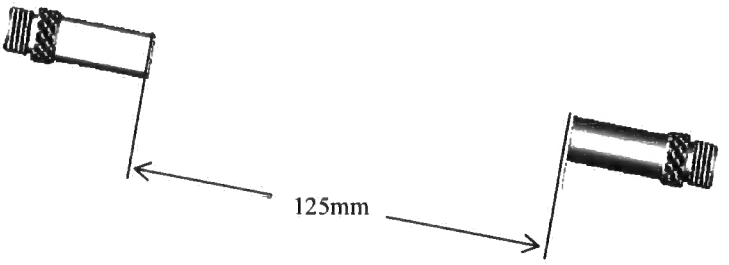

Figure 5.9. Diagram showing 125mm transducer separation

These experiments were carried out using two 5MHz transducers, with the transducers facing each other and an arbitrary separation distance of 125mm (Figure 5.9.) Figure 5.10. again shows the effect of having different pulse widths. A wide pulse width results in a narrow central lobe of the sinc function in the frequency domain. There will be a slight mismatch of the Tx and Rx crystal frequencies so again it is the sinc function effectively traversing the receiving frequency resulting in the initial peak. Now as the pulse gets narrower the central lobe of the sinc function gets wider and there will be less power in the receiving frequency resulting in a decrease in the voltage amplitude.

The voltage received at the transducer, displayed in the graph (Figure 5.10.), shows that the maximum response occurs at a frequency setting of just above 7MHz. This overall response is a combination of the frequency response of the transmitted pulse, the transducers, amplifier and the coupling medium. From this graph the operating frequency setting chosen for further experiments as 5MHz as it is just in the flat region of the overall response.

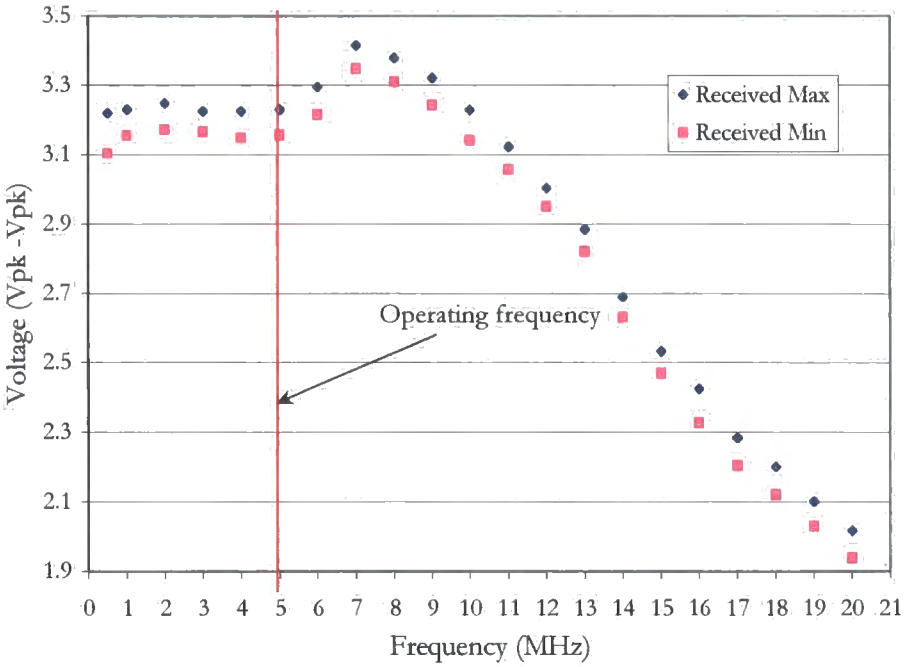

Figure 5.10. Plot of received voltage through 125mm water separation

5.4. Initial experiments to assess the use of a single transmitter-multi-receiver system

The first sets of experiments were carried out on a steel billet to assess whether signals could be detected from a receiving probe array. However, before this could be done, the billet required characterisation using traditional pulse/echo techniques to determine the type of defects present.

5.4.1. Characterisation of Billet

The billet was examined using a single transmitter/receiver probe placed directly on the steel billet via a water based coupling gel. This resulted in the possibility of defects within the near-field not being detected due to pressure wave minima.

To overcome this, the orientation of the billet was changed to give complete coverage. To ensure that only the compression wave mode was evaluated, only the signal prior to the back-wall echo was used in these experiments, as other, slower modes, may have added additional complexity and will not be supported by the immersion system.

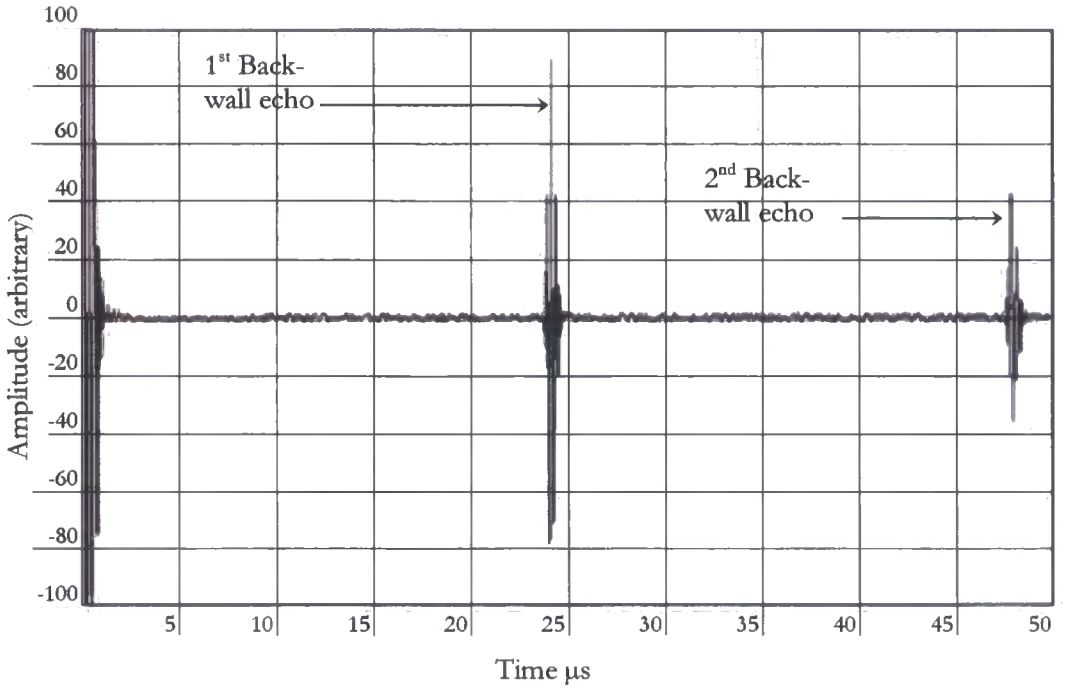

Figure 5.11. Scan of defect free section of billet showing 1st and 2nd back-wall echoes

A clean back-wall echo signal, one with no detectable defect, was established in a section of the material (Figure 5.11.). The compression wave velocity was then measured using the time of flight for the first and 2nd echo from the back–wall [8]. This was used to calculate wave velocity together with the measured material thickness as stated in BS EN 1223:2000, using Equation 5.2.

$$\frac{\text{Distance}}{\text{Velocity}} = \text{Transit Time} \qquad [5.2.]$$

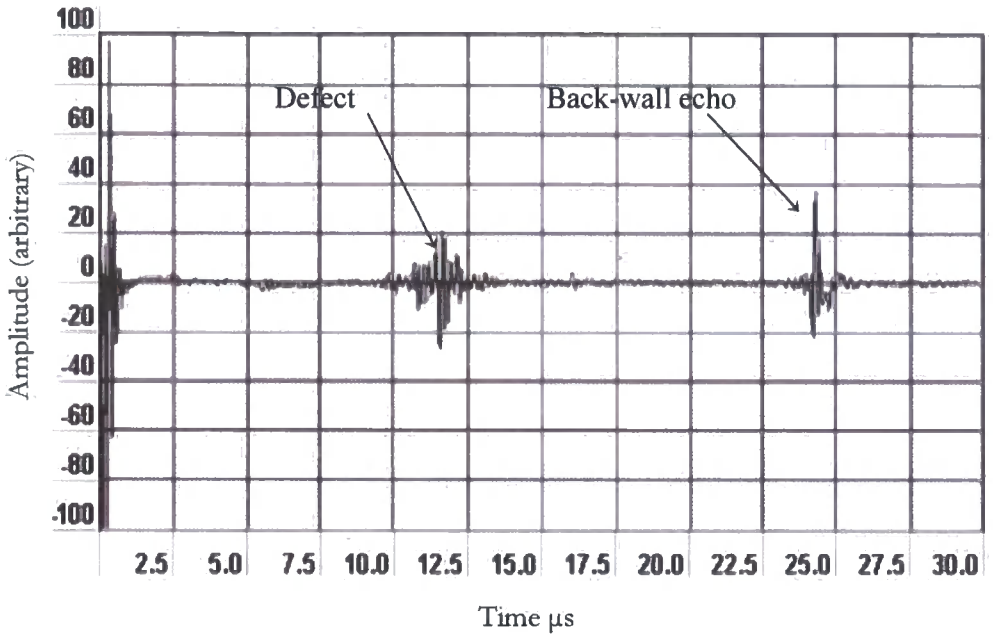

Figure 5.12. A-scan of the defect, taken from random position on the billet

When all of the data had been analysed it was deduced that the steel billet had a large centreline defect present in the core of the billet and this was present throughout the length of billet (Figure 5.12.)

5.4.2. Experiment to assess the use of passive receiver probes

It was decided to progress using the probe in contact with the material but with the introduction of two additional probes as signal receivers. This arrangement was chosen as a representative simulation of the array at the finishing mill (Figure 5.13.) The probes were fitted into a fixture to hold them parallel to each other, with 22.50 mm and 45mm probe separation, and held at 90^0 to the inspected surface (Figure 5.14.)

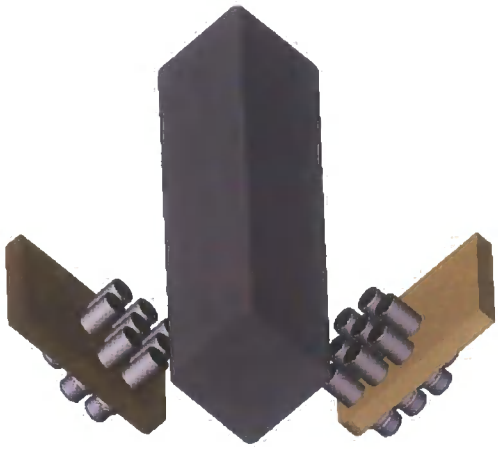

Figure 5.13. Representation of the transducer array at the finishing mill

The signal path lengths were calculated from the centreline of the transducers, with the transmitting signal propagating at normal incidence to the probe face, and with the reflected signal angle calculated away from the normal incidence.

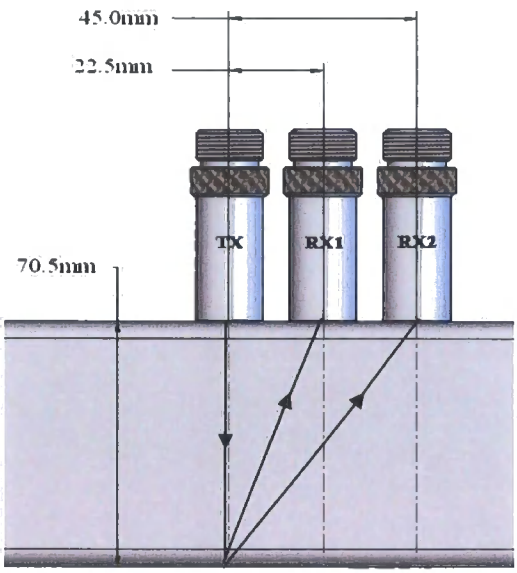

Figure 5.14. Experimental set-up showing transducer separation & signal paths

The procedure was to transmit using one probe (TX). This was connected to the pulser-receiver of the USPC 3100. The other two probes were connected to the oscilloscope and operated as passive receivers (RX). It was established that the receiver probes RX1 and RX2, electro-magnetically detected the initial pulse emitted from the transmitting probe. The USPC 3100 has a trigger facility, however during these initial experiments the initial pulse proved a reliable trigger source and was subsequently utilized as the triggering signal for the oscilloscope. According to Brooks (2003) "There is nothing inherently good or bad about electromagnetic coupling. Whether the consequences of this coupling are beneficial or not depends entirely on the circumstances"[9].

It was considered that when the transmitting probe received a reflected pulse then the neighbouring probes might also detect these via the electromagnetic coupling. This was not the situation however, as the timings would be almost identical for all of the probes within the system and was calculated as approximately 7.5ps over the separation distance of 22.50mm. This was calculated using the relationship stated in Equation 5.1. and the electromagnetic velocity as 299 793 +/- 0.3 km/s [10]. As this was not the case, the mechanism was discounted and the time of flight of the electro-magnetic signal was deemed negligible and subsequently ignored.

Table 5.1 Signal Path lengths and Angles

Transducers	Signal Path Lengths (mm) +/- 0.01mm	Velocity +/- 50m/s	Angle of Signal Paths	Time (μs) +/- 0.01 μs
TX-TX	70.50 + 70.50 = 141.00	5900 m/s	0.0^0	23.90
TX-RX1	70.50 + 74.00 = 144.50	5900 m/s	17.7^0	24.50
TX-RX2	70.50 + 83.64 = 154.14	5900 m/s	32.5^0	26.13

The three-probe array scanned the billet in a similar raster scan pattern as the single pulse/echo probe. The geometry of the array was drawn out to measure the timings of the received signals and to compare with the signals received at the flaw detector (Table 5.1.)

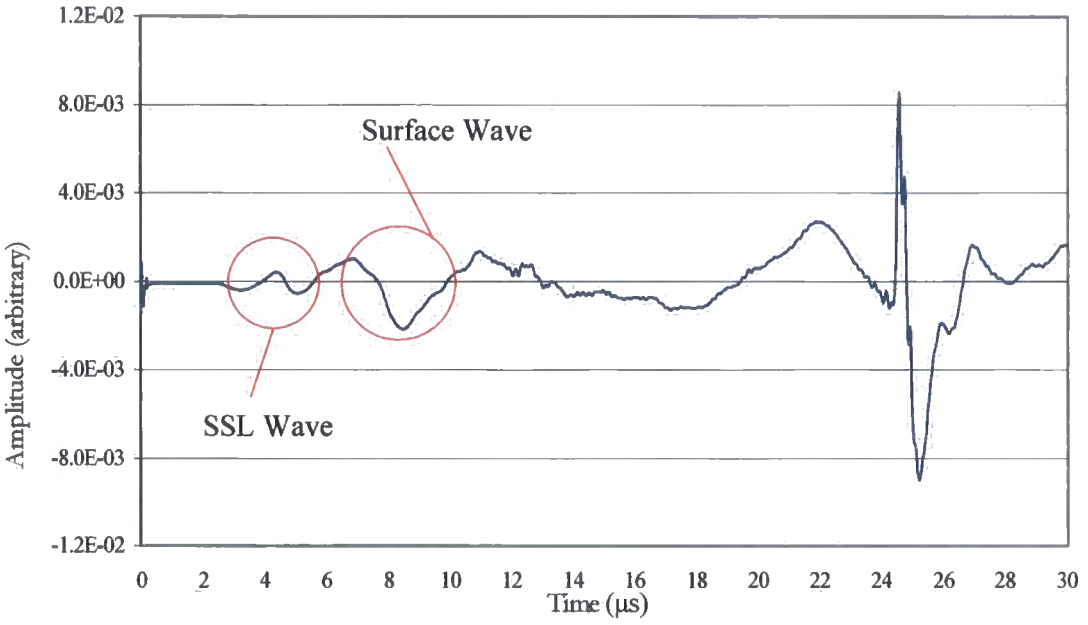

Figure 5.15. Signal received from transducer RX1

The received data from the passive receivers was captured using the oscilloscope and analysed (Figure 5.15 and 5.16). The scans consistently showed a low frequency high amplitude signal and a low frequency low amplitude signal arriving prior to the back wall echo. The high amplitude signal was evaluated through probe positioning and signal timings as a surface wave reflecting from the vertical walls of the block (Equation 5.3.). Surface waves (SW) propagate at a velocity of 0.92x shearwave velocity within the subject material [5], therefore the signal echoing from the sidewall travels a maximum of 25mm from the centre of the probe to the sidewall, with shearwave velocity of 3240ms[11].

Therefore:

$$SWV_s \text{ x } 25mm = 25\left(\frac{0.92}{3240}\right) = 0.00838 = 8.38\ \mu s \qquad [5.3.]$$

The lower amplitude signal arriving prior to the surface wave, was also evaluated through probe positioning and signal timings as a surface skimming longitudinal wave (SSLW) propagating at the same velocity as the longitudinal wave within the material [12]. Therefore:

$$SSLW\ V_c \text{ x } 25mm = 25\text{x } 5900 = 0.00423 = 4.23\ \mu s \qquad [5.4.]$$

The scans proved inconclusive; as the defect could not be readily identified in ether of the scans. The surface wave is an un-required signal and will therefore be treated as noise, and will require filtering out prior to any additional analysis. The subject of signal filtering will be introduced and addressed later in the project.

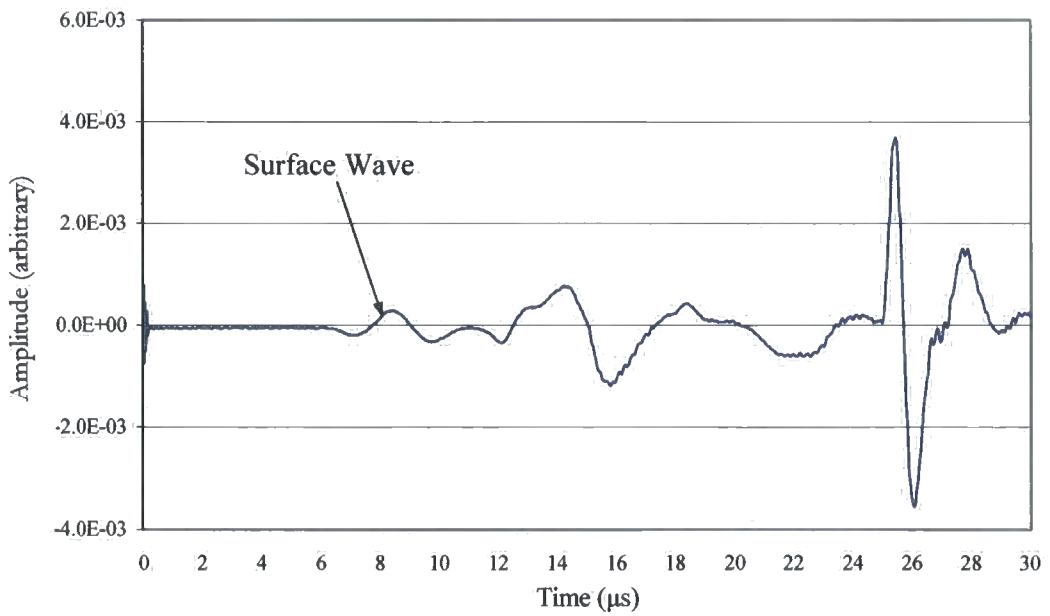

Figure 5.16. Signal received from transducer RX2

5.5. Further experiments to assess the use of passive receiver probes

5.5.1 Calibrated sample

As previously stated a billet of steel with known properties was required to eliminate as many variables as possible. It was decided that a V1 ultrasonic calibration block would be suitable for this purpose. The V1 calibration block is a certified defect free block of steel of known quality and surface finish and because of its commonality throughout the ultrasonic NDT community would be an aid to future experimental repeatability [13]. The V1 calibration block is manufactured to the following standards BS 2704:1978 DIN 54120 IIW (International Institute of Welding). It is machined from normalized low/medium carbon ferrite steel, to produce a fine homogeneous grain structure and has dimensional tolerances of ± 0.1 mm for the 25mm x 100mm x 300mm V1 (Figure 5.17.) Velocity tolerances are stated in the following standard, (EN 12223:2000) and declared 5920 ± 30 m/s for longitudinal waves. The specification states that it should be machined with a surface finish (R_a) value not greater than 0.8μm [13]. Surface roughness R_a is rated as the arithmetic average deviation of the material surface valleys and peaks [14].

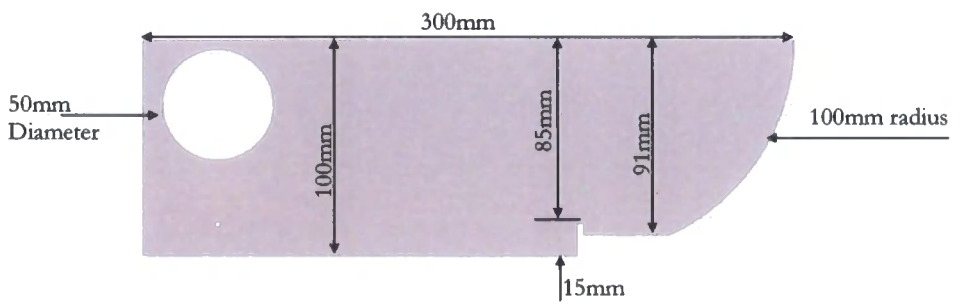

Figure 5.17. V1 ultrasonic calibration block

The series of experiments required the detection of a known defect; and for this the 2 mm wide notch that is 85 mm from the inspection surface of the V1 calibration block was deemed suitable to use as a pseudo defect. These experiments would be carried out with the probes in contact with the V1 block using the couplant stated in section 5.6. This series of experiments was also designed to evaluate the extent of the sound field that the transducers, adjacent to the transmitting transducer, could reliably detect and be repeated. The experimental results would then be assessed and compared the expected theoretical results.

The objective of this project is to evaluate an immersion system and therefore only compression waves are to be used. As compression waves have the greatest velocity of all the ultrasonic wave modes, it is only the area prior to the arrival of the signal received from the 100mm back-wall echo that is of concern. As an additional precaution, the experiments will concentrate on the signal that arrives prior to the back-wall echo, and employ a low pulse repetition frequency, to avoid stray echoes.

5.5.2. Pulse/Echo Scans

The aim of the first series of experiments is to evaluate what can be detected using the standard pulse/echo method at the stated probe separation distances. These tests would be used to simulate what the probes would have detected if this were an online static array system. This will also provide a point of reference for the materials examination when the additional probes are introduced.

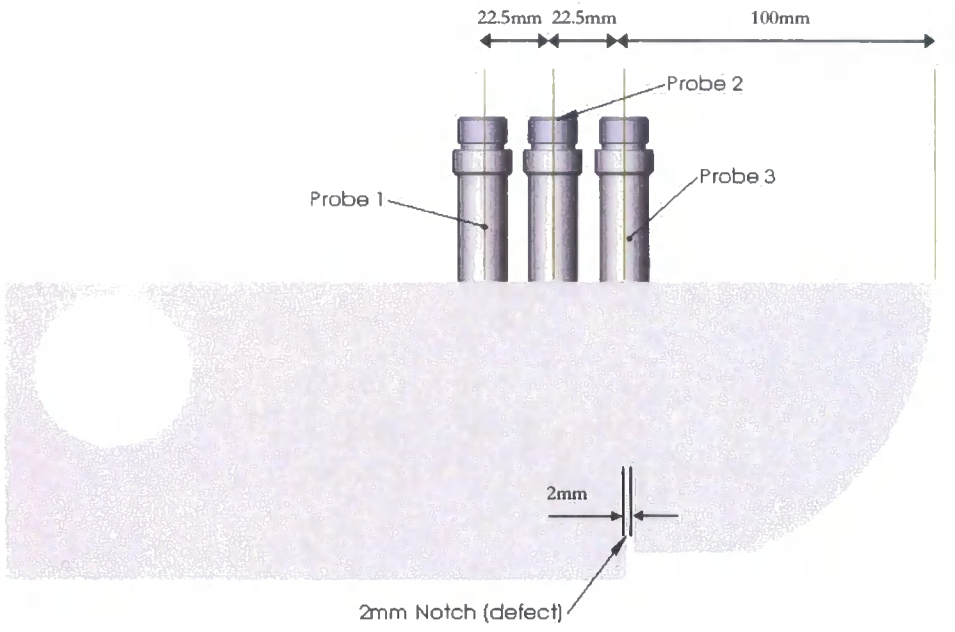

Figure 5.18. V1 calibration block with the probes in position

It was first necessary to determine the ultrasonic velocity within the V1 Calibration block. This velocity was measured using a single probe in pulse/echo mode as described by Webb and Wykes [15] and was calculated to be 5900ms^{-1} +/- 2% [16]. Each probe sequentially tested the calibration block in pulse/echo mode. The probes were positioned as shown in Figure 5.18. using the same 22.50 mm probe separation as used in the previous experiments carried out on the section of steel billet.

The A-scans that these examinations produced are displayed in Figures 5.19. 5.20. and 5.21. Figure 5.19. is of the full A-scan from the initial pulse to an arbitrary time after the back-wall echo, the remaining A-scans are of the back-wall echo and the portion of the signal directly preceding the back-wall echo, as this is the area where the notch would be displayed if detected.

Figure 5.19. shows the unprocessed pulse/echo A-scan from probe 3, which was positioned with 50% of the probe over the 100mm distance with the other 50% of the probe over the notch and the 91mm surface. Point 1 on the A-scan is the echo from the 2 mm notch at a distance of 85 mm from the transmitting probe. Point 2 is the echo from the 91 mm back-wall, and point 3 is the echo from the 100 mm back-wall.

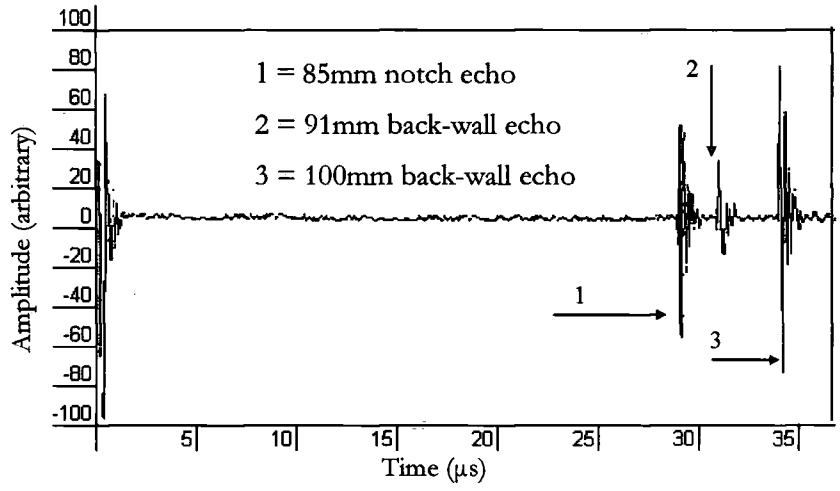

Figure 5.19. Trace of probe 3 in Pulse/echo mode

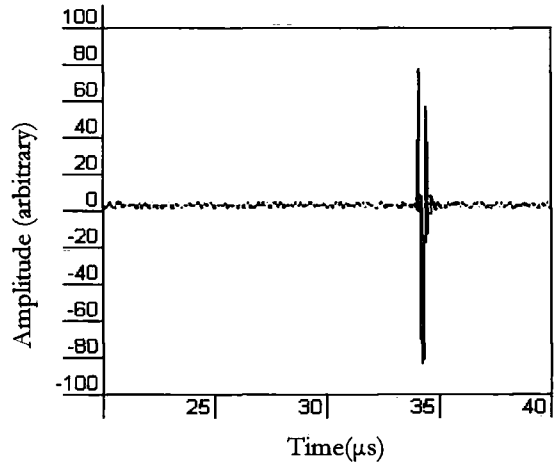

Figure 5.20. A-scan from Probe 2 with back-wall height set at 80%

This A-scan trace of the signal is clear and relatively easily interpreted with the notch having a SNR of 19.0dB. Because the features are located within the centre-line of the transducer, the signal is therefore reflected directly back to the same transducer. Figure 5.20. is the pulse/echo A-scan produced from the transducer at position 2 on the V1 block, and shows that the notch is indistinguishable above the background noise when the back-wall echo height is set at 80%.

Figure 5.21. is the A-scan trace from the transducer at position 2, with a increased signal gain of 60 dB and shows that the notch is evident, albeit with much-reduced amplitude. This increased dB gain is necessary because the transmitted signal striking the notch will be largely reflected away from the transmitting transducer. This increased gain is required due to the defect being 13 degrees from the centreline of the probe as shown in Figure 5.22. and outside the extremities of the main ultrasonic lobe, calculated using Equation 4.6. with the half beam width of this main lobe calculated at 8.36 degrees [8].

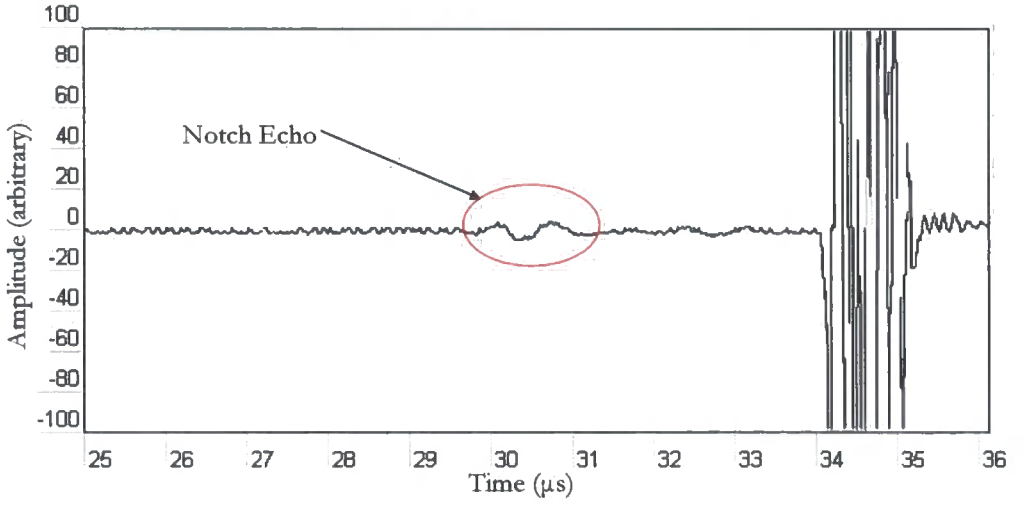

Figure 5.21. Trace from probe 2 with 60dB gain with the notch echo circled.

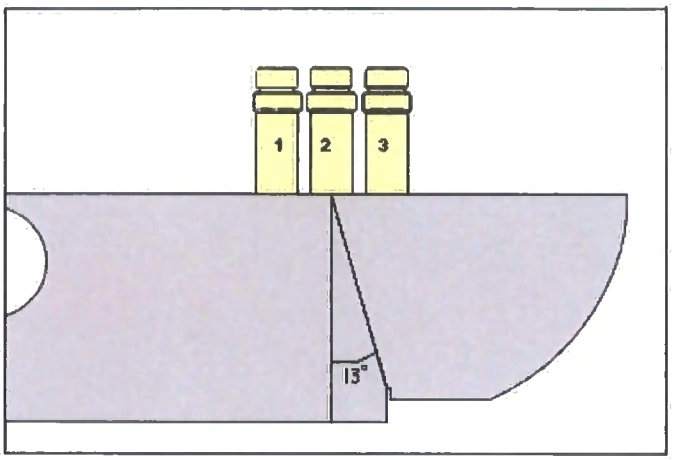

Figure 5.22. Drawing showing 13° angle to the notch

Figure 5.23. shows the pulse/echo A-scan for probe 1 with the back-wall echo set at 80% of the screen height, and the defect is indistinguishable above the level of the noise. The centre of probe 1 is at a 24-degree angle from the pseudo defect, as shown in Figure 5.24.

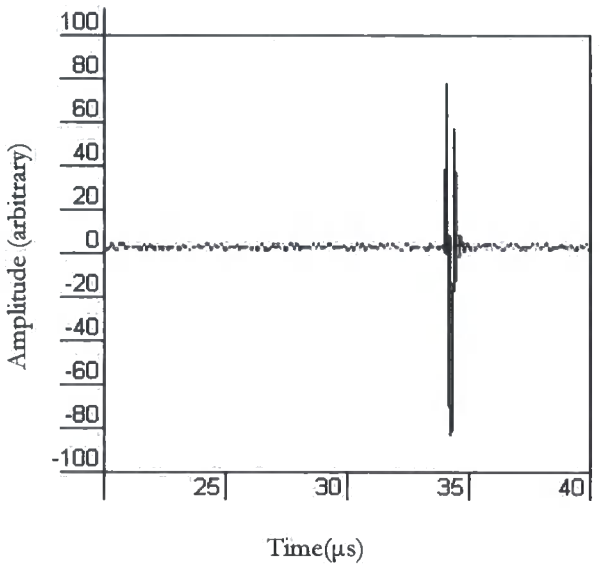

Figure 5.23. A-scan from Probe 1 with back-wall height set at 80%

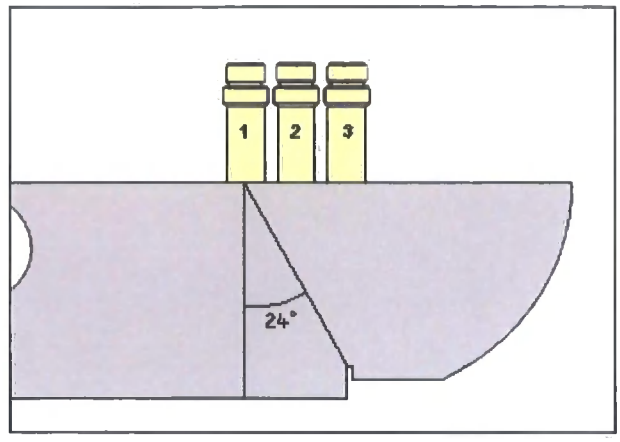

Figure 5.24. Drawing showing angle to the notch

The A-scan in Figure 5.25. shows that even with the high dB gain of 60dB used in the previous experiment (Figure 5.21.) the diffracted or non-specula reflected signal remains indistinguishable above the level of the noise. This is partially due to the defect being outside of the range of the diverging main ultrasonic lobe, and that the transmitted signal reflecting away from the transmitting transducer [17]. The other reason for the poor sensitivity of probe 1, is due to the high incidence angle, temporally smearing the signal which will also make the signal appear of lower frequency.

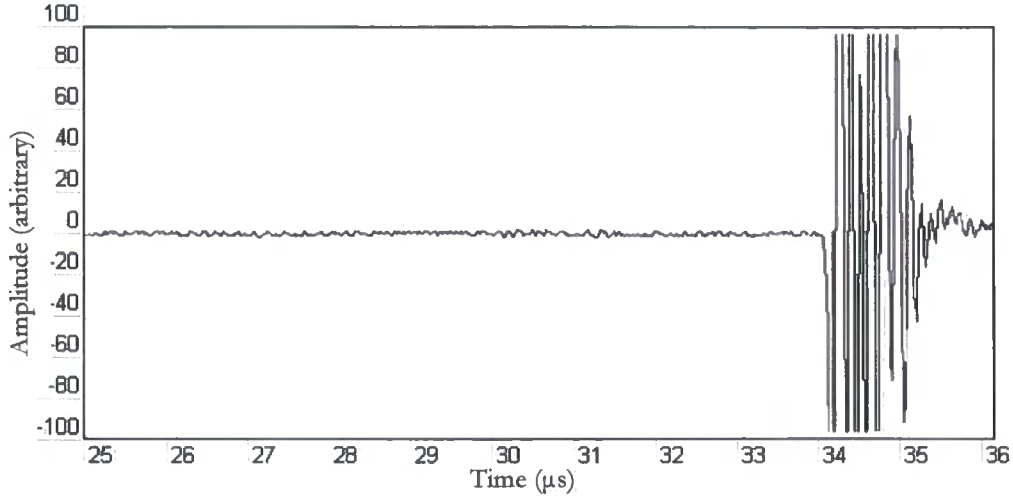

Figure 5.25. Trace from probe 1 with 60db gain showing no notch echo.

5.6. Multi-Probe Scan

The multi-probe apparatus consists of the three 5 MHz probes, placed in a linear arrangement with a fixed separation distance of 22.5 mm. The probes are at normal incidence to the upper surface of a V1 calibration block, as in the previous pulse/echo experiment (section 5.5.2.). Each probe in turn transmitted pulses, and the transit time of the returning pulses recorded. As discussed in the previously, the receiver probes electro-magnetically detected the initial pulse emitted from the transmitting probe, and this was utilised as the triggering signal for the oscilloscope [9].

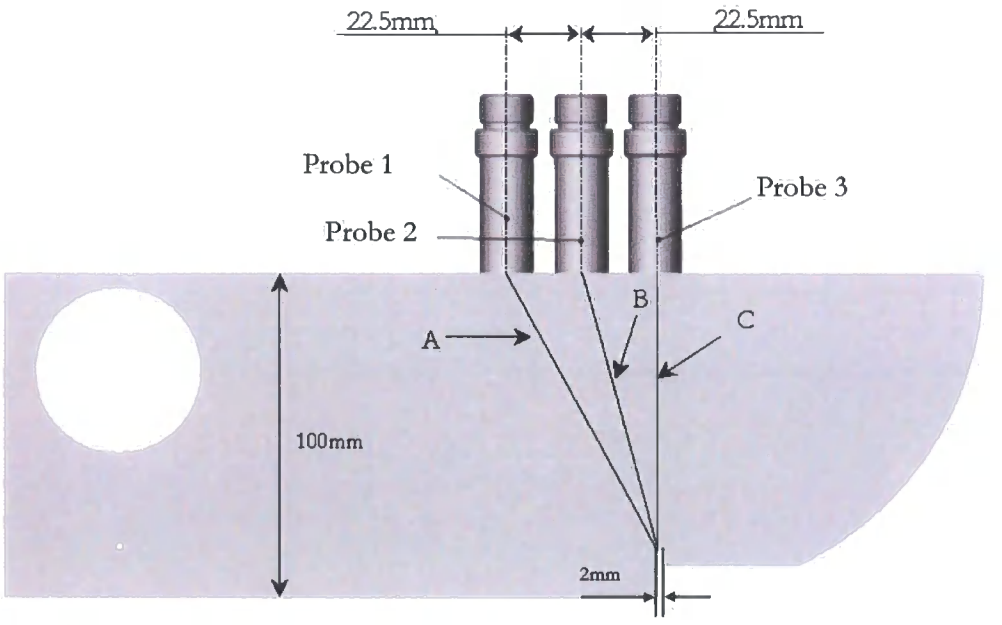

Figure 5.26. V1 calibration block showing signal paths and probe separation distances

The times between the transmitted and received signals were recorded, with a precision of 0.05μs, to determine the origin and path of the received signal. Figure 5.26. shows the geometry of the signal paths between the probes and the notch.

Table 5.2. displays these calculated times together with the calculated distances using 5900ms^{-1} for the speed of sound in steel and the relationship in equation 5.5.

$$\frac{\text{Distance}}{\text{Velocity}} = \text{Transit Time} \qquad [5.5.]$$

Table 5.2. Calculated signal time and distances to the notch at 5900m/sec

	A	**B**	**C**	**Backwall**
Distance, mm +/- 0.05mm	95.60mm	87.50mm	85.00mm	100.00mm
Time, μs +/-0.05 μs (@ 5900ms^{-1})	16.20μs	14.80μs	14.40μs	16.95μs

Table 5.3. Probe to probe times and distances form the notch (taken from Table 5.2.)

Signal Paths	**Theoretical (Calculated from distances)**	**Actual (from the A-scan graphs)**
A + B	31.10μs	30.95μs
A + C	30.60μs	30.40μs
B + C	29.20μs	29.20μs

The measured transit times are evaluated from the A-scans, using the time taken from the initial pulse to the point of first significant increase in amplitude. The theoretical times taken for a signal to travel the shortest path between the probes via the pseudo defect are shown in Table 5.3. together with the measured transit times of the signal. The tabled data sets show a strong time correlation, as the difference between the calculated and measured time show a less than 1% deviation.

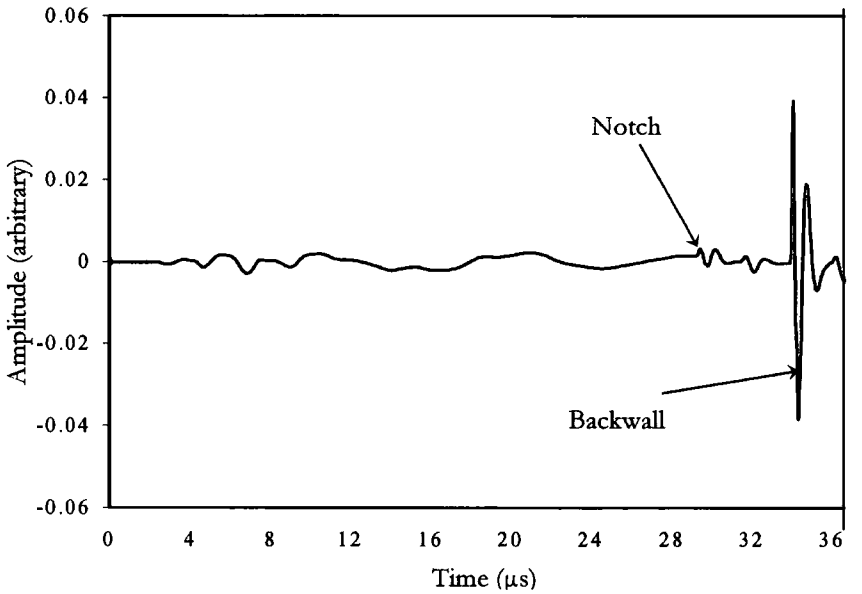

Figure 5.27. The A-scan show the signal received at probe 2, transmitted from probe 3, extending to 40μs after the initial pulse.

Figure 5.27. shows that the notch is detectable using the TX3 RX2 combination of probes, however the noise preceding the notch echo requires filtering to reduce its amplitude, and the SNR of the defect was calculated at –1.7dB using equation 4.19. After the back-wall echo it is not possible to distinguish between further echoes due to multiple internal reflections and mode conversion. Therefore, subsequent A-scan graphs display the only signal from the defect and first back-wall echo. The A-scans shown in Figure 5.28. was conducted using probes in positions 1 and 2. The A-scans are produced from the data received at the oscilloscope and transferred into Microsoft EXCEL.

The probes were used as alternate transmitter and receiver, however the displayed signals are very similar. This similarity is due to the signal paths being identical albeit in opposing directions. The most noticeable aspect of the A-scans displayed in Figure 5.28. is that the notch, circled in red, is visible considering the location of the two probes and there position relative to the notch. However it would prove to be difficult to automatically detect using signal thresholding techniques, due to the presence of low frequency noise and the amplitude of the signal.

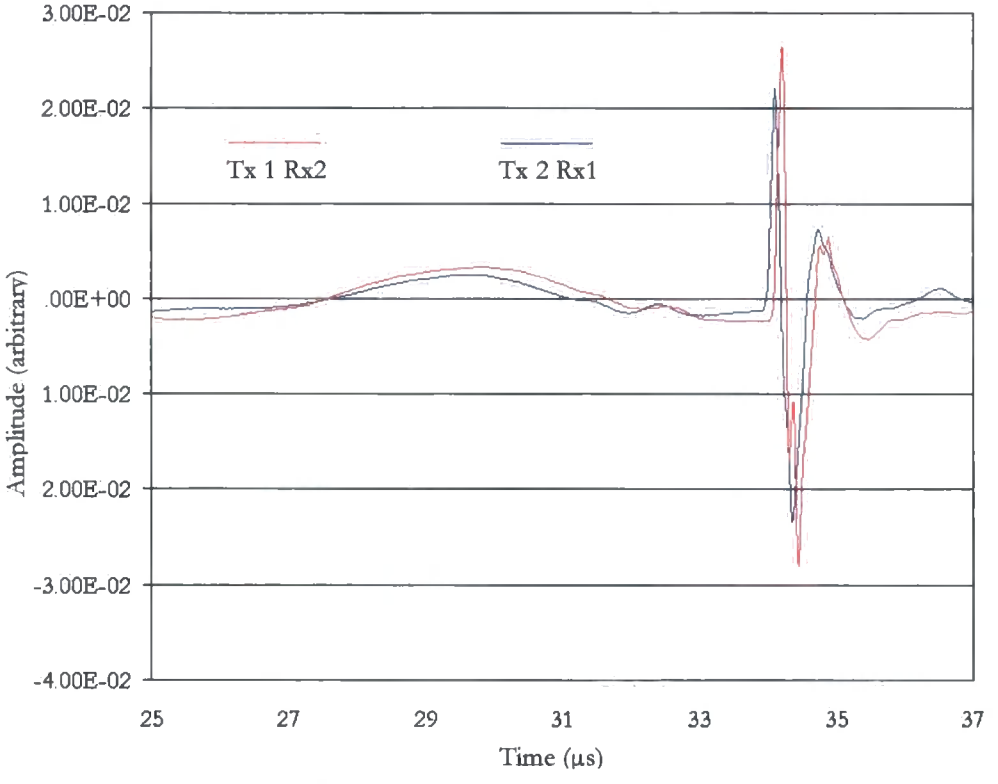

Figure 5.28. Tx 1 Rx2 and Tx 2 Rx1

The next stage of the experiment was conducted using the pair of probes with the greatest probe separation of 45mm. The notch echo, circled in red, is easily visible albeit a stretched and lower amplitude signal due to the smearing effect because of the angle of incidence.

There is also a signal of similar frequency, circled in green, following it and preceding the back-wall echo (Figures 5.29. and 5.30.) This second signal was initially dismissed as an anomaly, however the experiment was repeated numerous times and the second signal was a constant feature, and required investigation.

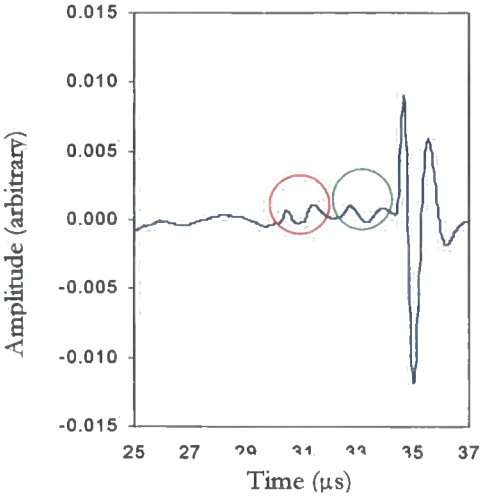

Figure 5.29. Tx-3 Rx-1

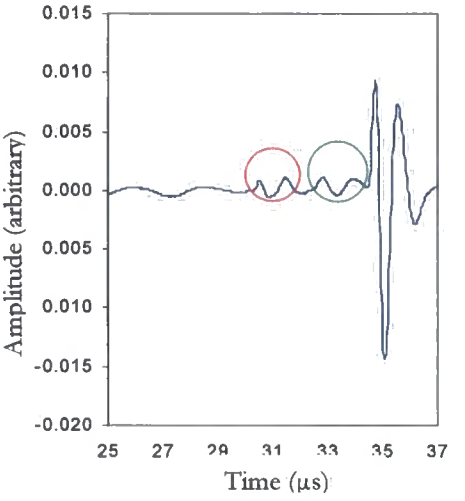

Figure 5.30. Tx-1 Rx-3

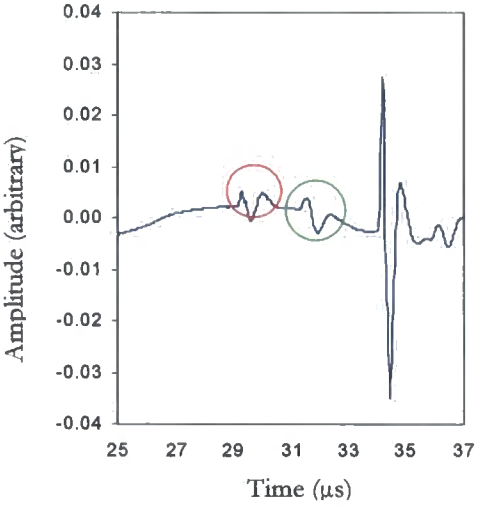

Figure 5.31. Tx-2 Rx-3

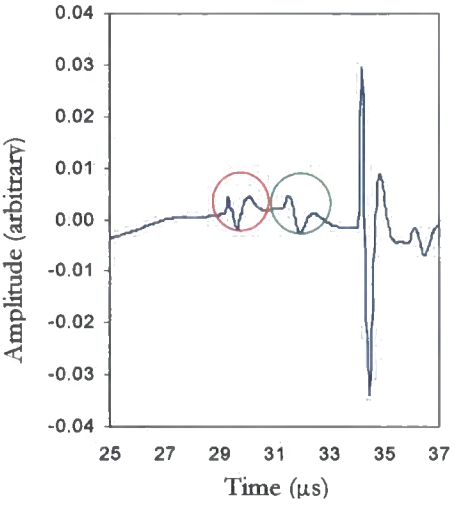

Figure 5.32. Tx-3 Rx-2

Figures 5.31. and 5.32. show the A-scans for the probes in positions 2 and 3 on the V1 calibration block. The signal from the notch is stronger and more readily identifiable as a 5 MHz signal than the previous series of probe pairings. This is due to the probes being both closer to the notch and that the notch lies closer to the centreline of the main ultrasonic lobe.

The A-scans also indicate the presence the second echo signal and again it is similar in frequency and amplitude as the notch echo signal. It was decided that this signal required additional investigation, this was conducted using several different methods and this is explained in the next section.

5.6.1 Spurious Echo Investigation

Certain assumptions were made based upon the previous experimental results, in that the ultrasonic wave was diffracting from the corner of the notch. However there are two signals present prior to the arrival of first back-wall echo. This second signal is present on all of the experimental results from the V1 calibration block that has the notch signal, and this section sets out to investigate the source of that second spurious signal. Speculation as to the source of the second signal gave four principle areas of investigation, these were:

1. Echo from the 91mm back-wall?
2. Mode converted echo from the near side of the notch?
3. Creep wave from the near side of the notch traversing along the surface of the notch then diffracting from the far side?
4. Sidewall reflected echo after diffraction from the notch?

The first stage of the investigation was to gain accurate data on the spurious echo. This was achieved by re-examining the data collected for the previous experiment on the V1 block, but with attention focused on the notch and spurious signal.

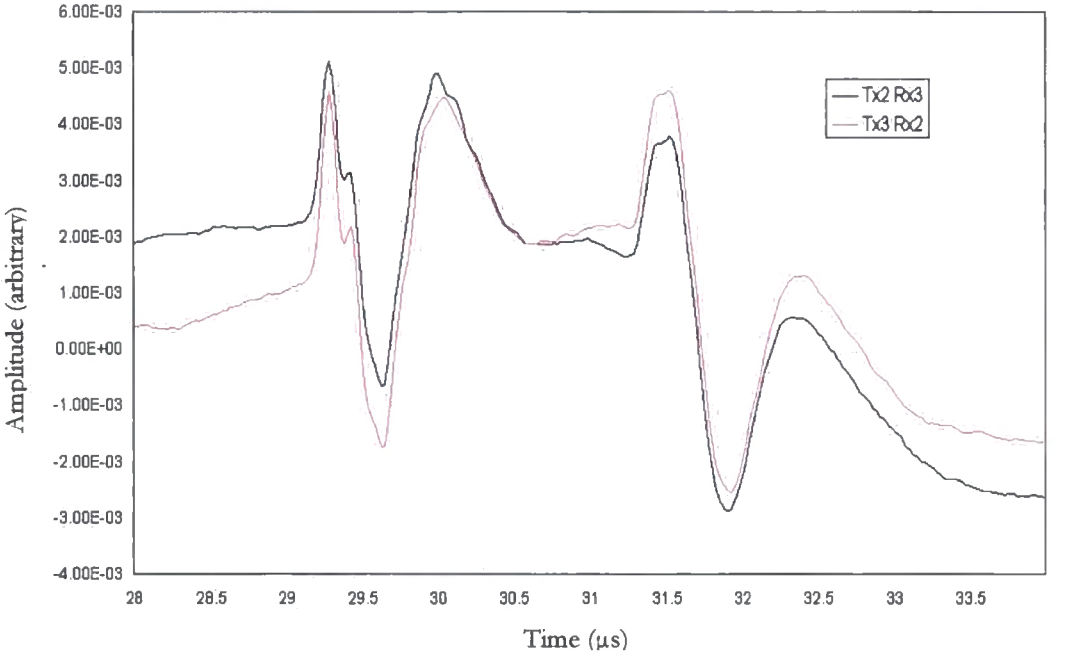

Figure 5.33. Graph using probes in positions 2 and 3

The experiments were repeated several times to ensure consistence in the readings, Figure 5.33. shows the signal received using probes 2 and 3 as alternate transmitter and receiver. As expected because the signal paths are over the same distance, the signal arrival times shown in this graph are identical.

This process was conducted using the other two pairs of probes (1 & 2 and 1 & 3) and the relevant graphs are displayed in Figures 5.34. and 5.35. showing a slight (0.1μs) time shift The collated signals were averaged and the results are displayed along with the calculated distances in Table 5.4.

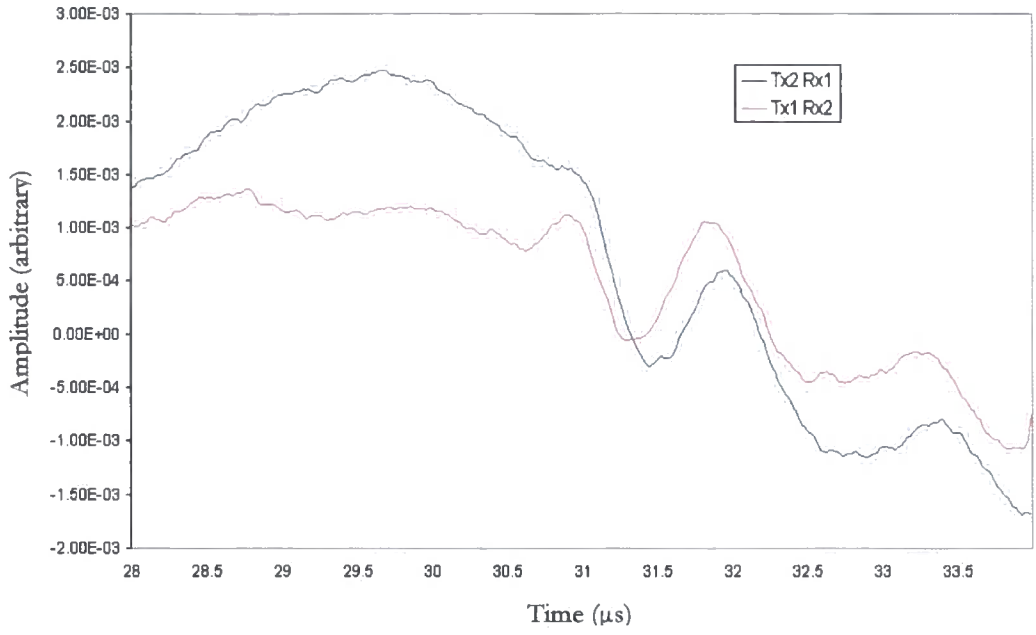

Figure 5.34. Graph using probes in positions 1 and 2

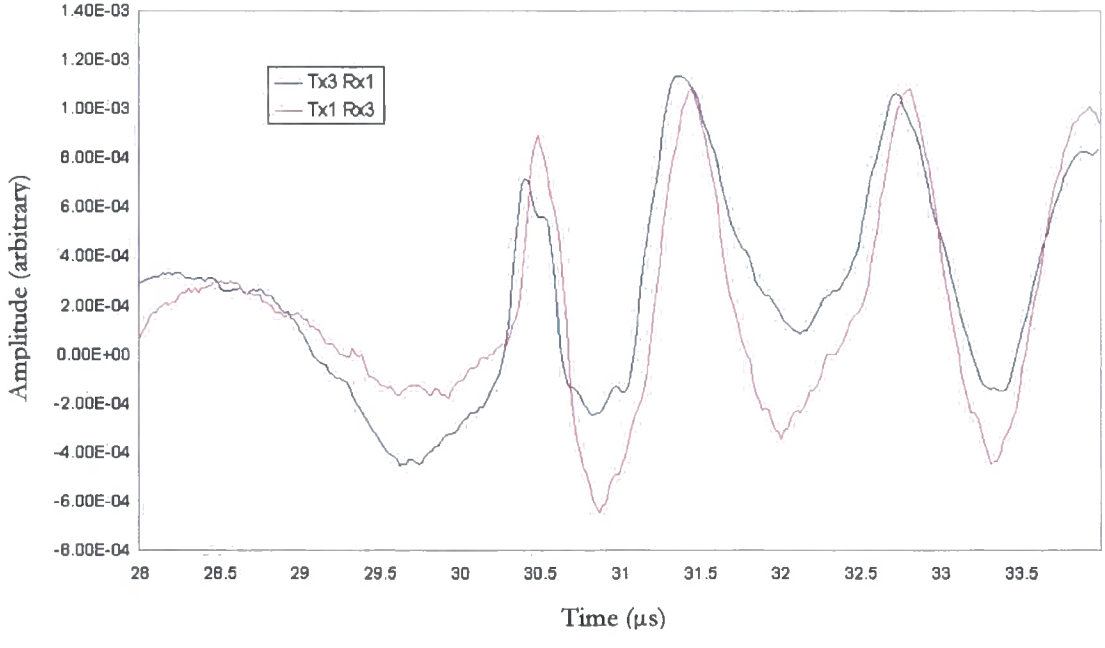

Figure 5.35. Graph using probes in positions 1 and 3

Table 5.4. Signal times and calculated distances for second signal

Probe pairs	Time μs +/-0.05 μs	Distance mm +/-0.05 mm
2 & 3	31.30	184.67
1 & 2	33.00	194.70
1 & 3	32.40	191.16

A method was required to evaluate the signal transit distances recorded in Table 5.4. and their possible paths. Kuo et.al. (1998) describe several methods of using time ellipses as a way of locating the tip of surface breaking cracks [18]. Their method was employed on surface breaking cracks on the inspected surface of the component, however the method could be adapted for a crack in this case the notch, on the reverse side of the component. The equations, 5.6. and 5.7., were used to calculate the ellipse of the spurious signal, with the ellipses being plotted against the V1 calibration block in Figure 5.36.

[5.6.]

$$\text{Vertical Distance from Probe Centres} = \sqrt{\left(\frac{\text{Signal Distance}}{2}\right)^2 - \left(\frac{\text{Probe Separation}}{2}\right)^2}$$

[5.7.]

$$\text{Horizontal Distance from Probe Centres} = \frac{\text{Signal Distance} - \frac{\text{Probe Separation}}{2}}{2}$$

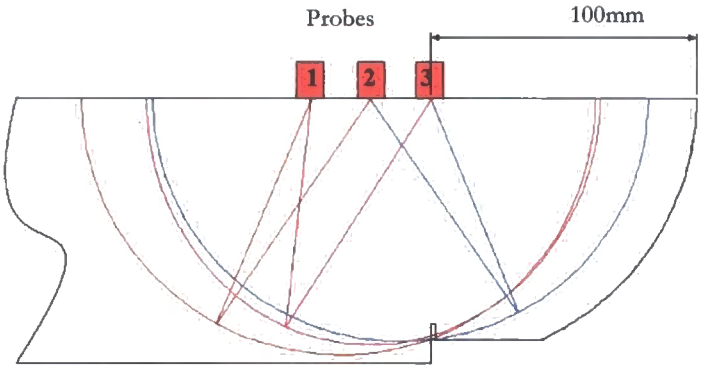

Figure 5.36. Drawing of spurious signal ellipses plotted against the V1 block

The ellipse test proved inconclusive as to the source of the spurious signal, however it did eliminate the possibility of the signal coming from the 91mm back-wall. This is because the signal times are not long enough and regardless of which pair of probes was transmitting or receiving, the signal would be speculatively reflected away from the receiver. The timings also show that the spurious echo signal could not be a mode-converted signal as the time calculation shown in Figure 5.36. and was conducted using the pair of probes that yield the clearest signals, probes 2 and 3. The velocity of the transverse wave was taken as 3200 m/sec. in steel [5].

Table 5.5. Longitudinal and transverse wave transit times for signal paths C & B

Signal path distance taken from Figure 5.9. (+/- 0.05mm)	Longitudinal wave @ 5900 m/sec (+/-0.05 μs)	Transverse wave @ 3200 m/sec (+/-0.05 μs)
(C.) 85.00mm	14.40μs	26.56μs
(B.) 87.90mm	14.90μs	27.69μs

$$\textit{Transit time} = C_T + B_L = 26.56 + 14.90 = 41.46\mu s \quad [5.8.]$$

$$\textit{Transit time} = C_L + B_T = 14.40 + 27.69 = 42.09\mu s \quad [5.9.]$$

It be seen from the transit times calculated in equations 5.8. and 5.9. the spurious signal is not a longitudinal wave, mode converted at the notch into a transverse wave. The time ellipses also show that the spurious echo is not a creep wave from the near side of the notch, traversing along the surface of the notch then diffracting from the far side to a receiver. This is because despite its name, a creep wave travels at the same velocity as its generating wave [6], in this case a compression wave. However a compression wave requires 0.34μs and a shear wave 0.63μs to travel the 2mm width of notch. This amount of time constitutes 1-2% of the total transit time and is within the anticipated margin of error and therefore additional tests are required.

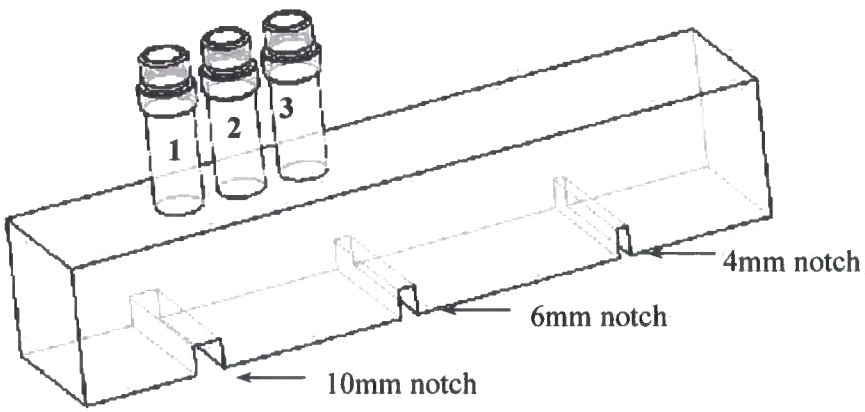

Figure 5.37. Line drawing of the experimental set-up including the transducers in position for examination of the 10mm notch

To investigate this a series of experiments were designed using a 50mm square section steel block containing 3 milled slots to a depth of 10mm and widths of 4mm, 6mm, and 10mm. The 10mm wide slot was initially used to consider if a creep wave was present on the top surface of the slot. The drawing (Figure 5.37.) shows the set-up with the probes in position to interrogate the 10mm slot area, with probe 1 directly over the edge of the notch. The experiment is similar in execution to that of the previous experiment so that the results are coherent and easier to interpret. The probes were positioned in the same linear relationship as previous experiment and on the centreline of the block.

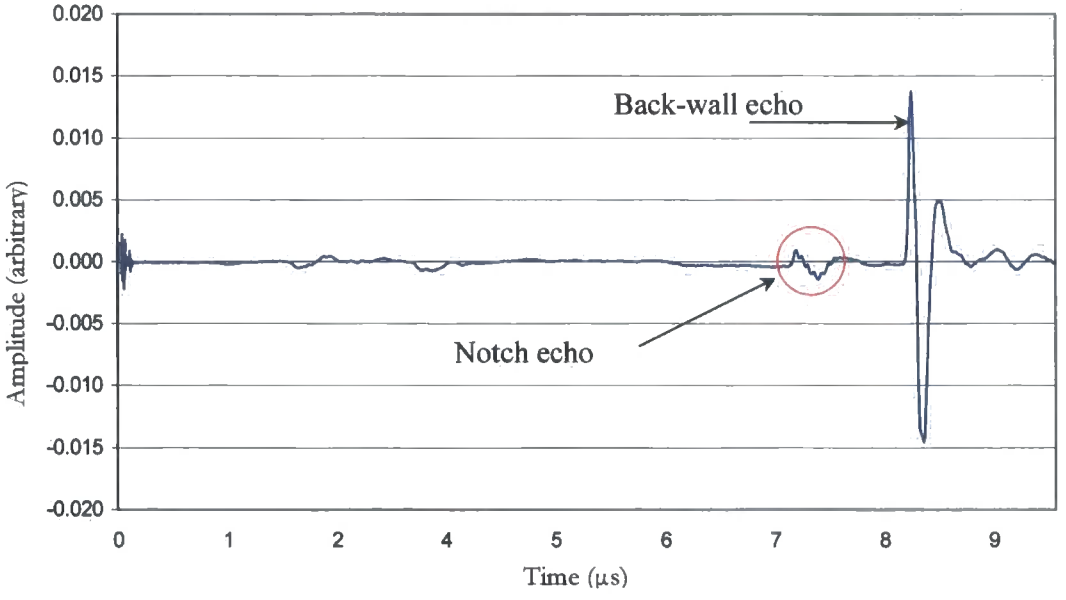

Figure 5.38. A-scan trace of signal transmitted from probe 1 and received at probe 2

Figure 5.38. shows the notch clearly visible circled in red, preceding that of the back-wall echo. This test procedure was conducted several times with the same result, and as can be seen from the A-scan, there is no second echo, following the notch.

As there is no second echo visible on the A-scan Figure 5.38. and the previous experiment indicated that the spurious echo was not due to a creep wave, the assumption was made that this was not the signals source.

However that the signal did not re-occur in a block 50mm in width but did occur in the V1 block which is 25mm in width, the presumption was made that the spurious echo was from side wall reflections. To verify this theory an A-scan was completed using the two probes with 22.5mm separation on the V1 block looking only at the 100mm backwall. As can be seen from A-scan (Figure 5.39.) there is a signal closely following the backwall echo that is the back wall echo, reflected from the sidewalls causing the signal delay.

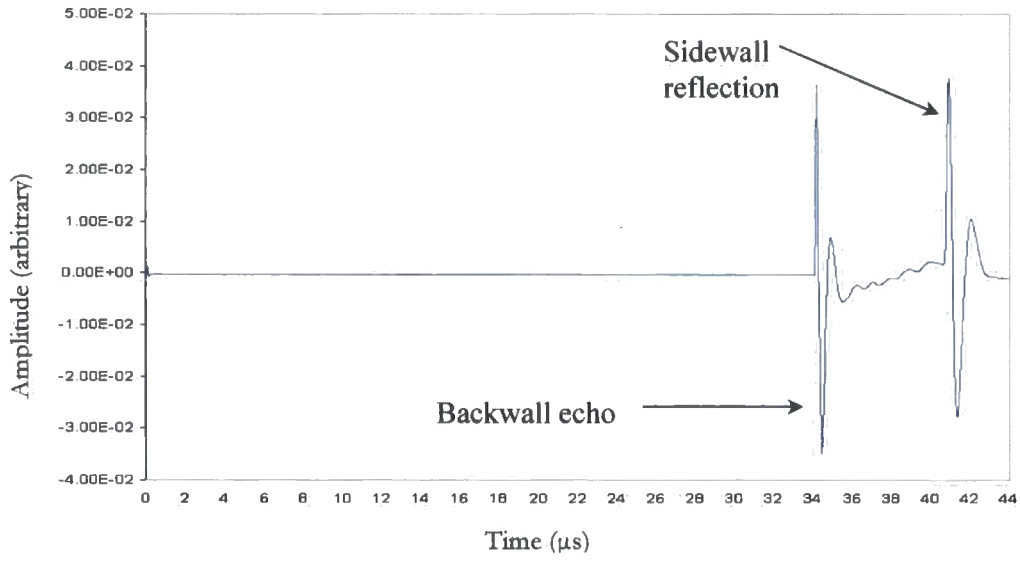

Figure 5.39. Signal showing 100mm backwall echo and the sidewall reflected delayed signal

5.7. Conclusion

The measurement system was characterised and suitable operating conditions were chosen, resulting in 5MHz frequency setting being employed for the duration of this project.

The test on the steel billet had proved inconclusive due partly to the fact that the defect was large and obscured the back-wall echo signal. It was suggested that the project progressed to an immersion test on the billet, with the additional probes in position. However it was decided that it was premature to move the project in this direction at this stage, as it added additional variables to the experiment. Because of the potential confusing signal traces, it was decided to eliminate as many of the variables as possible. The subsequent series of experiments was carried out on a subject containing a simple known target. The options considered included a section of billet with a flat-bottomed hole, as the target defect, as this method is widely employed within the NDT industry [6]. However as the quality of the material could not be assured, it was decided to use a V1 calibration block, as the steel was of certified quality (BS 2704:1978). The 2mm notch could be utilized as a pseudo defect, and as this was a standard calibration tool, it would aid repeatability.

The next section of the Chapter was initiated to evaluate the potential within the probe array to reliably detect a known defect. For this the 2mm wide notch that is 85mm from the inspection surface of the V1 calibration block was used as a pseudo defect.

The aim of this series of experiments was to evaluate what features within the V1 block the individual probes, while operating in standard pulse/echo configuration, could be discerned. The experiment was simulating what the probes would detect if this were an online system and to provide a point of reference for future experiments.

The first set of experiments using the V1 calibration block showed that the probe at position 3, could detect the notch and the back-wall echoes from both the 91mm back-wall and the 100mm back-wall. This was as expected because the probe was positioned directly above these features and therefore able to receive the directly reflected signal. That the probe in position 2 also picked up a returning signal from the 2mm notch however was unexpected. At 13 degrees away from the centreline of maximum intensity, the notch was outside of the stated theoretical extremities of the main ultrasonic lobe. This could also account for the large increase in signal gain required to detect the notch (Figure 5.21. and 5.25.). That the signal was detected and identified requires some form of non-specular reflection, the probable method of which is diffraction, as diffuse reflection requires a rough surface and the boundary variations to be of the same order of magnitude or larger than the ultrasound wavelength being used [19].

For the notch to be detected at the probe in position 2 using an automated system would prove problematic to threshold the defect due to low signal to noise ratio. Also operating at the required elevated levels of signal gain would lead to an increase in false alarms.

Section 5.5.3. was concerned with the spurious second echo and set out to investigate its source. This second signal was present on all of the experimental results from the V1 calibration block, and could not be ignored or dismissed as an anomaly. The procedure to discover the signals source proved to be longer and more involved than initially anticipated. However the evaluation showed that the signal was due to internal reflections owing to the V1 block being relatively narrow in profile and interacting with the diverging ultrasonic beam.

The investigation into the spurious signal, introduced a technique devised by Kuo et. al. (1998) [18] for measuring the depth of surface breaking cracks on the inspection surface, using pairs of half ellipses. This half ellipse method was adapted for use on the back surface of the V1 block, and was used successfully to evaluate the source of the echo. In the next chapter, the technique will be evaluated further and in detail.

This initial experimental work served to layout the path of the next series of experiments. These experiments will be conducted using the experience and understanding taken from this work, in that care must be taken as to the source of the echo signal and the half ellipse technique can be employed for echolocation.

5.8. References:

1. Chen, C.-T., *Digital Signal Processing; Spectral Computation & Filter Design.* 2001, New York, U.S.A.: Oxford University Press.

2. Soh, H.T., et al., *Silicon micromachined ultrasonic immersion transducers.* Journal of American Institute of Physics, 1996. **69**(24): p. 3674-3676.

3. Ladabaum, I., et al. *Silicon Substrate Ringing in Microfabricated Ultrasonic Transducers.* in *IEEE Ultrasonics Symposuim.* 2000. San Juan, Puerto Rico.. p.943-946

4. Payne, P.A., *Ultrasonic Transducers: Design, Construction and Applications.* International Journal of Materials, 1994. **9**: p. 403-427.

5. Krautkrämer, J. and H. Krautkrämer, *Ultrasonic Testing of Materials.* 1990, New York: Springer-Verlag. 677.

6. Birks, A.S. and R.E. Green Jr., *Ultrasonic Testing.* 2nd ed. Nondestructive Testing Handbook, ed. P. McIntire. Vol. 7. 1991, Baltimore, Maryland, U.S.A.: American Society for Nondestructive Testing. 893.

7. Wolfram, A. *Automated ultrasonic inspection.* in *15th WCNDT conference.* 2000. Rome, Italy: www.karldeutsch.de/PDF/Automated_UT_inspection_May00.PDF.

8. Hellier, C.J., *Handbook of Nondestructive Evaluation.* 2001, New York, U.S.A.: McGraw-Hill.

9. Brooks, D., *Signal Integrity Issues and Printed Circuit Board Design.* 2003, New Jersey: Prentice Hall.

10. Kingsbury, R.F., *Elements of Physics.* 1965, Princeton, New Jersey, U.S.A.: D. Van Nostrand Co. Inc.

11. Halmshaw, R., *Mathematics and Formulae in NDT.* 2nd ed. 1993, Northampton: The British Institute of Non-Destructive Testing.

12. Sathish, S., et al., *Local surface skimming longitudinal wave velocity and residual stress mapping.* The Journal of the Acoustical Society of America, 2004. **115**(1): p. 165-171.

13. Markucic, D., et al. *Quality Requirements for Ultrasonic Testing Calibration Blocks.* in *8th ECNDT.* 2003. Barcelona, Spain.

14. Pohanish, D. and C. McCauley, *Machinery's Handbook Pocket Companion: A Reference Book for the Mechanical Engineer.* 2000, New York, USA: Industrial Press Inc. 317.

15. Webb, P. and C. Wykes, *Suppression of second-time-around echoes in high firing rate ultrasonic transducers.* NDT & E International, 1995. **28**(2): p. 89-93.

16. Kumar, Y. and A. Kumar. *The Calibration of Ultrasonic Flaw Detectors.* in *NDE 2002 Indian Society for Non-Destructive Testing.* 2002. Chennai (Madras), India.

17. Ben Amor, M., et al., *Influence of attenuation on the behavior of refracted elastic waves at the interface between anisotropic media.* Ultrasonics, 2002. **40**: p. 561-565.

18. Kuo, M.K., et al., *Locating the crack tip of a surface-breaking crack. Part I. Line crack.* Ultrasonics, 1998. **36**: p. 803-811.

19. Charlesworth, J.P. and J.A.G. Temple, *Engineering Applications of Ultrasonic Time-of-Flight Diffraction.* Second Edition ed. Ultrasonic Inspection in Engineering, ed. M.J. Whittle. 2002, Baldock: Research Studies Press Ltd. 254.

Chapter 6.

Time Ellipse Defect Location

6.1. Introduction

This chapter further explores the potential for using the ellipse method, introduced in the previous chapter. In the previous chapter, the factors affecting the ellipse technique were investigated. In this section, the technique will be evaluated as a tool for locating the notch of the V1 calibration block. This sample was chosen as the material and propagation properties have already been characterised.

The method used during this series of experiments differs from the one utilised by Kuo et.al. (1998) [1] who employed the technique for the location of nearside surface breaking cracks. In their paper, the basic principle was to align the source and the receivers geometrically on either side of the surface-breaking cracks, which is similar to time-of-flight diffraction (TOFD), whereas the probes in this experiment would be positioned either above the defect or to one side of the defect.

The ellipse scans would be conducted using the identical probe configuration as all of the previous experiments i.e. 22.5mm and 45mm. Charlesworth et.al. (2002) during their study of the ToFD technique, advocated the use of multi-probe scans and specifically the use of different probe separations as a method for ensuring reliable detection [5].

6.2. Ellipse Equations

An ellipse has two axes of symmetry, the Major axis 2_a and the Minor axis 2_b [2]. In this experiment, each transmitter receiver pair was considered as the twin foci of the ellipse (F_1 & F_2).

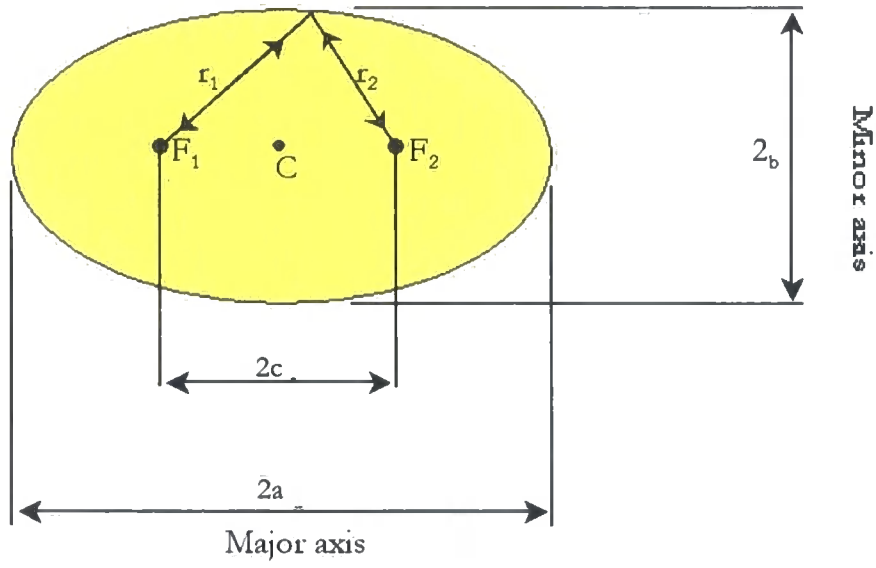

Figure 6.1. Diagram of the ellipse dimensional relationships

With the distance between the probes (2c) and half distance between the probe centres being the centre of the ellipse (C). The signal transit time between the probe pair of which has diffracted from the defect was considered as the radii (r_1+ r_2).

The following equations (Eq.6.1. and Eq.6.2.) provide the Minor and Major axis of the ellipse.

Minor Axis

$$2_b = 2\sqrt{\left(\frac{r_1 + r_2}{2}\right)^2 - \left(\frac{2c}{2}\right)^2} \qquad [6.1.]$$

Major Axis

$$2a = r_1 + r_2 \qquad [6.2.]$$

6.3. Ellipse Calculations

As discussed in the previous chapter (Chapter 7.3.), the probes are at normal incidence to the upper surface of a V1 calibration block and each probe sequentially transmitted pulses. The experiment was repeated several times and the average transit time of the signal returning to the two passive probes was recorded. The sampling frequency employed was 50MHz (20ns/point) to give accurate reproduction of the waveform [3]. This frequency was also sufficiently above that of the signal frequency of 5MHz, to avoid the problems of signal aliasing [4].

Table 6.1. displays the average of recorded times together with the distances calculated using 5900 m/s for the speed of sound in steel and the relationship in Equation 5.3.

Table 6.1 Signal path distance calculated at 5900m/sec

Signal path	Distance (mm) +/-0.05mm	Time (μs) +/-0.05μs
A & B	182.60	30.95
A & C	179.40	30.40
B & C	172.30	29.20

The calculated signal path distances were substituted into the two ellipse equations (Equation 6.1 and 6.2.) Using the dimensions calculated from the equations, ellipses were drawn and plotted against a drawing of the V1 calibration block.

Probes 1 and 2, signal path A-B.

$$\text{Minor Axis } 2_b = 2\sqrt{\left(\frac{182.61}{2}\right)^2 - \left(\frac{22.5}{2}\right)^2} \qquad [6.3.]$$

$$\therefore b = 90.61\text{mm}$$

$$\text{Major Axis } 2_a = 91.30 + 91.30 = 182.60 \qquad [6.4.]$$

$$\therefore a = 91.30\,\text{mm}$$

Probes 2 and 3, signal path B-C.

$$\text{Minor Axis } 2_b = 2\sqrt{\left(\frac{172.28}{2}\right)^2 - \left(\frac{22.5}{2}\right)^2} \qquad [6.5.]$$

$$\therefore b = 85.40\text{mm}$$

$$\text{Major Axis } 2_a = 86.15 + 86.15 = 172.30 \qquad [6.6.]$$

$$\therefore a = 86.15\text{mm}$$

Probes 1 and 3, signal path A-C.

$$\text{Minor Axis } 2_b = 2\sqrt{\left(\frac{179.40}{2}\right)^2 - \left(\frac{45}{2}\right)^2} \qquad [6.7.]$$

$$\therefore b = 86.83\text{mm}$$

$$\text{Major Axis } 2_a = 89.70 + 89.70 = 179.40 \qquad [6.8.]$$

$$\therefore a = 89.70\text{mm}$$

The resultant plot (Figure 6.2.) shows that the intersection of the three ellipses generated from the three pairs of probes, located the 2mm wide notch within the V1 calibration block with an accuracy of +/-0.5% of the travelled signal distance.

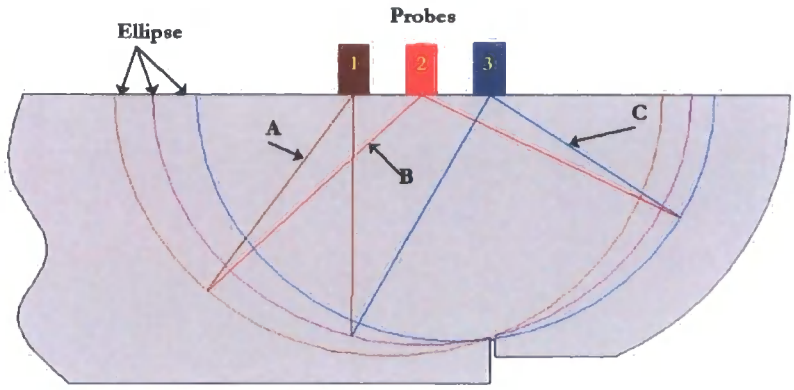

Figure 6.2. Drawing of ellipses plotted against the V1 block, showing signal paths

6.4. Conclusion

The first section of this chapter investigated the half ellipses as a geometric method of accurately locating a defect. Kuo et.al. (1998) had successfully employed the technique to size surface breaking cracks. The experimental work conducted using the ellipse method of geometric location described in this chapter shows that the technique was successfully adapted the to locate the defect on the bottom surface of the V1 calibration block. The use of three probes and the combination of signal paths provided data to locate the notch to an accuracy of +/-0.5%, using the intersection of the three ellipses. However, the weaker echo signals required a subjective approach in their time estimation. The next chapter will set out to address this problem with the application of DSP techniques to the signals.

This work was presented at the 30th Annual Review of Progress in Quantitative Non-destructive Evaluation (QNDE) July 27-August 1, 2003, held in Green Bay, Wisconsin U.S.A. Also a modified version of this work was published in the journal, Non-destructive Testing and Evaluation [6].

6.5. References

1. Kuo, M.K., T.R. Lin, P.L. Liu, and T.T. Wu, *Locating the crack tip of a surface-breaking crack. Part I. Line crack.* Ultrasonics, 1998. **36**: p. 803-811.

2. Stroud, K.A., *Mathematics for Engineering Technicians.* Vol. 2A, Practical Applications. 1981, Cheltenham, UK.: Stanley Thornes.

3. Fritsch, C., M. Parrilla, T. Sánchez, and O. Martínez, *Beamforming with a reduced sampling rate.* Ultrasonics, 2002. **40**: p. 599-604.

4. Chen, C.-T., *Digital Signal Processing.* 2001, New York: Oxford University Press, Inc. 440.

5. Charlesworth, J.P. and J.A.G. Temple, *Engineering Applications of Ultrasonic Time-of-Flight Diffraction.* Second Edition ed. Ultrasonic Inspection in Engineering, ed. M.J. Whittle. 2002, Baldock: Research Studies Press Ltd. 254.

6. Snowdon, P.C., S. Johnstone, and S. Dewey, *A 2D Static Ultrasonic Array of Passive Probes for Improved Probability of Detection.* Nondestructive Testing And Evaluation, 2003. **19**(3): p. 111-120.

Chapter 7.

Signal Echo Enhancement using DSP

7.1. Introduction

This chapter sets out to investigate and subsequently employ the most suitable digital signal filter to enhance the signal to noise ratio of the received ultrasonic signal. In previous chapters, the signal returning from the notch has been preceded by low frequency high amplitude noise. This has been identified using Equation 5.3. as a surface wave reflecting from the sides of the test material. It is however an un-required signal, and it will be treated as noise and filtered out, as this could cause problems with automated defect detection systems that rely upon signal thresholding, which requires the defect signal to be of greater amplitude than the ambient noise.

The MathWorks program, MATLAB®, is extensively used to apply several various signal filters in order to improve the signal to noise ratio (SNR). To obtain these results, the unprocessed signals were recorded using the digital oscilloscope with a sampling rate of 50M samples/sec (50MHz) as stated in Chapter 5., and transferred via Microsoft EXCEL digitally into MATLAB®.

The chapter will then progress and investigate the potential of combining the two techniques, that of ellipse geometry and the application of DSP to enhance the likelihood of detection of the defect within the V1 calibration block.

7.2. Digital Signal Processing

The discontinuity signals measured by an ultrasonic NDT system; include the effects of the measurement system, and are corrupted by different types of noise. According to Kazanavicius et.al. (2003), an A-scan signal may carry information on material properties and defects, but the information appears within, or together with, various guises of noise [2]. There is a complex interaction between the defect geometry, diffracted, mode converted waves and the back-scattered ultrasonic waves inside the test piece .

Current means of automated defect detection use various preset level gates within the flaw detector. The system is alerted when the amplitude level moves above or below the set threshold of the gate and is defined as monitor level or thresholding [3]. Much research has been done on ultrasonic signal processing, for more reliable and versatile signal processing techniques without a definitive solution [4].

It was decided to conduct the initial DSP filtering using the signal with the best signal to noise ratio (SNR) and with the most defined notch diffraction signal. The signals from the previous ellipse experiment were collated and transferred into MATLAB®.

These were examined and it was decided to use the signal from the probe pairing where the probe in position 3 was transmitting with the probe in position 2 receiving (Figure 7.1.). This signal had the most favourable SNR of -2dB calculated using the Equation 4.19.

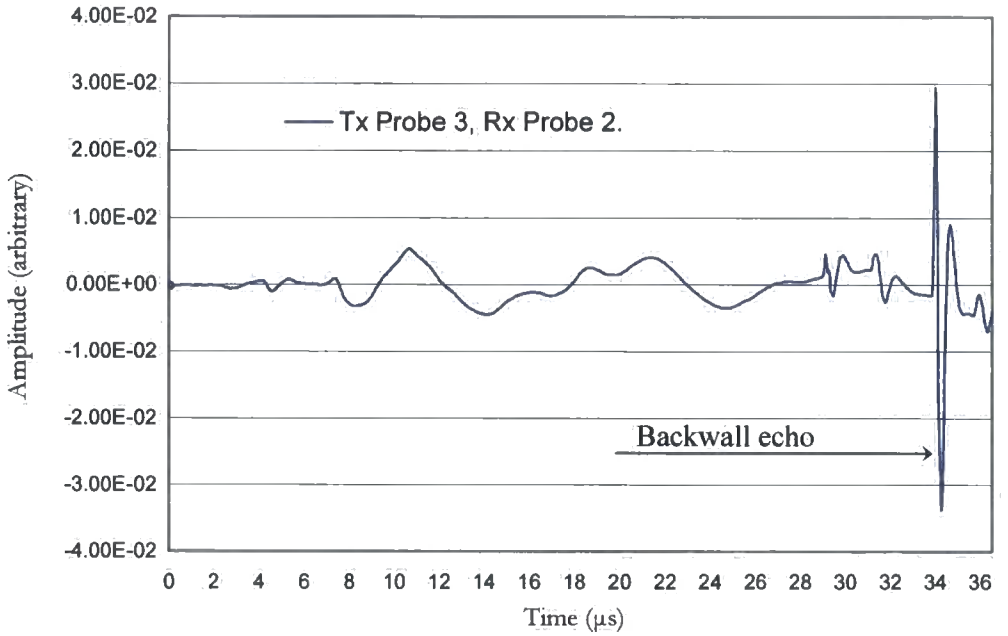

Figure 7.1. Graphical example of the signal transferred into MATLAB®

The filter design was completed, using the standard signal processing algorithms of the filter design and analysis tool (FDATool) and the signal processing toolbox (SPTool) within MATLAB®.

There are two primary types of digital filters used in DSP applications, the Finite Impulse Response (FIR) filter, and the Infinite Impulse Response (IIR) filter. The first digital filters applied during this experiment were FIR. These filters are mostly linear-phase; this refers to the condition where the phase response of the filter is a linear function of frequency. This consequently results in the delay through the filter being the same at all frequencies, however the filter does not cause phase distortion.

7.3. Cross-correlation Filtering

Several of the embedded algorithms were explored, with varying levels of success, however the one chosen gave greater consistency of results when applied to the signals received at the passive probe. The choice was made to design and use a matched filter to reduce the noisy signal. The cross-correlation or matched filter is used extensively in pattern recognition and signal detection [5]. The term cross-correlation comes from statistics, and what is defined here is more appropriately called a sample cross-correlation filter [6]. This is achieved by projecting one signal onto another as a means of measuring how much of the second signal is present in the first.

Several approaches to designing the signal for the filter were considered, these included;

- Designing the ideal 5MHz signal using the MATLAB® programme
- Using the defect echo
- Using a backwall echo

The first option of designing the ideal signal was dismissed as Kazanavicius et.al.(2003) suggest that the approach of signal processing should be conducted using the noisy signal itself to construct the signal processing method [2]. The backwall signal however, is for most pulse/echo inspections the main reflector and therefore easily obtained, and this was the signal used in the development of the filter.

A typical backwall echo was isolated from one of the many signals similar to that in Figure 7.2., and imported digitally into MATLAB® and evaluated using various algorithms.

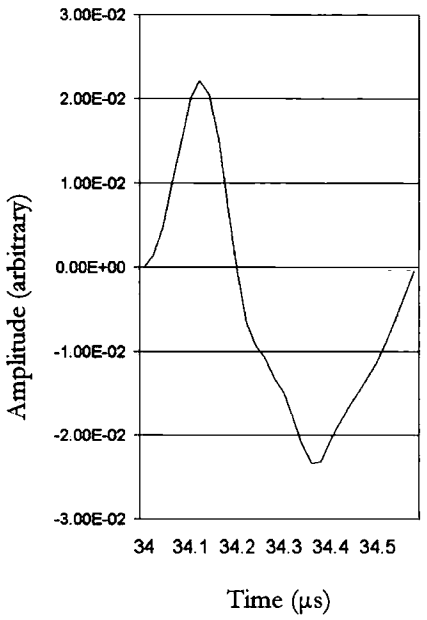

Figure 7.2. Isolated backwall echo signal

After one cycle through the filter the signal showed little improvement over the input signal. It was decided to undertake a multi-stage filter using the original sinusoidal correlation signal but using the product of the previous filtering operation. The product of the second filtering cycle was improved, in that the signal to noise ratio had been greatly enhanced. However, it was decided to repeat the procedure until the noise preceding the notch signal was of sufficiently low amplitude that the signal could be reliably and repeatedly threshholded.

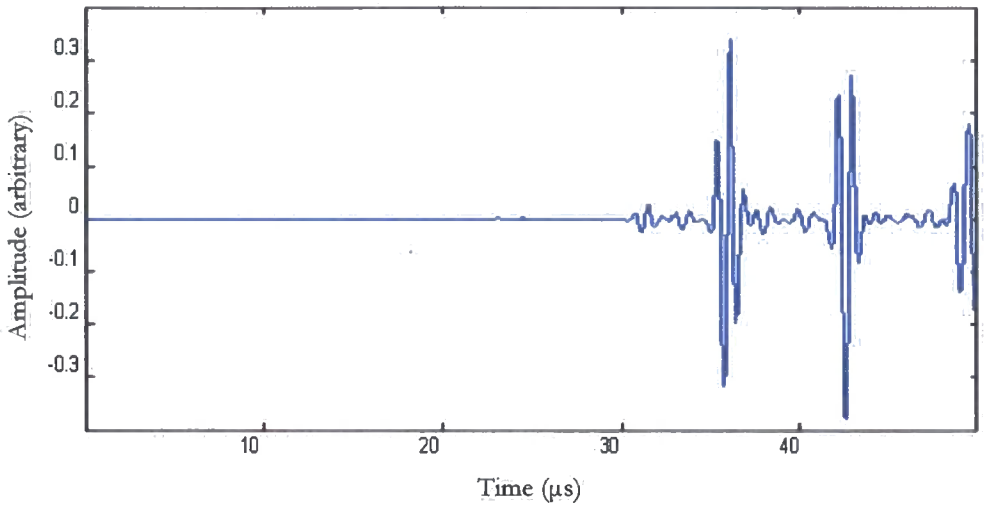

Figure 7.3. Signal after fourth filter cycle

As previously stated, because of the way that FIR filters operate, they cause a delay in the signal, and therefore every additional filtering operation causes additional delay. This signal required an additional two cycles to give the result in Figure 7.3., totalling four filter cycles. The signal to noise ratio was then re-calculated using the equation 4.19. for the filtered signal at 12.0dB.

The two signals were superimposed upon each other with the unfiltered signal shown in blue and the filtered signal in red, as in Figure 7.4. showing a time delay, estimated at 2μs, equating to a distance in the material of 12mm. The signal time is taken from the first point of significant deviation, as shown in Figure 7.8. This time delay is only of relevance to the accuracy of location of a defect, but not in detection of a defect.

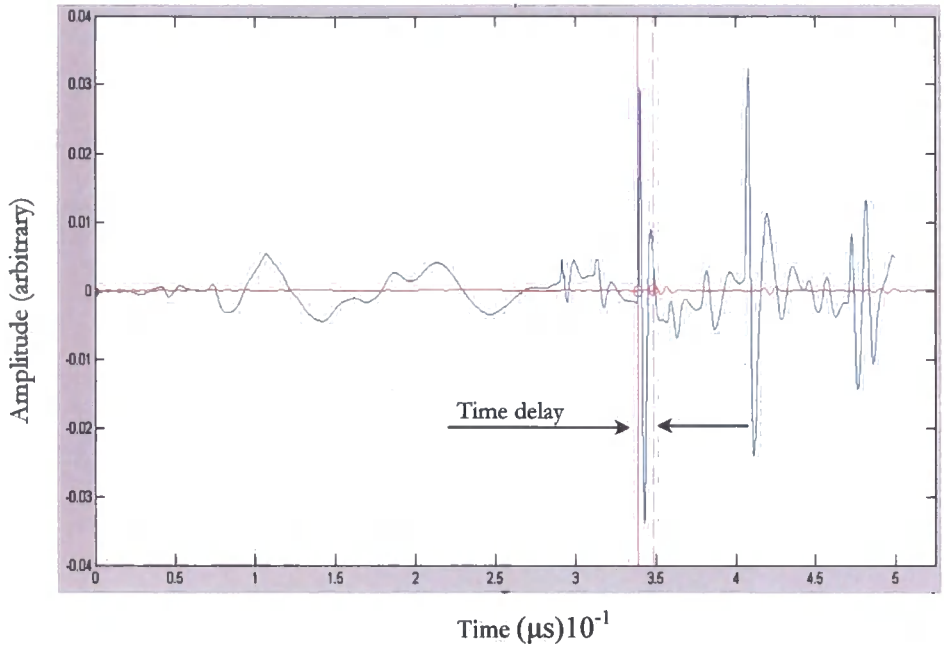

Figure 7.4. Unfiltered signal (blue) and 4th cycle filtered signal (red), with markers showing delay

7.4. Pass-band Filtering

The various filter parameter permutations available within the filter design and analysis tool (FDATool) and signal processing toolbox were explored and applied to the signal. The results were evaluated and of the multitude of parameter permutations, Figure 7.5. shows the parameters of the filter chosen with the best compromise of signal time delay and signal to noise ratio. Figure 7.6. shows the Tx3 Rx2 signal with the application of the 10th order FIR bandpass filter. Due to the linear-phase FIR filtering process the resultant signal shows time delay as with the correlation filter. The delay was measured by superimposing the filtered signal upon the unfiltered signal, as shown in Figure 7.7. Figure 7.8. is a close up of the two signals with the unfiltered signal in red and the bandpass signal in blue. The signal to noise ratio was then re-calculated, using the equation 4.19. at 17.0dB for the band-pass filtered signal.

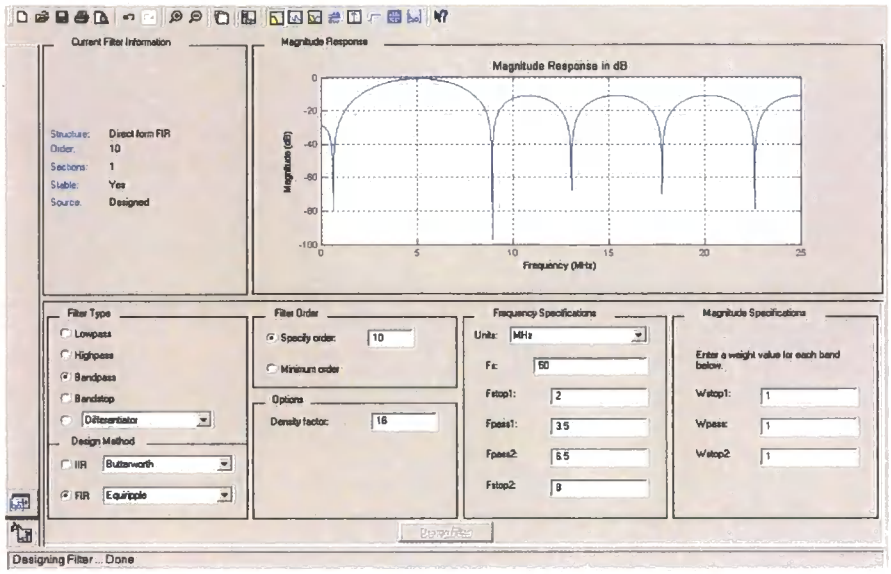

Figure 7.5. Example of the filter design tool interface screen

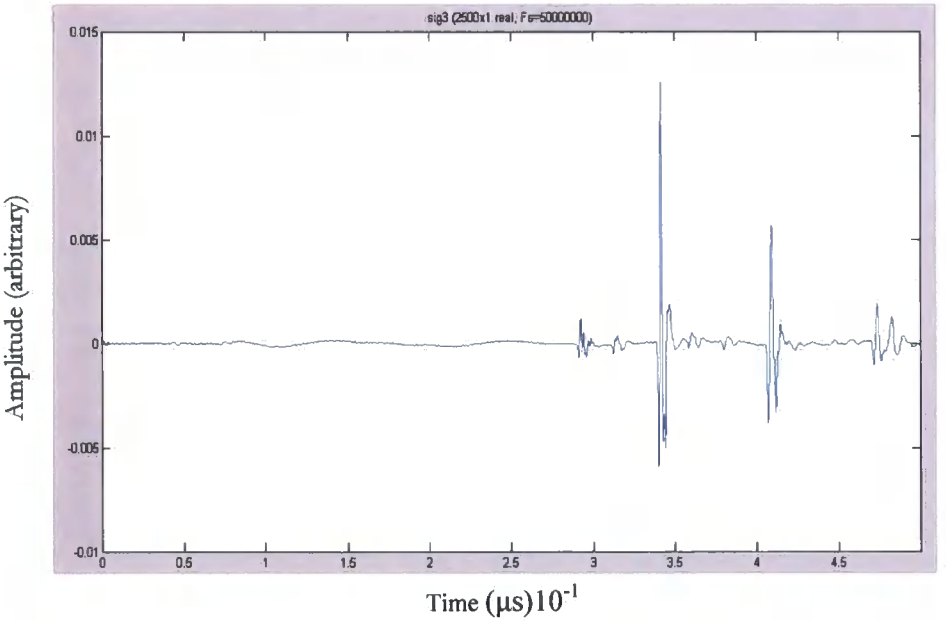

Figure 7.6. Bandpass filtered signal

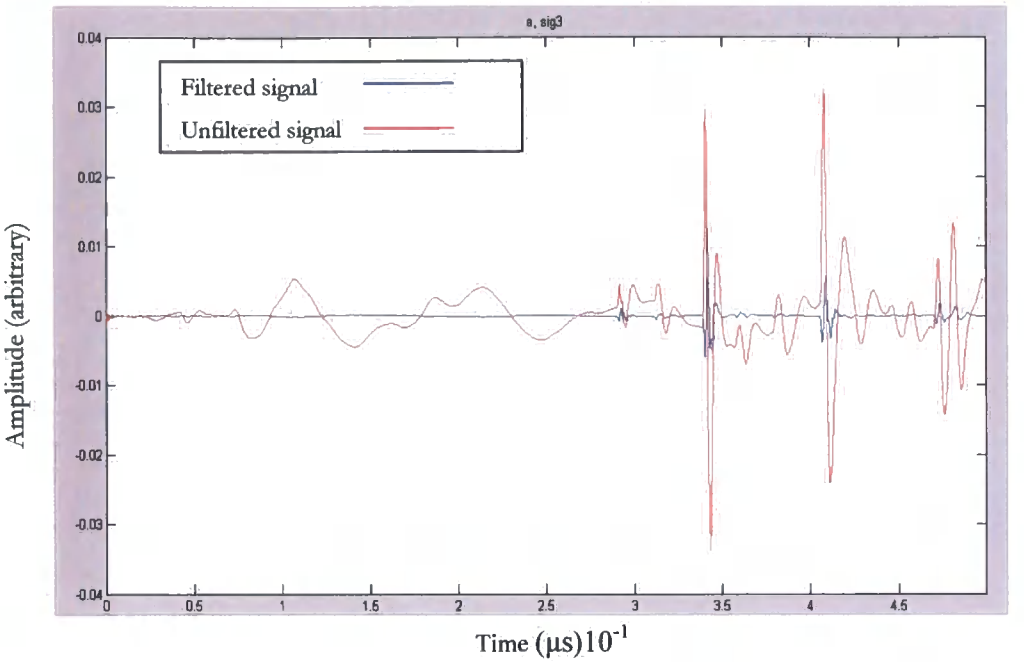

Figure 7.7. The bandpass filtered signal (blue) and unfiltered signal (red) showing time delay

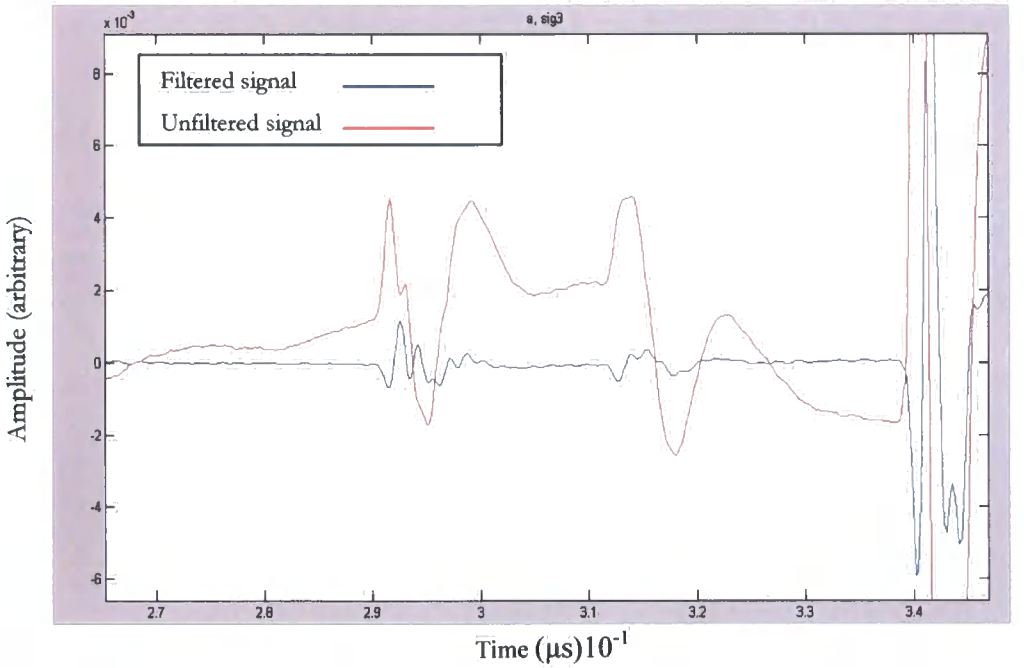

Figure 7.8. Close-up of bandpass filtered signal (blue) and unfiltered signal (red)

7.5. Filtering a Weak Echo Signal

It has being shown that Digital Signal Processing (DSP) can improve the signal to noise ratio of the defect echo signal. However to this point the DSP had only been applied to the signal from adjacent probes with the strongest echo signal, but to confirm the choice of filter, it must also realise the defect from the weaker echo signals scattered from the defect. The signals were re-examined and it was decided to use the signal from the probe in position 3 with the probe in position 1 receiving the signal. This signal had the least favourable SNR, calculated using the equation 4.19. as –5.5dB. The notch echo was still distinguishable from the noise, however it would not be revealed by signal thresholding methods.

7.6. Cross-correlation Filtering of a Weak Echo Signal

The first of the two most successful FIR filters form the previous experiment, the cross-correlation filter, was applied to the weaker signal. The cross-correlation filter used the same backwall echo signal (Figure 7.2.), as the previous experiment. This enabled a true evaluation of the filter as it had been applied to both a strong and weak echo signal. After the first cycle through the filter the signal showed little improvement over the input signal. It was decided to again employ a multi-stage filtering approach as in the previous experiment. This was conducted using the original sinusoidal correlation signal but using the product of the previous filtering operation. The procedure was repeated through six cycles until the noise preceding the notch signal was sufficiently low in amplitude that the signal could be reliably threshholded

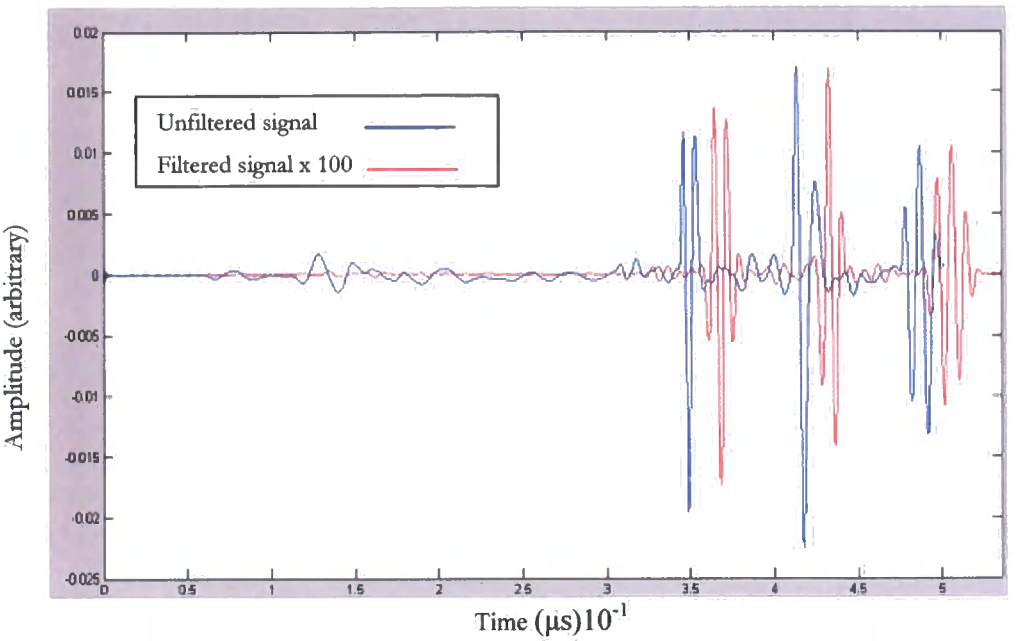

Figure 7.9. Unfiltered signal (blue) and 6th cycle filtered signal (red) increased in amplitude by 2 orders of magnitude

Figure 7.9. shows the unfiltered signal overlaid with the filtered signal, however the filtered signal has been increased in amplitude by 2 orders of magnitude to increase visual clarity of the graphical representation. The delay due to the filtering mechanism was measured at 2.5μs equating to a distance of approximately 14.75mm in steel. The signal to noise ratio was re-calculated at 9.5dB.

7.7. Pass-band Filtering of a Weak Echo Signal

The filter designed for theTx3 Rx2 signal, the 10th order FIR bandpass filter (Figure 7.8.), was applied to the weaker echo signal, Tx3 Rx1. This enabled a true evaluation of the filter as it had been applied to both a strong and weak echo signal.

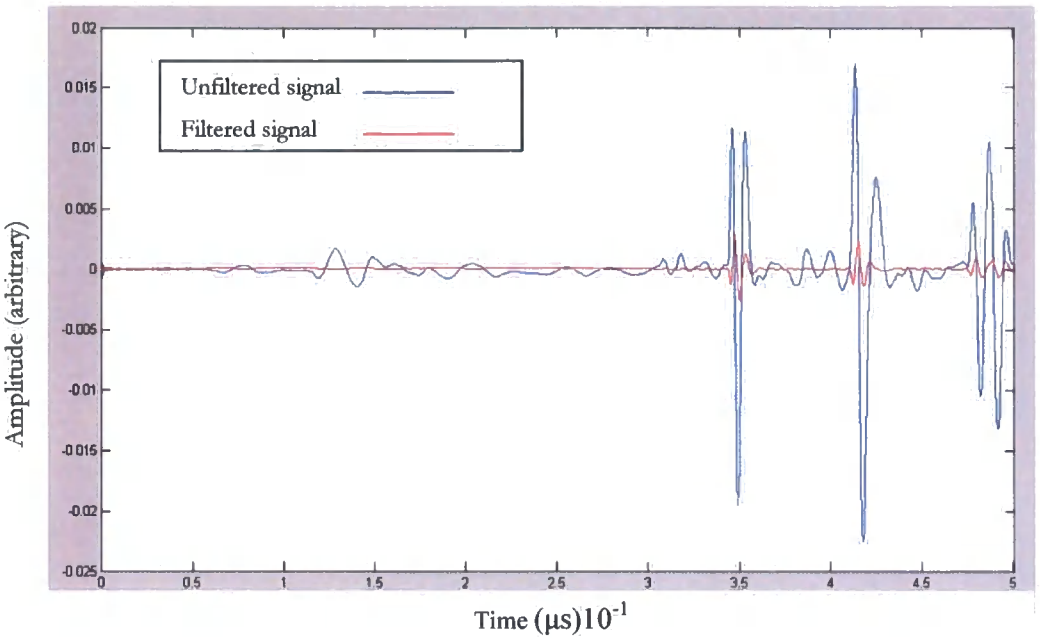

Figure 7.10. Bandpass filtered signal and unfiltered signal

The delay due to the filtering mechanism was measured in MATLAB® at 0.2μs equating to an approximate distance of 1.2mm in steel. Figure 7.10. is the graphical representation of the two signals with the unfiltered signal in blue and the bandpass signal in red. The signal to noise ratio was re-calculated at 7.2dB.

7.8. Combining the Techniques

This experiment would prove the effectiveness of the techniques amalgamation to form a system for the detection and location of defects. The experiment will use the most effectual filter from the previous section the FIR bandpass filter. The experiment was repeated numerous times at a sampling frequency of 50MHz, the average signal transit time was recorded, with a resolution of 0.05μs. The signal was then transferred digitally into MATLAB® were the filter was applied. A time correction of 0.2μs was applied to

all the filtered signal times to compensate for the filtering effect. However the time of 0.2μs is for the total transit time within the material, equating to 1.2mm, which is also the wavelength of the ultrasound within the material. This equates to a maximum effective location accuracy of λ/2 (0.6mm) [8], even without the compensation, the location of the defect would not be overly affected. Table 7.1. displays the average of filtered times with the corresponding distances calculated using 5900 m/s for the speed of sound in steel and the relationship shown in Equation 7.1.

Table 7.1. Filtered signal path distance calculated at 5900m/sec

Signal path	Distance (mm) +/-0.05 mm	Time (μs) +/-0.05 μs
A & B	184.10	31.20
A & C	180.50	30.60
B & C	172.90	29.30

The results displayed in Table 7.3. are the distances when 1.2mm is subtracted, to compensate for the effect of the filter. The ellipse equations 6.1. and 6.2. were applied to the corrected distances in Table 7.3. and the results plotted against the V1 calibration block.

$$\frac{\text{Distance}}{\text{Velocity}} = \text{Transit Time} \qquad [7.1.]$$

The difference in distances between the unfiltered signal and the filter-corrected signal are listed in Table 7.4. This shows that the largest difference in distance is 0.60mm (<0.5%), between probes 2 and 3, and is equivalent to the effective minimum defect detection of half of the wave length (λ/2) [8].

Table 7.3. Filtered signal path distance calculated at 5900m/sec

Signal path	Filtered signal distance (mm) +/-0.05mm	Corrected distances (mm) +/-0.05mm
A & B	184.10	182.90
A & C	180.50	179.30
B & C	172.90	171.70

Table 7.4. Signal path distance differences

Signal path	Unfiltered distance +/-0.05mm	Filtered and corrected distances +/-0.05 mm	Difference between filtered and unfiltered distance
A & B	182.60mm	182.90mm	0.30mm
A & C	179.40mm	179.30mm	0.10mm
B & C	172.30mm	171.70mm	0.60mm

Table 7.5. Signal to Noise Ratios (dB)

Probe Pairs	Unfiltered Signal	Bandpass filtered Signal	Correlation Filtered Signal
Tx3 Rx2 signal	-2.0dB	12.0dB	17.0dB
Tx3 Rx1 signal	-5.5dB	7.2dB	9.5dB

Two variations of FIR filters were evaluated, a bandpass filter and a correlation filter using an isolated backwall echo as the filter signal. The signal required several passes through the correlation filter to effectively improve the signal to noise ratio (Table 7.5.)

7.9. Conclusion

The first section of this chapter investigated the half ellipses as a geometric method of locating a defect. The experimental work conducted in this chapter show that the technique could be adapted the to locate the defect on the bottom surface of the V1 calibration block. The use of three probes and the combination of signal paths provided data to locate the notch, using the intersection of the three ellipses, to an accuracy of <0.5% of the transit distance. However, the weaker echo signals required a subjective approach in their time estimation.

The MATLAB® filter design and analysis tool (FDATool) and signal processing toolbox (SPTool) were employed to design and develop a FIR bandpass filter, and effectively apply the filter to the signals. The developed filter was similar in its effectiveness to the correlation filter in improving the signal to noise ratio. However, the time delay imparted upon the signal was a tenth of that of the correlation filter, and thereby chosen as the most effectual filter for this application, with the SNR results shown in Table 7.5. The application of the FIR bandpass filter to the weaker echo signals enabled the signal to be thresholded, and thereby objectively measure their transit times. The application of the ellipse geometry equations to the FIR filtered signals proved that the techniques were compatible and that with relatively basic signal time correction the defect could be located.

This work was presented at the 30th Annual Review of Progress in Quantitative Non-destructive Evaluation (QNDE) July 27-August 1, 2003, held in Green Bay, Wisconsin U.S.A. Also a modified version of this work was published in the journal, Non-destructive Testing and Evaluation [9]

7.10. References

1. Kuo, M.K., T.R. Lin, P.L. Liu, and T.T. Wu, *Locating the crack tip of a surface-breaking crack. Part I. Line crack.* Ultrasonics, 1998. **36**: p. 803-811.

2. Kazanavicius, E., A. Mikuckas, I. Mikuckiene, and V. Kazanavicius, *Noisy signal processing in real time DSP systems.* Ultragarsas Journal, 2003. **46**(1): p. 31-36.

3. Birks, A.S. and R.E. Green Jr., *Ultrasonic Testing.* 2nd ed. Nondestructive Testing Handbook, ed. P. McIntire. Vol. 7. 1991, Baltimore, Maryland, U.S.A.: American Society for Nondestructive Testing. 893.

4. Fomitchev, M.I., Y.E. Grigorashvily, and S. Volkov, *Ultrasonic pulse shaping with optimal lag.* International Journal of Imaging Systems and Technology, 1999. **10**(5): p. 397-403.

5. Chen, J., Y. Shi, and S. Shi, *Noise analysis of digital ultrasonic nondestructive evaluation system.* International Journal of Pressure Vessels and Piping, 1999. **76**(9): p. 619-630.

6. Smith III, J.O., *Mathematics of the Discrete Fourier Transform (DFT), with Music and Audio Applications.* 2003, Stanford, California: W3K Publishing.

7. Hasnselman, D. and B. Littlefield, *Mastering MATLAB 6: A Comprehensive Tutorial and Reference.* 2001, New Jersey: Prentice Hall.

8. Diederichs, R., *The Online Journal of Nondestructive Testing.* 2005, www.ndt.net.

9. Snowdon, P.C., S. Johnstone, and S. Dewey, *A 2D Static Ultrasonic Array of Passive Probes for Improved Probability of Detection.* Nondestructive Testing And Evaluation, 2003. **19**(3): p. 111-120.

Chapter 8.

Multi-Probe Scan

8.1. Introduction

The project remit required that the inspection be carried out on an immersed and moving steel billet. This required two additional variables into the development of the system. It was decided that the immersion section of the project be conducted as the last section of the project. The moving billet experiment would be conducted by indexing the transducer array by a specific distance after each individual pulse examination was conducted. This procedure will then be repeated over the designated area of the V1 block to be examined.

As previously stated in section 2.2. of this thesis, each individual 10mm diameter probe is firing every 8mm of billet, when travelling at 1m/s. However the scans for this experiment will be conducted in 1mm increments, this being the lower figure of the 1-2mm that is stated by Wolfram (2000) [1], equating to 60 individual A-scans of the V1 block.

This chapter will also bring together the elements of the project that form the Normal Probe Diffraction technique (NPD) the term given to the amalgamation of the processes elements. These elements comprise of the scanning of the billet, ellipse geometry location of the defect, and the Digital Signal Processing.

8.2. Detection Limits

This experiment would be completed using the V1 calibration block utilised as the test material. It was necessary to ascertain the extent of the region of which the passive probes could receive the diffracted signal from the notch. This would minimise the quantity of individual readings required of each scan. The method was to use two probes, one as the dedicated transmitter the other as the receiver, and scan the V1 block maintaining the 22.5mm probe separation.

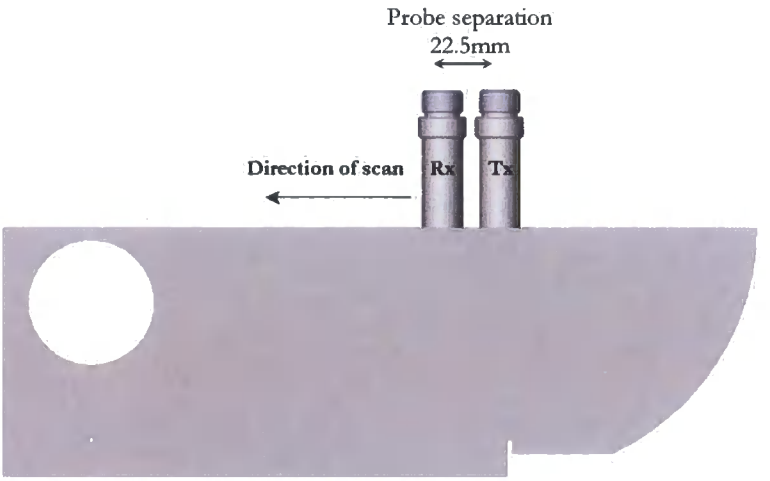

Figure 8.1. Probe positions and direction scan

The transducer array scanned the V1 block until the notch signal was indistinguishable from that of the background noise. The starting position of the probes was with the transmitting probe positioned directly over the notch, and the receiver over the 100mm bottom surface (Figure 8.1.). The experiment was repeated numerous times, alternating the probes used and their position within the two probe array.

The results were collated and filtered with the FIR filter designed in the previous chapter (section 7.6.), using Microsoft EXCEL and MATLAB®. The signal threshold for this experiment was set at 6dB Signal to Noise Ratio and any signal above this would indicate positive defect detection.

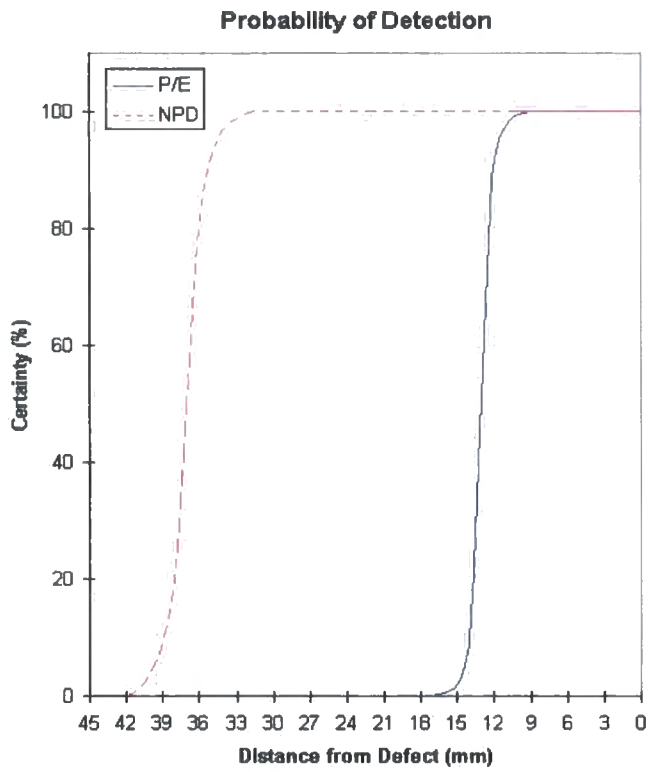

Figure 8.2. Comparison of Probability of Detection for NPD and Pulse-Echo

The scans showed that the diffracted signal was detectable by the passive probe, when the receiver was over 42mm from the notch and the transmitter 20mm from the notch. Figure 8.2. shows the increase of detection ability using the standard single-probe-multi-receiver scan over the conventional single-probe pulse/echo scan. It shows that the NPD system starts detecting the defect at a lateral distance of 41mm from the defect whereas the pulse-echo probe needs to be within a range of 15mm. However, at the 41mm distance the reliability of detection was erratic, and only became stable when the distance from the notch was less than 35mm (Figure 8.2.) The detection limit is defined by Birks (1991) as the smallest measurement having a probability of 97.5% of not being caused by noise [2]. The application of the limits advocated by Birks, equates to a distance from the notch of 33mm. From these results it was decided to scan for 60mm, i.e. 30mm either side of the notch.

8.3. Scanning the V1 Block

The method was to use two probes, one as the dedicated transmitter the other as the receiver, and scan the V1 block maintaining the 22.5mm probe separation. The starting position of the probes array was with the centre of the array 30mm from the notch, with the transmitting probe facing the radius of the V1 block (Figure 8.3.). The scan was conducted in 1mm increments, being the lower figure of the 1-2mm that is stated by Wolfram (2000) [1], that is 60 individual A-scans of the V1 block.

To make the data more manageable and easier to analyse, a matrix was formed from the data using Microsoft EXCEL, allowing the A-scans to be stacked, creating a B-scan of the V1 block (Chapter 3.2.) [3].

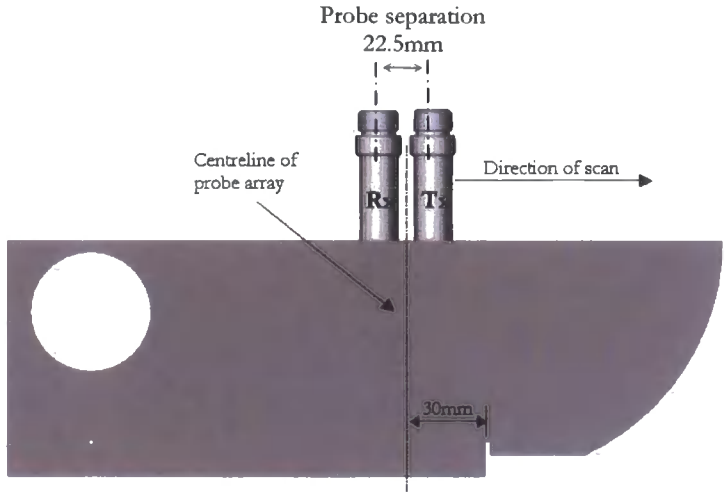

Figure 8.3. Probe transmitter/receiver location and direction of scan

The collated data was interrogated with the B-scan result plotted in Figure 8.4. with the first 20μs of the signals removed as it contained no relevant data. Removing the first 20μs of the signals and concentrating on the defect also negated the lengthy process of filtering the 60 individual A-scans. The filtering of the scan would be added to the process later in the experiment.

The greyscale B-scan shows all of the features of the V1 block, the 100mm backwall, the notch and the 91mm backwall, that are recognised by their time position on the scan. However, the greyscale graduation can be adjusted for the signal amplitude, effectively making it a signal threshold, and required some diligence in ensuring a linear scale.

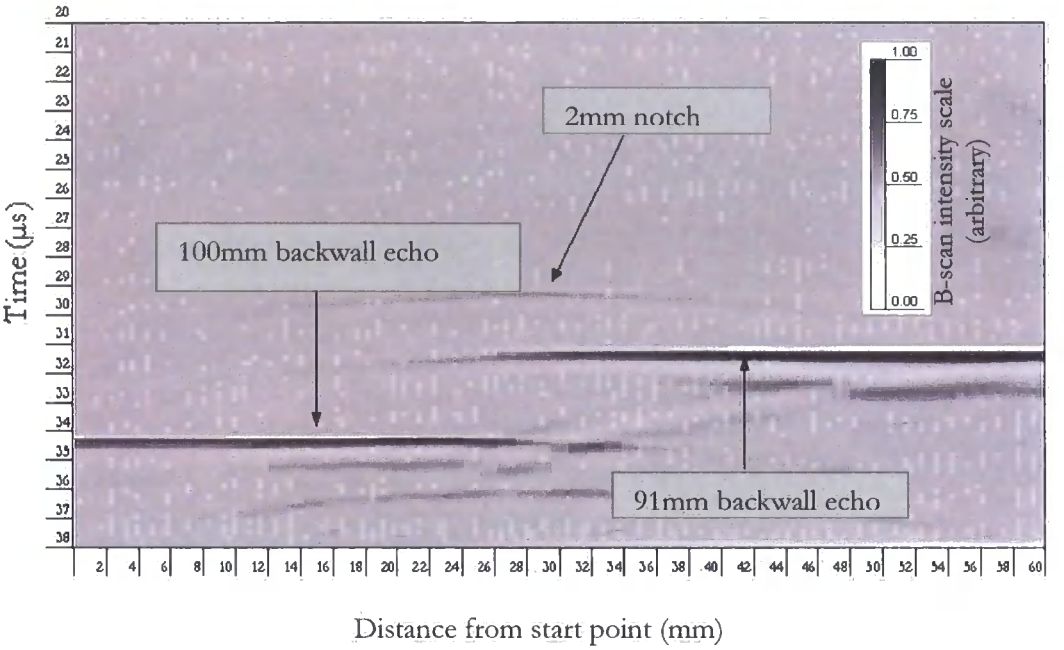

Figure 8.4. Unfiltered B-scan plot of the V1 calibration block

The NPD array scan of the V1 block has indicated that the technique could potentially be adapted to operate on a moving steel billet, however because the signal has been entered into a DSP system, it could be further manipulated to enhance the signal, and therefore its detectability. It was noted that the methods were similar to that of the Synthetic Aperture Focusing Technique (SAFT). However whereas SAFT uses a form of a delay and sum algorithm for signal enhancement [4], essentially a time shifting a B-scan; the NPD technique employs the delay of the diffracted signal, for geometric defect location.

8.4. Filtering the B-scan

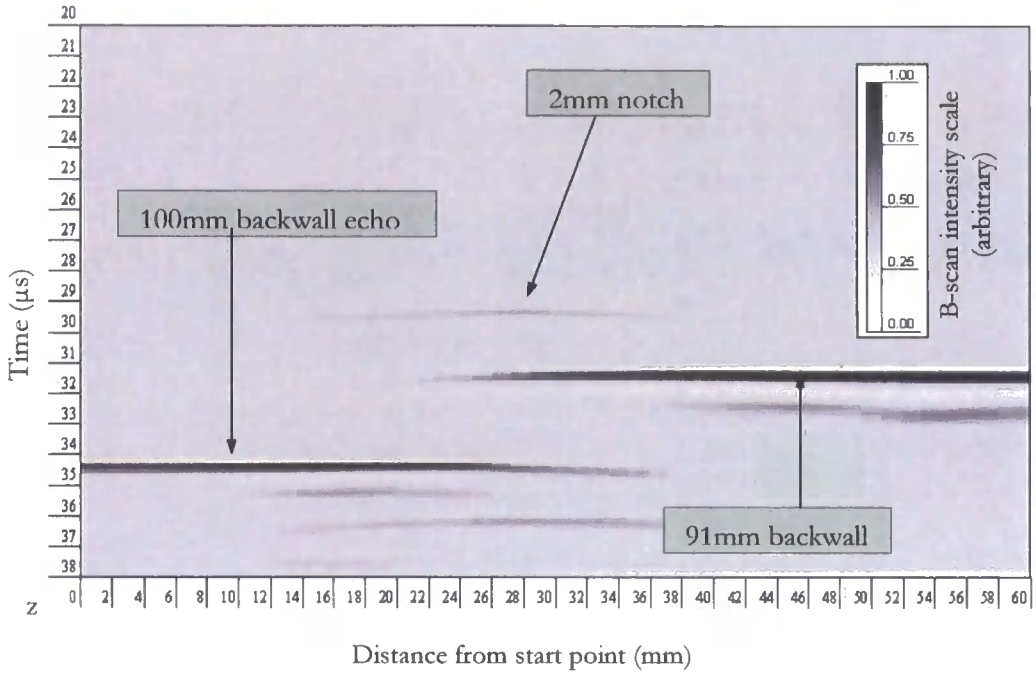

Figure 8.5. Filtered B-scan plot of the V1 calibration block

The digital data that formed the B-Scan of the previous experiment was imported into MATLAB® to be filtered. The previously developed filter, the FIR filter designed in chapter (Chapter 7.6.), was applied to the signals. The resultant signals were collated, stacked and plotted out graphically re-forming the B-scan. The application of this filter would facilitate the application of a defect detection threshold level enabling the defect to be detected automated system. The filtered B-scan in Figure 8.5. shows much less noise and the features are clearly defined, with the notch at 29µs, the 100mm backwall at 34µs and the 91mm backwall at 31µs.

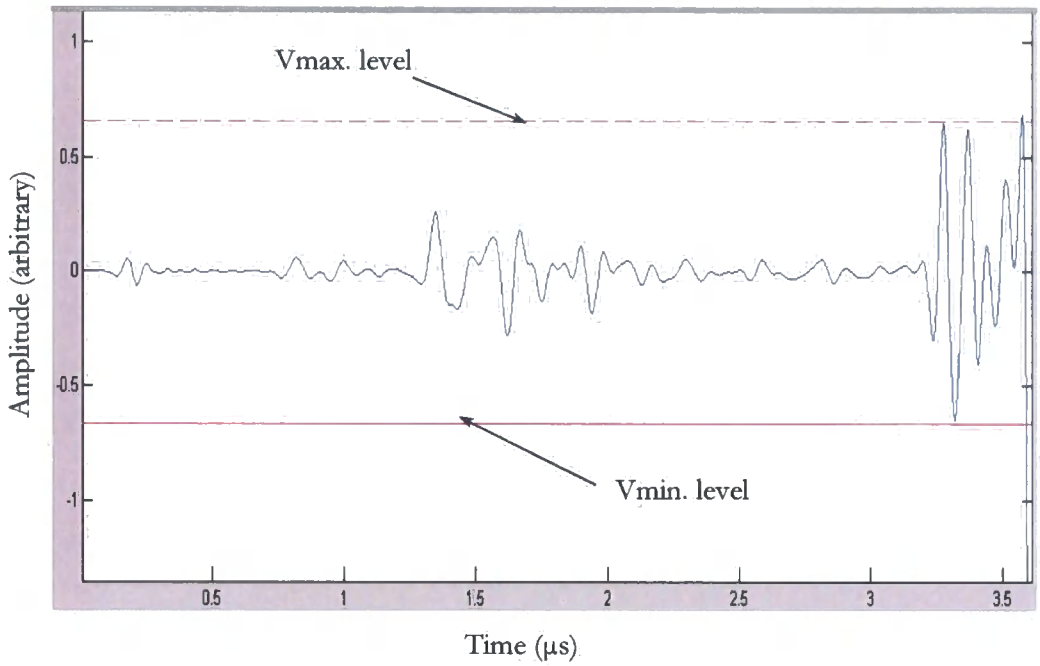

Figure 8.6. Measured Vmax and Vmin signal levels

The next stage of the signal processing was to set the Signal to Noise Ratio level, as the SNR can be enhanced substantially after the threshold processing [5]. In the previous section the SNR level was successfully set at 6dB, and this was the chosen level. The SNR was determined by measuring the level of signal and noise from individual A-scans from the filtered B-scan digital matrix. The two measured signal levels were inserted into the equation 4.19. this determined the SNR, which using Figures 8.6. and 8.7. was calculated as 7.8dB. The level was then set and applied using the MATLAB® signal processing toolbox (SPTool).

When the signal matrix is displayed graphically as a B-scan, the result of the application of the DSP can be readily appreciated (Figure 8.8.). The B-scan shows the three features of the 100mm, 91mm, and the notch, more clearly defined than in the previous B-scan graphics.

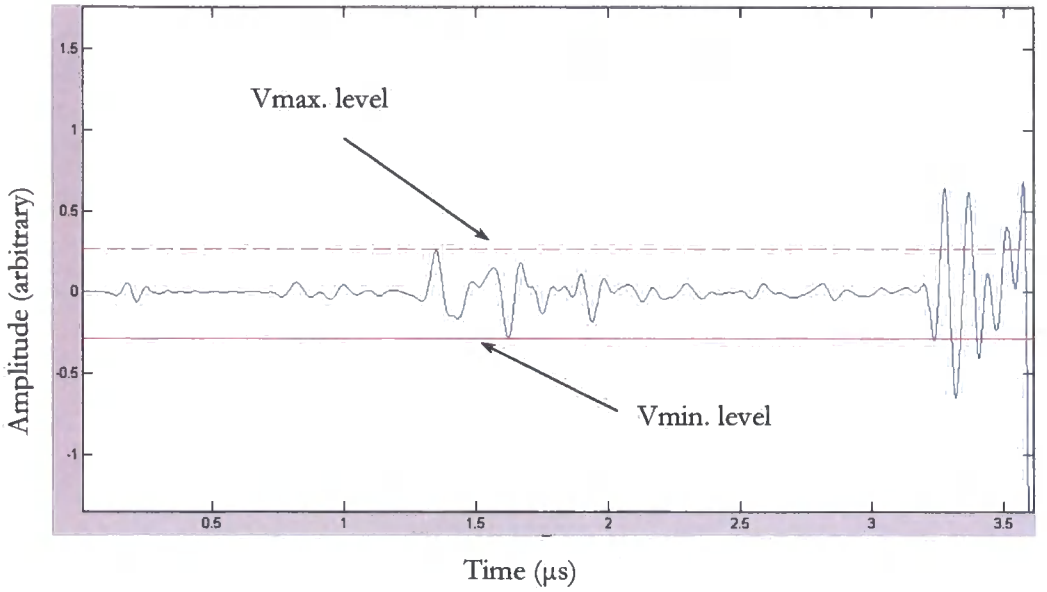

Figure 8.7. Measured Vmax and Vmin noise level

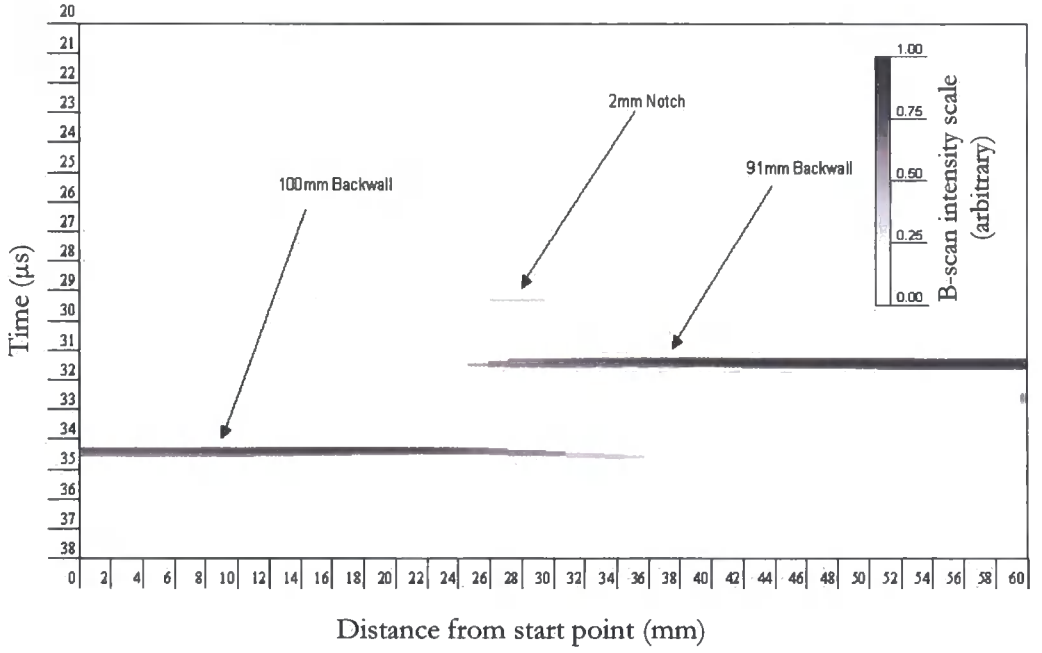

Figure 8.8. Filtered and thresholded B-scan plot of the V1 calibration block

8.5. The NPD System

Described in this section is the layout design of the potential automated defect detection system, incorporating all of the successful elements developed during the project. The order in which the individual elements are positioned within the system is significant. The positioning within is required to maximise the processing power and to minimise the overall financial cost. A block diagram was designed and drawn for the proposed system, and is displayed in Figure 8.9.

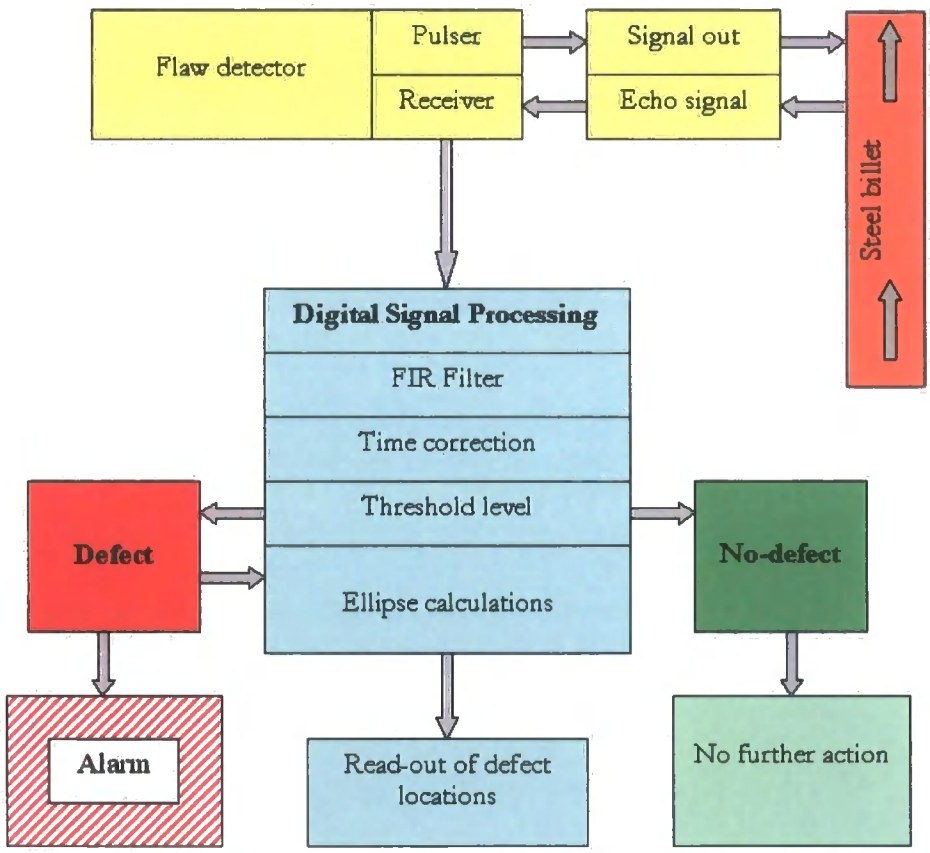

Figure 8.9. Block diagram of the proposed system

The ultrasonic pulse is generated in a generic transmitter/receiver – flaw detection system, with the received signal being diverted into the Digital Signal Processor. The signal is then filtered to maximise defect detection, and time corrected, to remove the delay imparted during the FIR filtering process. It is envisaged that the filtering process could have variable parameters, depending upon the input frequency. The threshold level may require a parameter variance, dependent upon material dimensions and sensitivity required. The output signal now has two alternatives. This is dependent upon how the threshold DSP has categorised the signal as either defect, or no-defect.

If no-defect is registered, then no further action is required. If however a defect has been identified, then the signal remains within the DSP system for additional processing. This additional processing is the application of the ellipse equations for the geometric location and positioning of the defect. The data on the defect could be displayed as 3-dimensional co-ordinates, or be graphically displayed.

8.6. Conclusion

The project required that the inspection be carried out on an immersed and moving steel billet. The immersion experiments are conducted later in the project, in Chapter 10. Indexing the probes a specific distance over the billet and recording the individual A-scans overcame the problem of conducting the examination on a moving billet, successfully simulating the billet traversing the probe array.

The extent of the region of which the passive probes could receive the diffracted signal from the notch was ascertained to minimise the length of the scan. These scans showed that the diffracted signal was detectable at over 40mm from the notch by the passive probe receiver, after filtering. The results indicated that the signal could be reliably and repeatedly detected from a distance from the probes of 33mm from the defect with a >6dB Signal to Noise Ratio.

The results from the unfiltered scan (Figure 8.4.) showed that the passive probe could reliably define the features within the V1 block. The unfiltered B-scan showed a graininess indicating background noise; also, the graphics displayed long diffraction arcs from the notch. Once the filtering process had been applied (Figure 8.5.), the B-scan was cleaner in appearance with the notch in particular being more clearly defined.

The next stage of the filtering process was to threshold the filtered signal, this proved to be successful as the background noise and the diffraction arc from the notch were

effectively filtered out (Figure 8.8.). The process demonstrates that time of flight diffraction can be realized using passive normal probes (Normal Probe Diffraction, NPD) to effectively locate and realise defects.

The use of a NPD system could increase the throughput speed of the steel billet due to its increase of volumetric inspection per individual transducer pulse. A proposed system was designed and laid out in the form of a block diagram and is displayed in Figure 8.9., with the various elements shown in there relative positions. The design of a working system will be addressed in the final chapter, conclusions and further work.

The first section of this chapter covering the signal detection limits and the filtering of the signal matrix formed part of a poster presented at The 31st Annual Review of Progress in Quantitative Non-destructive Evaluation (QNDE) held in Golden, Colorado U.S.A. 2004.

A journal paper based upon this work was presented at The 42nd Annual British Conference on NDT held in Bransford, Worcester U.K. on 16-18 September 2003, and subsequently published in the Insight journal of the British Institute of Non-Destructive Testing [6].

8.7. References

1. Wolfram, A. *Automated ultrasonic inspection.* in *15th WCNDT conference.* 2000. Rome, Italy: www.karldeutsch.de/PDF/Automated_UT_inspection_May00.PDF.

2. Birks, A.S. and R.E. Green Jr., *Ultrasonic Testing.* 2nd ed. Nondestructive Testing Handbook, ed. P. McIntire. Vol. 7. 1991, Baltimore, Maryland, U.S.A.: American Society for Nondestructive Testing. 893.

3. Hellier, C.J., *Handbook of Nondestructive Evaluation.* 2001, New York, U.S.A.: McGraw-Hill.

4. Lingvall, F., *A method of improving overall resolution in ultrasonic array imaging using spatio-temporal deconvolution.* Ultrasonics, 2004. **42**: p. 961-968.

5. Chen, J., et al., *Noise analysis of digital ultrasonic nondestructive evaluation system.* International Journal of Pressure Vessels and Piping, 1999. **76**(9): p. 619-630.

6. Snowdon, P.C., et al., *A 2D Static Ultrasonic Array of Passive Probes for Improved Probability of Detection.* Nondestructive Testing And Evaluation, 2003. **19**(3): p. 111-120.

Chapter 9.

NPD Applied to a Section of Steel Billet

9.1. Introduction

The application of the developed technique has so far been conducted using a known test sample containing a pseudo defect, the V1 calibration block. In this chapter, the technique is applied to the original 70mm x 70mm section of steel billet first used in Chapter 5 of this thesis. The first part of this chapter describes the general experiment set-up using an immersion multi-probe transmitter/receiver array and a 2.5mm diameter 10mm deep flat-bottomed hole as a simulated defect machined into the steel billet. The identical inspection is then repeated on a billet containing a defect produced during its manufacture.

This series of experiments completes the remit of the project and the investigation into the development of a potential system or techniques' using an array of normal angle immersion probes for billet inspection. Geometric defect location using ellipse calculations have been characterised in numerous previous experiments, and will therefore not form part of the final series of tests.

9.2. General Experimental Set-Up

A section of steel billet was characterised in terms of the presence and approximate location of defects using a single probe pulse-echo method. A defect was then simulated in the section by machining a 2.5mm diameter flat-bottomed hole machined to a depth of 10mm [1]. The use of a flat-bottomed hole is a standard method for characterising defect detection instrumentation. The following series of experiments are conducted as immersion tests, and use a similar stand off distance of 70mm, to that of the bar mill. The probes were held stationary above the billet, while the billet was indexed passed the array. The temperature of the water was thermostatically regulated at 24 +/- 1 degrees Celsius, as this is above that of the ambient temperature of room, and was chosen to give consistent readings regardless of the surrounding environmental conditions. The set-up was pre-tested to ensure that the indexing mechanism operated as expected, with the probe holder remained static over the period of the tests (Figure 9.1.)

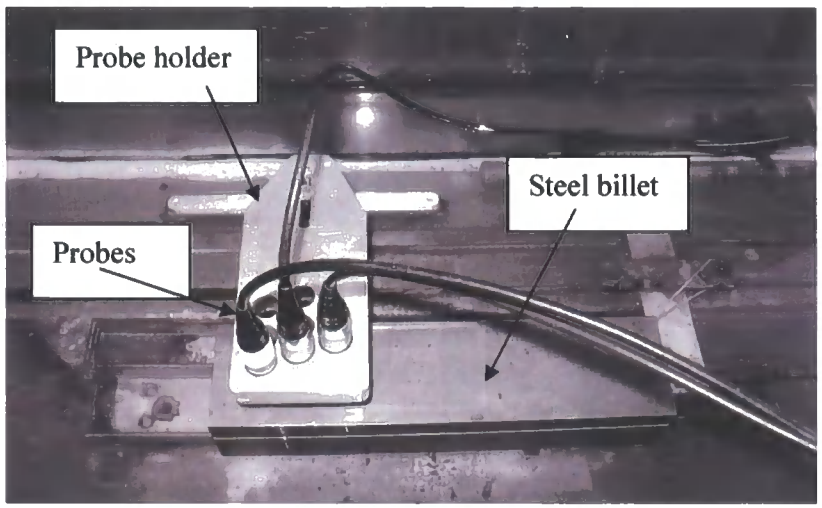

Figure 9.1. Photograph of an immersion set-up used during initial pre-trials

The Doppler effect of the propagating wave through the moving billet was also considered. Using equation 7.1. and with the wave front propagating at 5900m/s, the signal transit time through the 70mm square section steel billet is 23.73μs. The transit time of the signal within the water was also calculated using a signal velocity of 1480m/s as 94.59 μs. Therefore with the steel billet moving at 1m/s, the billet will have moved 0.11832 mm, during the 118.32μs, and was considered negligible. Numerous individual A-scans were conducted over the section of the billet containing the 10mm deep, 2.5mm diameter flat-bottomed hole defect, to ensure that the investigation was conducted over the correct section of steel billet.

9.3. Immersion Inspection of a 2. 5mm Flat-bottomed Hole

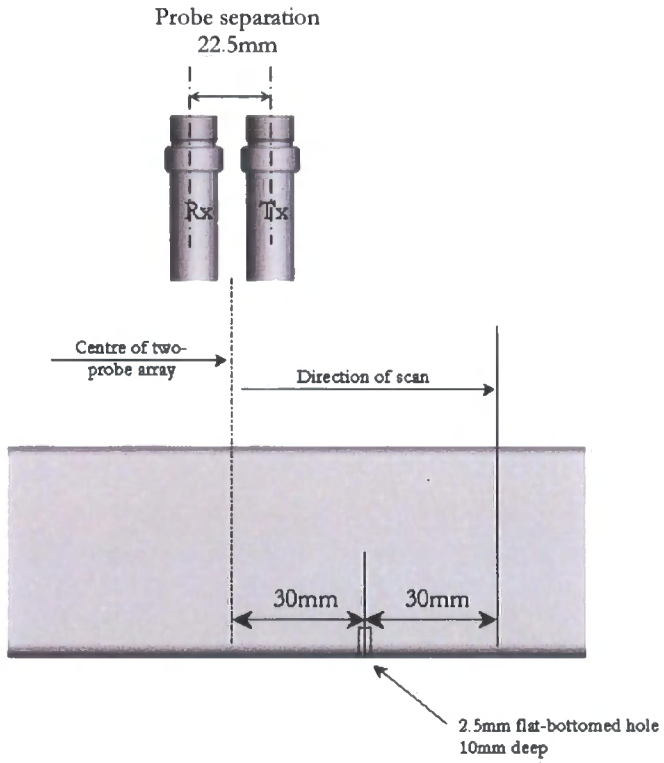

Figure 9.2. Drawing of the immersion set-up used for the flat-bottomed hole test

The scan of the steel billet was conducted over a distance of 60mm and sampled at 1 reading per probe position every 1mm [2]. The method was to use two probes, one as the dedicated transmitter the other as the receiver maintaining the 22.5mm probe separation as used in previous experiments.

The 10mm deep, 2.5mm diameter flat-bottomed hole was located on the underside of the billet as shown in Figure 9.2. The starting position of the scan was with the centre of the two-probe array 30mm from the centre of the flat-bottomed hole (Figure 9.2.) To make the data more manageable, a matrix was formed from the data using Microsoft EXCEL, allowing the data to be plotted using 3-dimensional graphics and stacked to create a B-scan (Chapter 4.2.) [3].

9.4. B-scan of the Flat-bottomed Hole

The first 40μs of the signals transit time through the water was removed as it contained no data relevant to the experiment, and therefore the B-scan starts just prior to the water/steel interface. The FIR bandpass filter developed previously in Chapter 8.6. was applied to the B-scan signals displayed in this section (Figure 9.3.) The diffraction arc formed from the 2.5mm flat-bottomed hole (the defect) can be readily identified in the B-scan displayed in Figure 9.3. with the signal to noise ratio calculated at –2.1dB using the equation 4.19. Behind the defect, the backwall echo signal shows a reduction in amplitude due to the ultrasonic energy being dissipated by the defect [3]. The reduction in backwall amplitude is more apparent when the signal matrix is displayed in a three dimensional matrix, as displayed in Figure 9.4. with the greater amplitude represented by the darker shade.

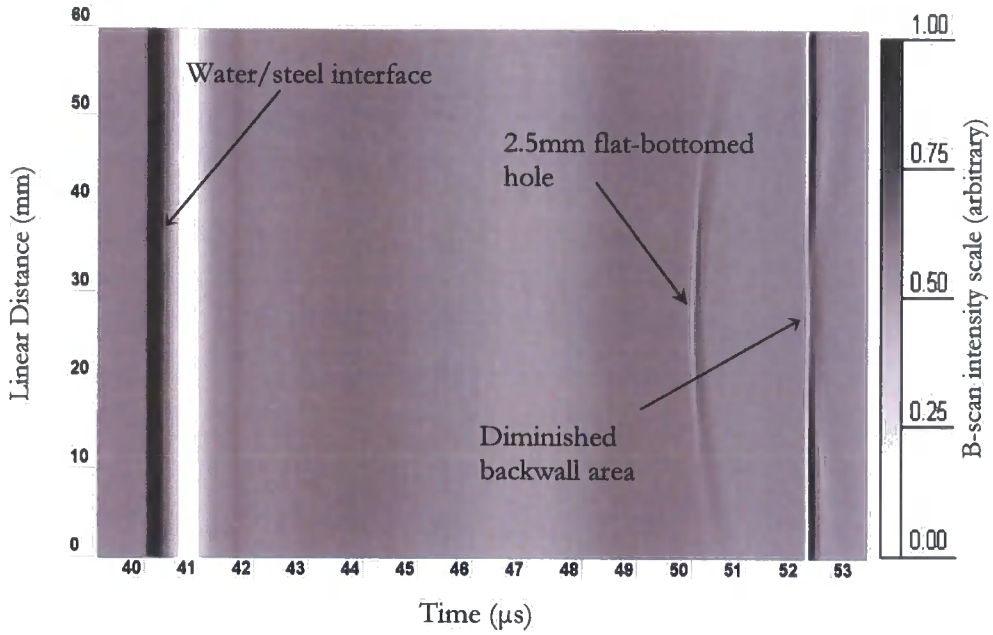

Figure 9.3. **B-scan of 2.5mm flat-bottomed hole**

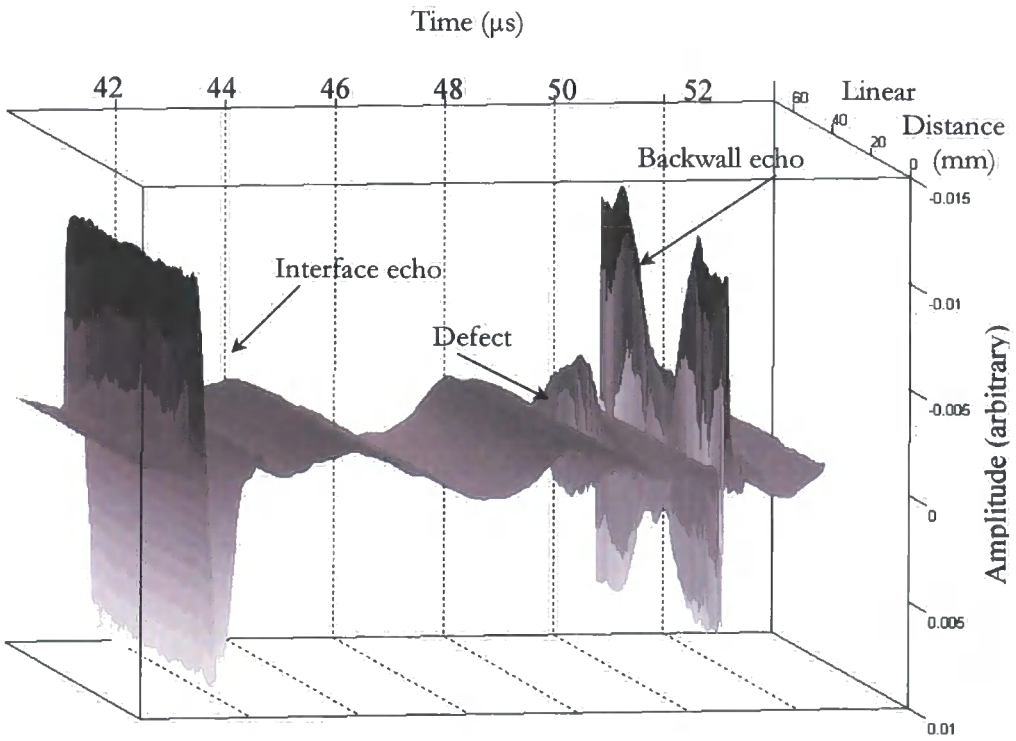

Figure 9.4. **3D time domain data display of 2.5mm flat-bottomed hole**

9.5. NPD applied to a Naturally Occurring Discontinuity

The next experiment carried out on the steel billet required the use of all of the positions of the probe array holder (Figure 3.3.) The central probe position of the array used as the dedicated transmitter (Figure 9.5.) The diagram in Figure 9.5. shows the probe array holder over the steel billet, with the positions of the probes labelled A to H, with the probe in position E as the dedicated transmitter. As previously stated in section 4.2. the oscilloscope has only two input channels and therefore the experiment required the receiving probes position, within the probe holder, to be alternated to simulate a complete array. The scan was conducted over a distance of 60mm and sampled at 1 reading per probe position every 1mm [2].

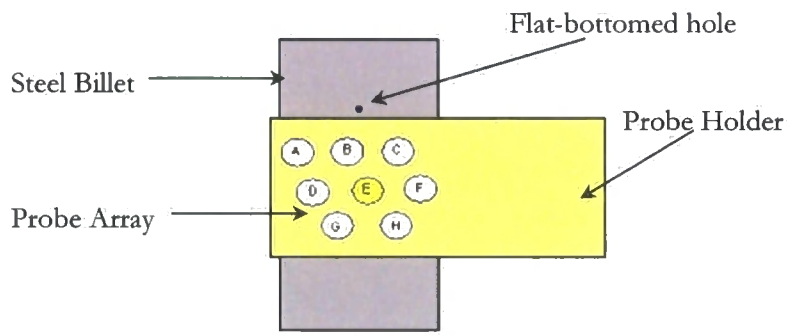

Figure 9.5. Diagram of the probe holder showing billet with flat-bottomed hole and probe array

The signal corresponding to a reflection from the signal can be seen on several of the unfiltered B-scans and indicate that the defect is identifiable by visual observation with the passive probes. However, because of the way B-scans display the signal i.e. they are A-scans rotated 90 degrees around the *y-axis* and stacked, the defect is not as readily recognisable as in previous experiments displayed in A-scans.

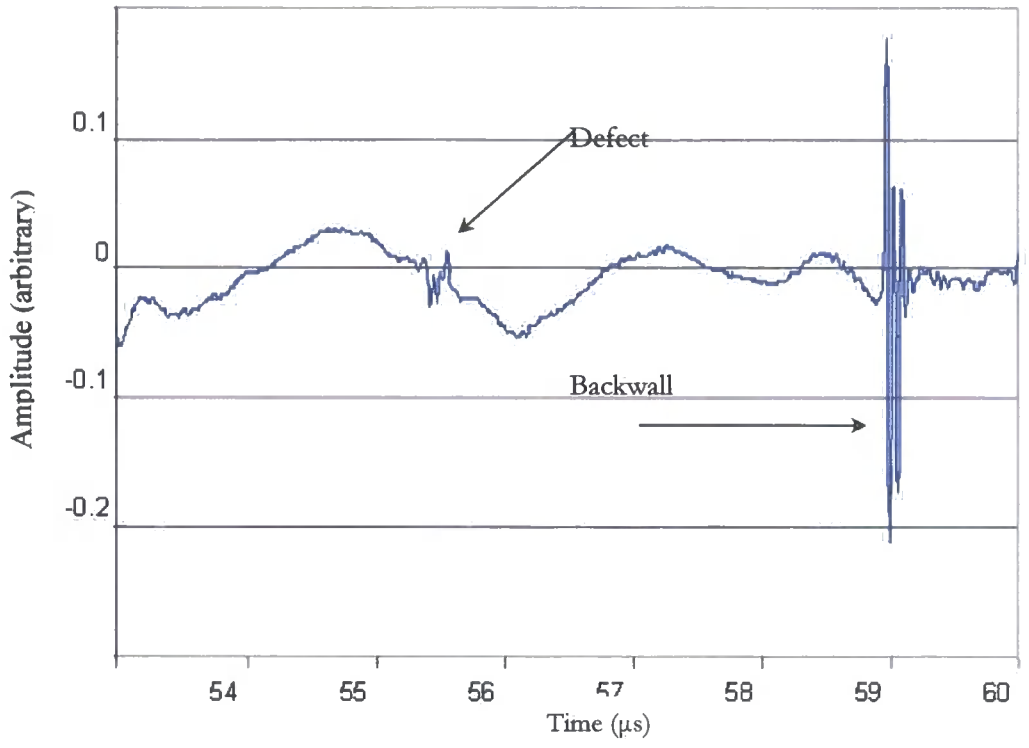

Figure 9.6. **A-scan from a typical section of steel billet (Probe D at 17mm)**

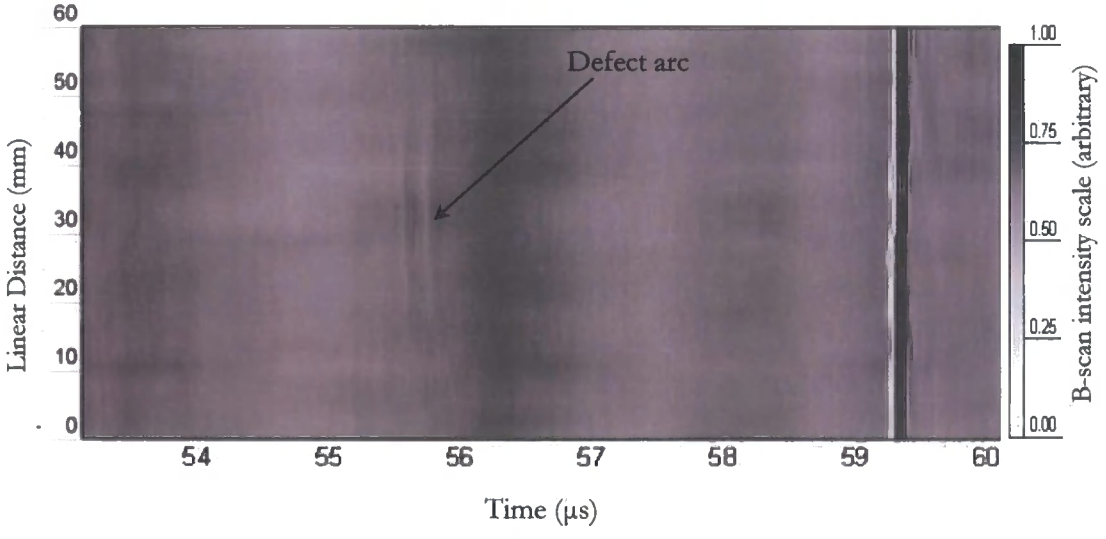

Figure 9.7. **B-scan showing defect arc taken from Probe D**

An example of this is the A-scan in Figure 9.6. showing the defect identifiable within the noise, whereas in the B-scan from developed from probe D (Figure 9.7.) the defect is difficult to extrapolate from the background noise, this is due to a low signal to noise ratio of – 4.5dB calculated using equation 4.19. The defect was only visible on the B-scan generated from the signal received at probe position G. All of the B-scans generated from this test are available in the Appendix.

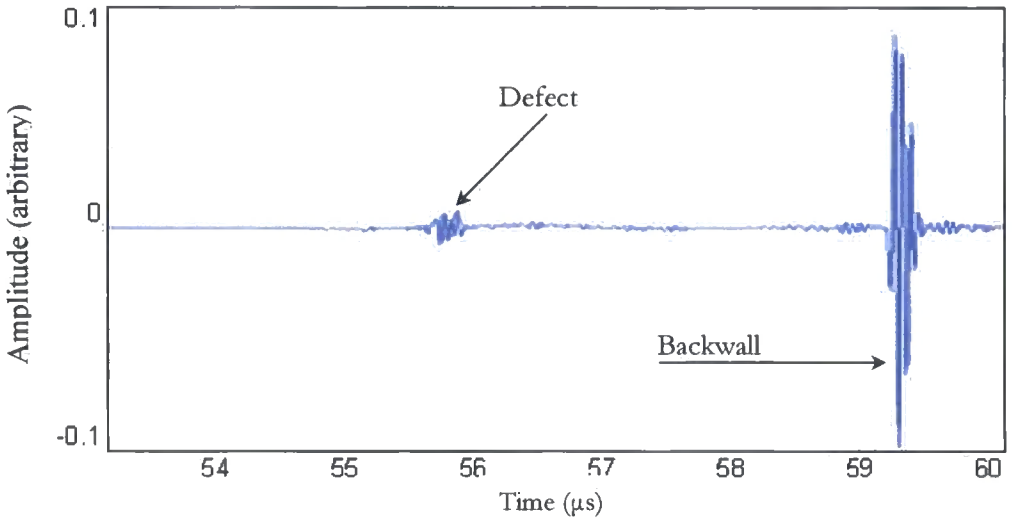

Figure 9.8. Filtered A-scan from Probe D

The signal displayed in Figure 9.8. was received at the probe in position D of the array, and filtered using the FIR bandpass filter developed previously in Chapter 8.6. Once the filter has been applied, the defect is more readily identifiable and could be thresholded with a SNR of 17.0dB (Figure 9.8.). This indicates that with the application of DSP techniques, a single A-scan signal, analysed within an automated defect detection system, has greater detection capability than displaying the stacked unfiltered A-scan signals as a B-scan. However, an automated system using filtered B-scans, could provide an even greater detection capability, but this would also require a significant increase in computer processing power.

9.6. Conclusion

The geometric defect location using the ellipse calculations have been proved in numerous previous static billet experiments. However it would require a significant amount of development time to be successfully adapted for use on a moving steel billet. As the project contained time constraints, it was decided that the geometric location method would not be included in the final series of tests.

The application of the NPD technique had up to this chapter been developed only using the V1 calibration block as a test sample. During these experiments, the technique detected the 2mm notch that was used as a defect with a SNR of –1.5dB. However, because of the additional complexities associated with immersion testing coupled with the extra problems of mode conversions, refraction etc., the technique would therefore require additional development to be employed on a moving submersed steel billet.

In this final chapter of the thesis, the technique was applied to a section of steel billet 70mm x 70mm in cross-section. A 2.5mm flat-bottomed hole was used as defect, and a pseudo scan was conducted on the billet (Figure 9.3.). The 2.5mm flat-bottomed hole was apparent in the B-scan, through the diffraction arc formed, and thereby detecting the flat-bottomed hole with a SNR of –2.1dB using the NPD process.

The technique was subsequently applied to the section of steel billet with a naturally formed discontinuity. The defect was located prior to the NPD scan using a single pulse/echo probe scan, and conducted to ensure that a discontinuity was present in the section under inspection.

The scan was conducted using all of the positions of the array, with each individual probe giving a different perspective of the defect. Several of the probes did not indicate the presence of the defect. This is due to the shape of the defect or unfavourable defect orientation in relation to the probes concerned. The SNR was improved significantly from –4.5dB of the unfiltered signal to 17.0dB using the technique.

The remaining probes received an echo signal from the defect of varying clarity. Because the defect was naturally formed void with an uneven surface structure, how the signals arrived at the transducers (diffraction, reflection, refraction etc.) was uncertain, however the signal was successfully interpreted and the defect detected.

The displaying of the signals as filtered A-scan stacked to form B-scans is the simplest way of displaying the signals resulting from the application of the NPD technique. Due to the amount of data involved, it is the only practical method for manual inspection, as if the data was displayed as A-scans, 420 individual A-scans would have required analysis. This requires the designed automated system to have sufficient digital signal processing power to manipulate the volume of data received.

The experimental work conducted during this project has repeatedly proved that under laboratory conditions, the use of the passive probes in conjunction with the application of DSP can enhance the detection of discontinuities within steel sections.

9.7. References

1. Birks, A.S. and R.E. Green Jr., *Ultrasonic Testing.* 2nd ed. Nondestructive Testing Handbook, ed. P. McIntire. Vol. 7. 1991, Baltimore, Maryland, U.S.A.: American Society for Nondestructive Testing. 893.

2. Wolfram, A. *Automated ultrasonic inspection.* in *WCNDT conference.* 2000. Rome, Italy. www.karldeutsch.de/PDF/Automated_UT_inspection_May 00

3. Hellier, C.J., *Handbook of Nondestructive Evaluation.* 2001, New York, U.S.A.: McGraw-Hill.

Chapter 10.

Conclusions and Further work

The remit of the project was to investigate and develop the present ultrasonic system currently employed at the steel mill. The motivation being that the system is not being fully utilised to its full potential in that only one probe, within the array, is in use at any time. Therefore, if more than one probe or all probes could be simultaneously used, the system could be operated more effectively, theoretically leading to a faster throughput of inspected material, or increased defect detection sensitivity, or higher reliability of defect detection, or a combination of the gains. The system developed in this project was initially to be designed as an immersion technique using an array of normal angle probes used for billet inspection. However the technique developed is potentially transferable to other ultrasonic multi-probe array applications.

The preliminary experiment of the project was conducted on a section of steel billet, and proved inconclusive due to the received signals being complex and not immediately interpretable. This was due partly to the fact that the defect was large and unknown and it was decided that there were too many variables for the initial experiment.

Because of the complexities of signal trace, it was decided to eliminate as many of these variables as possible. The subsequent series of experiments were therefore carried out on a subject containing a simple known target.

It was decided to use a V1 calibration block as the quality of the material could be assured [1], and the 2mm notch could be utilized as a pseudo defect. The first series of experiments on the V1 block indicated that the signal from the 2mm notch was detectable from outside that of specular reflection. Also, at 13 degrees away from the centreline of maximum intensity; the notch was also outside of the stated 20dB drop inspection zone of the main ultrasonic lobe [2]. This required a form of non-specular reflection as the method of signal propagation. The probable method of this being diffraction, because diffuse reflection requires a rough surface and the boundary variations to be of the same order of magnitude or larger than the ultrasound wavelength being used [3], and the V1 block had a known surface finish. The experiments showed that the signal generated from one probe was detected by the reflection off the backwall outside the 20dB drop inspection zone of the main ultrasonic lobe, and that the notch was detected through signal diffraction. The next experiment was conducted to determine the origin of a spurious echo generated within the V1 block. This experiment also introduced the ellipse method of geometric defect location technique devised by Kuo et. al. (1998) [4]. The experiment indicated that the echo was from an internal sidewall reflection, due to the 25mm width of the V1 block.

Chapter 6 of this thesis further developed the ellipse method to locate the defect on the bottom surface of the V1 calibration block by using the three probes and the combination of signal paths, locating the notch by using the intersection of the three ellipses, achieving an accuracy of <0.5% of the transit distance.

The weaker echo signals received during the ellipse experiment however required a subjective approach in their time estimation and to address this problem it was decided to employ DSP techniques to the signals. The MATLAB® filter design and analysis tool (FDATool) and signal processing toolbox (SPTool) were employed to design, develop and effectively apply the various filters to the echo signals. Two variations of FIR filters were extensively evaluated, a bandpass filter and a correlation filter. The successful application of the FIR bandpass filter to the weaker echo signals enabled the signal to be thresholded, and thereby measure their transit times. The appliance of the designed correlation filter, improved the SNR form –2.0dB to 17.0dB, with the band pass filter achieving an improvement from –2.0dB to 12.0dB when applied to the same signal. However the time delay imparted upon the signal was a tenth of that of the correlation filter, and thereby selected as the most effectual filter for this application.

The work conducted to this point was presented at the 30th Annual Review of Progress in Quantitative Non-destructive Evaluation (QNDE) July 27th -August 1st, 2003, held in Green Bay, Wisconsin U.S.A. A modified version of this work was also published in the journal, Non-destructive Testing and Evaluation [5].

The project then investigated the potential of combining the two techniques, that of ellipse geometry and the application of DSP to enhance the likelihood of detection of the defect within the V1 calibration block. The application of the ellipse geometry equations to the FIR filtered signals proved that the techniques were compatible and that with relatively simple signal time correction the defect could be located. The process demonstrates that time of flight diffraction can be realized using passive normal probes (Normal Probe Diffraction, NPD) to effectively locate and realise defects.

A journal paper also based upon this work was presented at The 42nd Annual British Conference on NDT held in Bransford, Worcester U.K. on 16-18 September 2003, and subsequently published in the Insight journal of the British Institute of Non-Destructive Testing [6].

The project brief required the inspection to be conducted on a moving section of steel billet. This was initially conducted on the V1 block by indexing the probes to a specific distance over the block and recording the individual A-scans, and simulating the material traversing passed the probe array.

This work formed part of a poster presented at The 31st Annual Review of Progress in Quantitative Non-destructive Evaluation (QNDE) held in Golden, Colorado U.S.A. 2004. A copy of the poster is available in the appendix of this thesis.

A proposed system was designed and laid out in the form of a block diagram giving an explanation to the proposed system. The design and development of system hard and software was considered as the main area for future development and research.

In April 2005, a paper on this development work was presented by Lei Zhang, at the Institute of Materials, Minerals and Mining Conference on advances in on-line instrumentation for materials characterisation in the metals industry. A second paper was presented at the British Institute of Non-Destructive Testing Annual Conference 2005. Copies of both papers are available in the appendix of this thesis [7, 8].

The final chapter of the thesis concludes with the inspection of a section steel billet. The developed NPD technique was applied to a section of billet containing both a 2.5mm flat-bottomed hole, and a void, formed during the steel making process. The technique located both types of defect.

At the commencement of this project, phased array systems were complex and costly for implementation into a steel mill, requiring additional technician training. The reduction in cost of processing power and reduced production costs has however increased the accessibility of these systems. The development of more user friendly and simpler user interface has also reduced the training required on these systems.

The Normal Probe Diffraction technique developed increases the detection of a defect within a static probe array, using standard low cost normal angle probes. The project has repeatedly proved that under laboratory conditions, the use of the passive probes in conjunction with the application of DSP can enhance the detection of discontinuities within steel.

10.1. References

1. Markucic, D., V. Mudronja, S. Mahovic, and B. Runje. *Quality Requirements for Ultrasonic Testing Calibration Blocks.* in *8th ECNDT.* 2003. Barcelona, Spain. P.353-375

2. Krautkrämer, J. and H. Krautkrämer, *Ultrasonic Testing of Materials.* 1990, New York: Springer-Verlag. 677.

3. Charlesworth, J.P. and J.A.G. Temple, *Engineering Applications of Ultrasonic Time-of-Flight Diffraction.* Second Edition ed. Ultrasonic Inspection in Engineering, ed. M.J. Whittle. 2001, Baldock: Research Studies Press Ltd. 254.

4. Kuo, M.K., T.R. Lin, P.L. Liu, and T.T. Wu, *Locating the crack tip of a surface-breaking crack. Part I. Line crack.* Ultrasonics, 1998. **36**: p. 803-811.

5. Snowdon, P.C., S. Johnstone, and S. Dewey, *A 2D Static Ultrasonic Array of Passive Probes for Improved Probability of Detection.* Nondestructive Testing And Evaluation, 2003. **19**(3): p. 111-120.

6. Snowdon, P.C., S. Johnstone, and S. Dewey, *Improving the Probability of Detection for a 2D Ultrasonic Array using Digital Signal Processing Techniques.* Insight (Journal of The BINDT), 2003. **45**(11): p. 743-745.

7. Zhang, L., S. Johnston, P.C. Snowdon, and S. Dewey. *Normal Probe Diffraction - Improving the capability of industrial ultrasonic probe arrays.* in *The IoM3 Conference.* 2005. London.

8. Zhang, L., S. Johnstone, P.C. Snowdon, and S. Dewey. *Real-Time DSP System for Normal Probe Diffraction Technique.* in *The 44th Annual British Conference on NDT 2005.* Harrogate, UK.

Improving the probability of detection for a 2D ultrasonic array using digital signal processing techniques

P C Snowdon, S Johnstone and S Dewey

Based on a paper presented at NDT 2003, the 42nd Annual British Conference on NDT, Worcester, September 2003.

An experiment was conducted to investigate the potential of using a linear array of probes consisting of a single transmitter (Tx) and multi-passive receivers (Rx) to improve defect detection. The array consisted of three 5 MHz straight-beam probes were located at distances of 22.5 mm and 45 mm from the transmitter. A V1 calibration block was used to ensure repeatability, and the 2 mm notch was utilised as substitute defect. The probes were used in a single transmission with dual-receiver formation in alternate positions. This experimental set-up was used to reveal the clearest interpretation of the received signal. The readings were taken from the area before the first echo to eliminate confusion due to the sidewall reflections.

Ultrasonic theory suggests that the reflected beam intensity would have insufficient signal-to-noise ratio (SNR) to be of practicable use with this probe array geometry. Work presented in this paper shows that the pre-processed SNR (in the order of 1.5 dB for a distance of 22.5 mm and less than zero at 45 mm), can be improved to around 20 dB by DSP techniques.

1. Introduction

The steel industry is under constant pressure to deliver higher quality defect-free material at lower cost to customers; however zero-defects is a questionable target[1]. This has led to improved manufacturing processes and the need for more reliable, faster testing methods. The standard method for defect detection is pulse/echo using relatively low-cost probes. To improve on this, the industry is tending to move towards phased array technologies. These systems are relatively expensive, complex in set-up, and have a propensity of being application-specific. The work presented in this paper is a further advancement of background work[2] and this paper describes efforts to extend this method for improving the probability of detection (PoD). This has been made possible due to increases in computer speed, improved hardware and developments within the field of Digital Signal Processing (DSP).

To investigate this proposal, the usable extent of the generated sound field needed to be characterised. It was decided that a standard V1 (BS 2704) ultrasonic calibration block would be used as the test material since this certified defect-free steel would aid repeatability. Predetermined problems were with signal strength, as diffracted signals are weak in comparison to reflected signals. There is therefore a dilemma with the setting of the sensitivity of the flaw detector. DSP may have solutions to this problem. To enhance the SNR and therefore the PoD several methods of DSP were discussed. The received signals where processed off-line.

Paul C Snowdon and Sherri Johnstone are at the School of Engineering, University of Durham, County Durham, DH1 3LE, UK. Tel: +44 (0)191 3342445; E-mail: paul.snowdon@durham.ac.uk

Stephen Dewey is at Corus plc, Swinden Technology Centre, Rotherham, South Yorkshire, S60 3AR, UK.

2. Background theory

Traditional pulse/echo detection operates, according to Snell's Law[3], in that if the defect is at normal incidence to the probe, the signal reflects back to that transmitting probe. If the defect is not at normal incidence the signal is reflected away from the probe and the defect is not actively detected. The probability of detection of this defect would be improved if a receiver probe were in a position to detect this angled reflection. The work presented in this paper extends on this concept of multi-probe detection. The literature shows that, typically, a single probe will detect defects within a given beam angle (Eqn.1) determined by the SNR[4]. Because in this instance the defect is outside this beam angle, the amplitude of the signal will be relatively small. This technique cannot solely rely on direct signal reflection, utilising other physical properties, that of non-specula refection, and diffraction. Examination of the literature on the potential of time-of-flight diffraction (TOFD)[5] for techniques of small signal detection showed little has been done with probes at normal incidence to the material interface. Hence, the method investigated in this report is referred to as normal probe diffraction (NPD).

$$Siny_{dB} = k_{dB}\left(\frac{\lambda}{D}\right) \quad \text{.....(1)}$$

3. Experiments

The apparatus was set up as shown in Figure 1. This consisted of three 10 mm-diameter 5 MHz straight-beam probes placed in a linear arrangement, normal and in contact with the upper surface of a V1 calibration block. The 2 mm-wide notch, 85 mm from the inspection surface was chosen as a pseudo defect. Each probe was then excited in turn using a USPC 3100 in pulse/echo mode and A-scans produced (Figures 2 and 3). The next part of the experiment was to fire one probe, while the remaining two probes acted as passive receivers (for example probe 1 was excited and probes 2 and 3 acted as receivers). These two probes were connected to a Hewlett Packard 'Infinium' oscilloscope and the results stored. The probes were excited at a frequency of 5 MHz and sampled at a frequency of 50 MHz, avoiding problems of aliasing[6]. The signals where transferred digitally into MatLab, and various digital

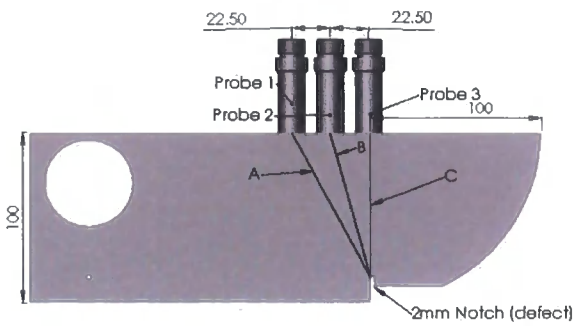

Figure 1. Probe geometry

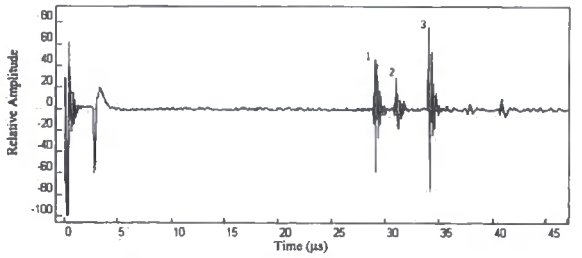

Figure 2. Trace of probe 3 in pulse/echo mode

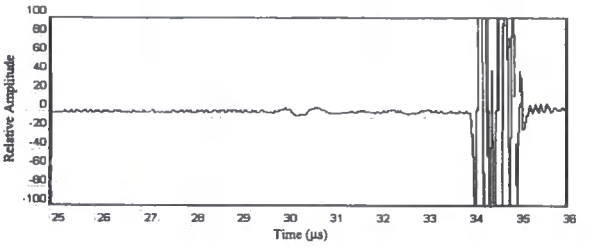

Figure 3. Trace of probe 2 in pulse/echo mode

filters applied to increase the SNR. Initially various low- and pass-band infinite impulse response (IIR) filters were applied. The SNR was improved; however it was anticipated that because of the identifiable sinusoidal signature at 5 MHz that correlation filtering would be a better solution[7]. A backwall echo trace from a typical scan was isolated and transposed as the correlation signal and was utilised within MatLab as a matched filter.

3.1 Probe triggering

It was found that the receiver probes detected the initial pulse emitted from the transmitting probe electromagnetically. This was suitable, therefore, for triggering the oscilloscope. The times between the transmitted and received signals were recorded with a precision of 0.05 μs to determine the origin and path of the received signal and analysed. Figure 1 also shows the basic geometry of the signal paths and Table 1 shows the signal distances and relative times using a velocity of 5900 m/s.

Table 1. Signal time and distances at 5900 m/s

	A	B	C	Backwall
Distance, mm ± 0.1 mm	96.18	87.93	85.00	100.00
Time, μs ± 0.05 μs (@ 5900 m/s)	16.30	14.90	14.40	16.95

4. Results

Figure 2 shows the pulse/echo A-scan from probe 3. Point 1 is the notch, point 2 is the step at 91 mm, and point 3 is the 100 mm backwall. Figure 3 is the A-scan from probe 2 and shows that the notch is distinguishable, albeit at a high gain (50 dB), but the notch remained undetectable at probe 1. A complete set of results is presented by Snowdon & Johnstone[2].

The graphs showed similarity of signals between corresponding pairs of probes irrespective of transmitting or receiving, therefore only one Tx/Rx arrangement for each probe pair is presented. Interpretation of the graphical results shows that the diffracted signal can be picked up from the passive probes. The first backwall echo can be clearly identified by the frequency (5 MHz) and signal strength. A signal of similar frequency can be observed preceding it (signal of interest). The subsequent graphs are of this area only (*ie* the area of the defect and the backwall echo).

It was decided that initially the signal processing work should be applied to the signal with the highest signal-to-noise ratio, and therefore the signal from Tx-3 Rx-2 was chosen.

Table 2. Probe to probe distances

Path	Theoretical time, μs (from Table 1)	Measured times, μs ± 0.05 μs (from graphs)
A + B	31.20	30.90
A + C	30.70	30.40
B + C	29.30	29.20

The results of using a 20th order bandpass filter is shown in Figure 7. It shows that the defect is clearly visible with a SNR of about 20 dB. The result of applying the matched filter shown in Figure 8 shows a similar SNR with less distortion of the defect signal.

5. Discussion

The results show that probes adjacent to the transmitting probe do detect signals. These correspond to the shortest signal paths via defects that are outside the normal detection range of the transmitting probe (Table 2). It is reasonable to assume that the signal has arrived at the receiving probe, via the 2 mm notch (pseudo defect), in a non-specula manner by diffracting from the edge of the notch[8]. This demonstrates that time-of-flight diffraction can be realised using normal probes NPD to locate defects that are outside the detection range of the transmitting probe.

5.1 Reliability of detection

Figures 4 to 6 show that the amplitude of the diffracted signal is small compared to the back wall signal, even when one of the probes is directly above it. Thus, without signal processing it would require a skilled operative to detect it. However, both the passband and matched off-line filters enhance the signal enough to enable a thresholding algorithm to be applied. It can also be seen that the matched filtered output resembles the raw signal to a greater extent than the passband filtered output.

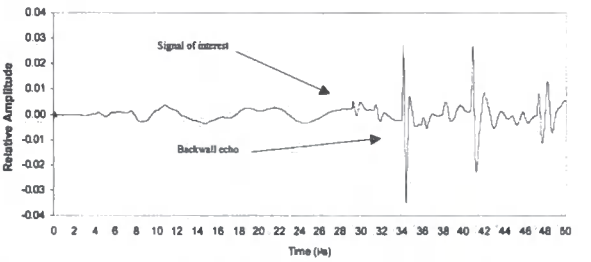

Figure 4. The received signal at probe 2, transmitted from probe 3 (Tx-3 Rx-2)

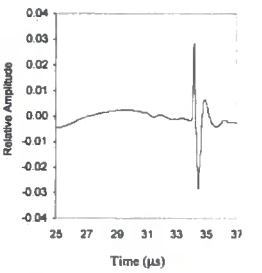

Figure 5. Tx-2 Rx-1

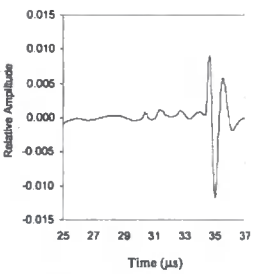

Figure 6. Tx-3 Rx-1

6. Conclusion

The work presented shows that the use of a single excitation multi-passive probe system increases the scan volume for a single measurement when compared with a single pulse/echo transducer. The mechanism for detection has been shown to be normal probe diffraction, that is when the defect is beyond the detection volume of the transmitter and its direct reflection. Since the system uses

standard low-cost normal angle probes the system is relatively cheap to implement, especially when compared to phased array systems.

The diffracted signals have varying signal-to-noise ratios depending on the position of the defect and in some instances the raw signal is barely visible. This has been overcome by the use of small signal extraction methods that are currently employed in communication and radar technologies. Of the various types of filter applied to the signal, the correlation filter gave the best results. The correlation filter applied has increased the signal-to-noise ratio sufficiently to facilitate the application of a thresholding algorithm for the detection of the diffracted signal.

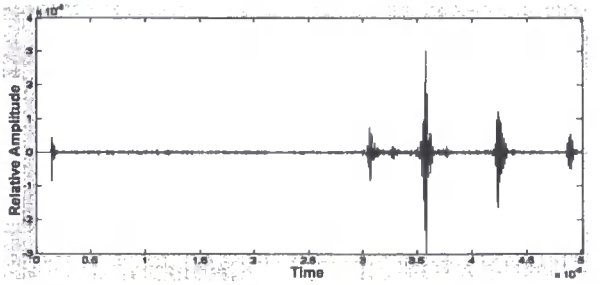

Figure 7. Passband filtered signal (Tx-3 Rx-2)

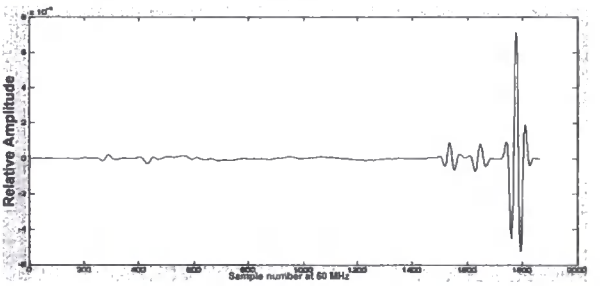

Figure 8. Correlation filtered signal (Tx-3 Rx-2)

Acknowledgements

The authors wish to thank the EPSRC for their financial contribution in funding this project.

References

1. Wolfram, A. *Automated ultrasonic inspection.* in *WCNDT conference.* 2000. Rome, Italy.
2. Snowdon, P C, S Johnstone, and S Dewey. *A 2D static ultrasonic array of passive probes for improved Probability of Detection.* in *QNDE.* 2003. Green Bay, USA.
3. Payne, P A. *Ultrasonic transducers: design, construction and applications.* International Journal of Materials and Product Technology, 1994. **9**: p 403-427.
4. Kartalopoulos, S V. *Fault Detectability in DWDM (Dense Wavelength Division Multiplexing): Toward Higher Signal Quality and System Reliability.* 2001: Wiley-IEEE Press.
5. Charlesworth, J P and J A G Temple. *Engineering Applications of Ultrasonic Time-of-Flight Diffraction.* 2nd ed. 2001, Exeter: Research Studies Press Ltd. 254.
6. Chen, C-T. *Digital Signal Processing.* 2001, New York: Oxford University Press, Inc. 440.
7. Chen, J, Y Shi, and S Shi. *Noise analysis of digital ultrasonic nondestructive evaluation system.* International Journal of Pressure Vessels and Piping, 1999. **76**: p 619-630.
8. Krautkramer, J and H Krautkramer. *Ultrasonic Testing of Materials.* 4th ed. 1990, Berlin, Heidelberg, New York: Springer-Verlag. 677.

16wcndt

16th World Conference on Non-Destructive Testing

Montréal, Canada
August 30~September 3, 2004

Organised by the Canadian Society for Nondestructive Testing and the 16th World Conference Organising Committee

To register for further announcements, contact: ***Conference Secretariat***, c/o Events International Meeting Planners Inc, 759 Square Victoria, Suite 300, Montréal, Québec, Canada H2Y 2J7
Tel: +1 (514) 286 0855; Fax: +1 (514) 286 6066; E-mail: info@eventsintl.com; website: www.wcndt2004.com

Real-Time DSP System for Normal Probe Diffraction Technique

Lei Zhang, Paul C. Snowdon, Sherri Johnstone
Affiliation
School of Engineering, University of Durham, County Durham DH1 3LE, UK
0191 3342542
Lei.zhang3@dur.ac.uk

Steve Dewey
Corus plc. Swinden Technology Centre, Rotherham, South Yorkshire S60 3AR, UK

Abstract

In steelmaking, on-line defect position and real-time size detection are desired. Many methods have been tried and developed for achieving a reliable cost-effective solution. Ultrasonic detection is commonly used in this field of non-destructive testing (NDT) in the steel industry. Traditional ultrasonic defect detection systems use an array of probes in which each probe pulses and receives sequentially. One new ultrasonic detection technology-Normal Probe Diffraction (NPD) has been proven to enhance the probability of detection for steel testing in the previous research.

In this project, a rapid Digital Signal Processing (DSP) prototype for realising the real-time system is modelled and simulated to implement the NPD technique. A DSP integrated development board is used to implement the NPD algorithm and process the digital signal in real-time. An analog expansion daughterboard is also applied in order to gain a fast digital-to-analogue conversion speed for the desired high frequency pulse signal. Variable frequency and wave shape pulse signals can be used in order to gain the best testing effect. A custom high frequency high voltage power amplifier is also designed to get a good response from the transducers. To remove the randomly distributed background noise that disturbs the recognition of the defect echoes and increase the behaviour of the system, several DSP algorithms such as correlation are applied and different filters including FIR filter and IIR filter can be chosen for experiments as well.

The developed real-time system will help increase the probability of detection of defects in steel billets and produce low-cost system solution for ultrasonic billet inspection in steel industry.

1. Introduction

Various defects such as inclusions, bubbles and cracks can affect the quality of the steel and may cause tremendous waste in the steel industry; therefore the detection and recognition of these defects without destructing the tested object is becoming increasingly significant. In steelmaking, on-line defect position and real-time size detection are desired under the urgent requirement for higher quality products. Many methods have been tried and developed for achieving a reliable cost-effective solution. Ultrasonic detection is commonly used in this field of non-destructive testing (NDT) in the steel industry. Traditional ultrasonic defect detection systems use an array of probes

in which each probe pulses and receives sequentially. One new ultrasonic detection technology-Normal Probe Diffraction (NPD) has been proven to enhance the probability of detection for steel testing in the previous research [1]. In this work, the necessary real-time system is simulated with software and the corresponding hardware is to be realised and tested to demonstrate the result. In order to gain the best testing effect, a high voltage amplifier is designed for the high frequency output ultrasonic to get a good response from the transducers and gain a better feedback from the tested object. A variable frequency and pulse shape can be completely and flexibly controlled in real-time. To remove the randomly distributed background noise that disturbs the recognition of the defect echoes and increase the behaviour of the system, several Digital Signal Processing (DSP) algorithms are applied and different filters can be chosen for real-time analysis as well.

2. Normal Probe Diffraction

2.1 Background Knowledge

The nature of the project dictates the specific areas of concentrated ultrasonic research, however all areas of wave propagation are to be briefly researched to ensure no potential avenue is overlooked.

The transducer forms the core of all non-destructive ultrasonic inspection procedures, and whether a work-piece can be inspected or not depends upon the acoustic properties they possess. The choice of the correct transducer is therefore indicative for the quality and the reliability of inspection results. Ultrasonic transducers work almost exclusively according to the piezoelectric effect, and there are four fundamental transducer types: Straight beam transducers, Angle beam transducers, Delay line transducers and Twin crystal transducers. In this project, the straight beam transducer is initially required and is dictated by the remit. This type of transducer has one main drawback, in that the poor recognition of near-to-surface discontinuities due to the width of the initial pulse, however in this project it is the core of the material that is of most interest.

Transducers also differ with respect to the size of the active piezoelectric elements, their frequency, bandwidth and the basic design. The selection of bandwidth is essential for achieving certain test results - narrow bandwidth for highly sensitive testing, or broad banded for high resolution testing. The sound field characteristics of a transducer, is generally derived from the diameter and the frequency of the piezoelectric element.

The Near Field is the region in an ultrasonic beam that is subject to variations of intensity due to diffraction effects. It extends from the source of radiation to a point just short of the far field. Diffraction is a particular example of wave interference and is common to all wave motion. Defect detection in the near zone should be avoided unless the characteristics of the probe used are accurately known. Figure1 shows the near field N, the angle of divergence of γ and the far field for a typical circular probe.

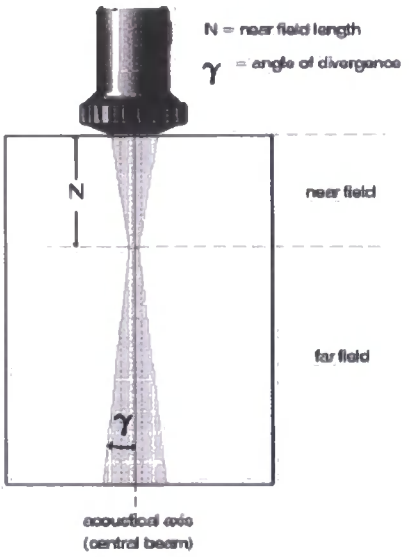

Figure 1 Near Field

The near field equation:

$$N = \frac{D^2 - \lambda^2}{4\lambda}$$

Where

D	=	the diameter of a flat circular oscillator (probe/transducer)
λ	=	wavelength of the ultrasound
N	=	length of near zone

Wavelength equation:

$$\lambda = \frac{c}{f}$$

Where

f	=	frequency
c	=	acoustic velocity
λ	=	wavelength

Acoustic velocity is dependant on the material of propagation, and in general, is constant for any frequency and wavelength. The mode of the wave however does affect the velocity, in that longitudinal waves have greater velocity than transverse waves. In steel, longitudinal waves have an acoustic velocity of 5.9 km/s compared to transverse waves with an acoustic velocity of 3.2 km/s.

2.2 Ultrasonic Detection Methods

Ultrasonic detection techniques have developed at a tremendous rate to fulfil the requirement for high quality defect free material in many industrial and research applications. The basic method is Conventional Pulse-Echo Method. As dictated by its name, conventional Pulse-Echo method use an array of probes in which each probe pulses and receives sequentially. This method was replaced gradually by some new

techniques such as Time-of-Flight Diffraction (TOFD) and NPD, because these new methods collect extra information from diffracted signal which was previously discarded by the pulse-echo detection. The TOFD technique uses angled beam probes to pick up the diffracted signal, while NPD can get the same result with normal probes by using multi-receivers.

Both the TOFD and NPD ultrasonic technique relies on the diffraction of ultrasonic energies from 'corners' and 'ends' of internal structures in a component under test. This is in contrast to conventional pulse echo method which relies on directly reflected signals from internal structures and only can test the depth of the defect, while the latter two methods can detect the flaw in 2D and could be improved to 3D detection by using an array of probes.

2.3 Previous Research

The previous research has investigated the potential within a current multi-probe ultrasonic detection system installed at a steel mill. Extensive laboratory experiments were carried out using the transducer array geometry, to extract additional information from passive probes. The apparatus was set up as shown in Figure2.

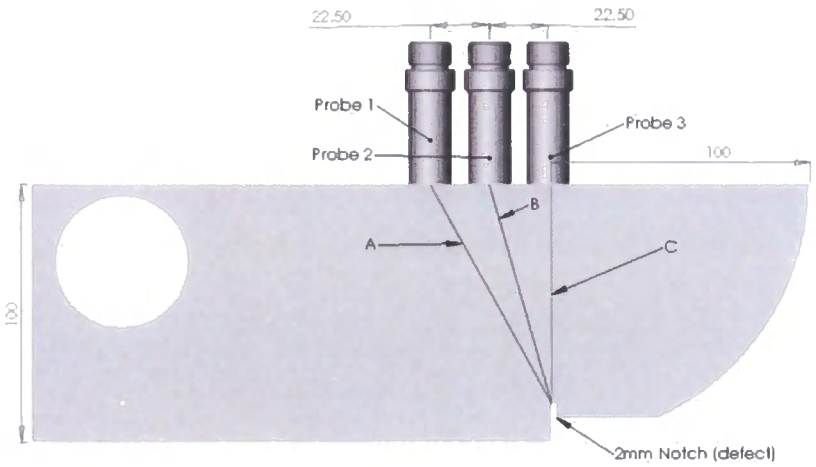

Figure 2 Normal Probe Diffraction

Figure 3 shows the increase of detection ability using the standard single-probe-multi-receiver (SPMR) system over the conventional single-probe-single-receiver (SPSR) system. It shows that the NPD system starts detecting the defect at a lateral distance of 41mm from the defect whereas the pulse-echo probe needs to be within a range of 15mm. The physical principle behind this system uses diffracted waves from the edge of the defects and thus it is particularly effective for the increased detection and sizing of centre-line defects. This technique is defined as Normal Probe Diffraction (NPD), which has been successfully applied offline on a V1 calibration block and a single billet, but has not yet been applied for real-time control.

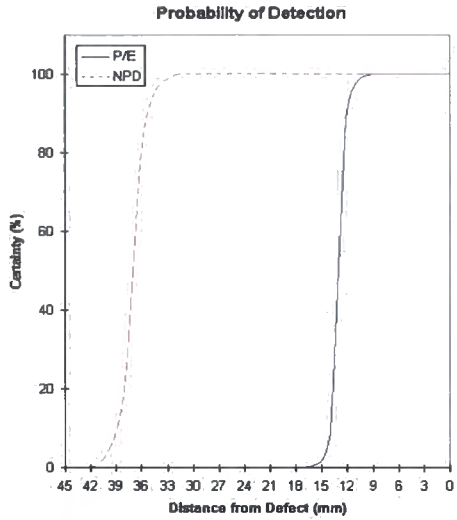

Figure 3 Comparison of Probability of Detection for NPD and Pulse-Echo

Experiments show that the defect detection range can be increased by collecting the diffracted pulse on all the neighbouring probes. This is due to the defect being detected several times per pulse. The research project involves in developing a real-time laboratory based prototype which can detect defects using two methods: the standard single probe pulse echo technique and NPD, and testing the system on a V1 calibration block and a steel billet. In this project, the transmitting and receiving electronics are developed to enable the NPD technique to be applied in real-time.

2.4 NPD Algorithm

The NPD algorithm uses three probes – one transmitter and two receivers. Each transmitter receiver pair are considered the be the foci of two ellipses, each of which pass through the defect. By solving these two ellipse equations, both the vertical offset/defect depth (y0) and the horizontal offset (x0) can be calculated to locate the defect. An ellipse and the coefficients are shown in Figure 4. The relative equations are also listed as follow.

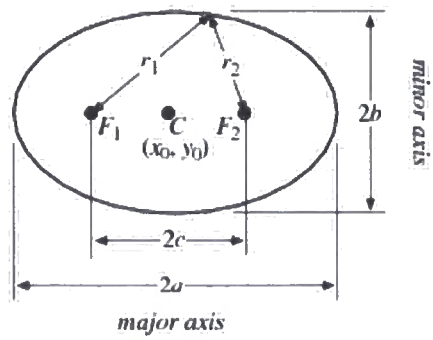

Figure 4 Ellipse

The ellipse equations:

$$(\frac{x}{a})^2 + (\frac{y}{b})^2 = 1$$

$$a^2 = b^2 + c^2$$

$$r_1 + r_2 = 2 * a$$

Table 1. Transmit Distance and Time

Path	Distance (mm)	Time (us)
A	96.18	16.3
B	87.93	14.9
C	85	14.4
Backwall	100	16.95

*Note: d = v * t; v = 5900 m/s*

Table 1 gives out the tested distances of path A, B and C in millimetre, with the theoretical time in microsecond calculated from the distances with the velocity of 5900m/s. The experiment setups and ellipse graphs for double probes and triple probes are shown separately in Figure 5 and Figure 6. The distance between each two probes is set to 22.5mm and the depth of the defect (notch) is 85mm (2).

For double probe NPD, probe 1 transmits signal and then receives the diffracted signal, so the first path is 2 x B and forms a circle whose radius (R) is B. The second path is formed by transmitter probe 1 and receiver probe 2, making an ellipse whose major axis equals to B plus C.

Similarly, for triple probes NPD, probe 1 only transmits signal and forms two ellipses with receiver probe 2 and receiver probe 3. The major axes for each are A plus B and A plus C separately.

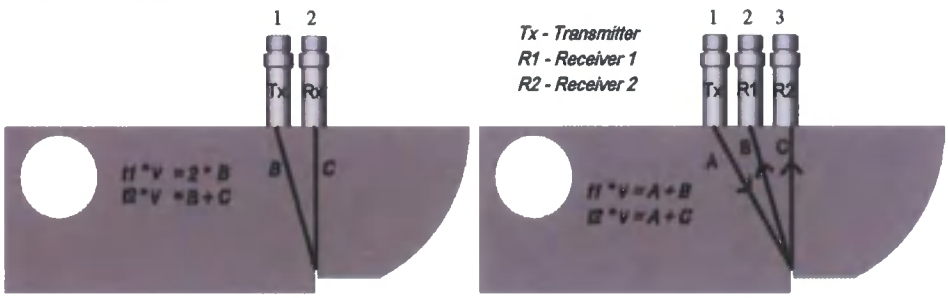

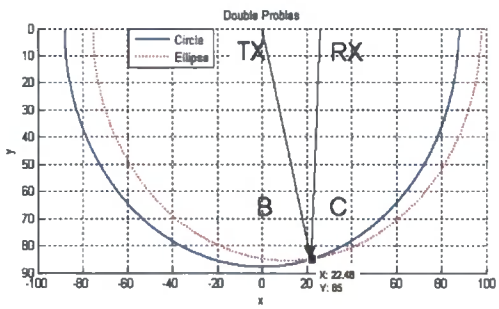

Figure 5 Double Probes Scheme

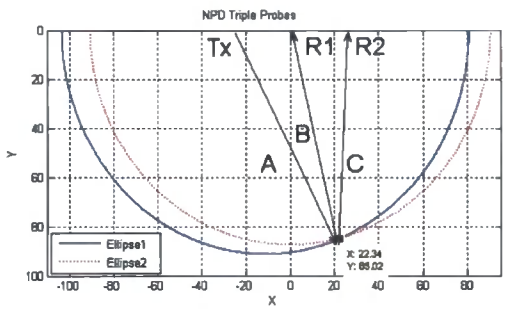

Figure 6 Triple Probes Scheme

2.5 NPD Simulation Model

Simulink Models have been built to simulate the Pulse-echo, Double Probes NPD and Triple Probes NPD algorithms. Figure 7 shows that by calculating the time delay of two transmit paths – t1 and t2, the algorithm can locate the pseudo defect in 2 dimensions. These blocks can be called as individual functions during the idle time in real-time data acquisition.

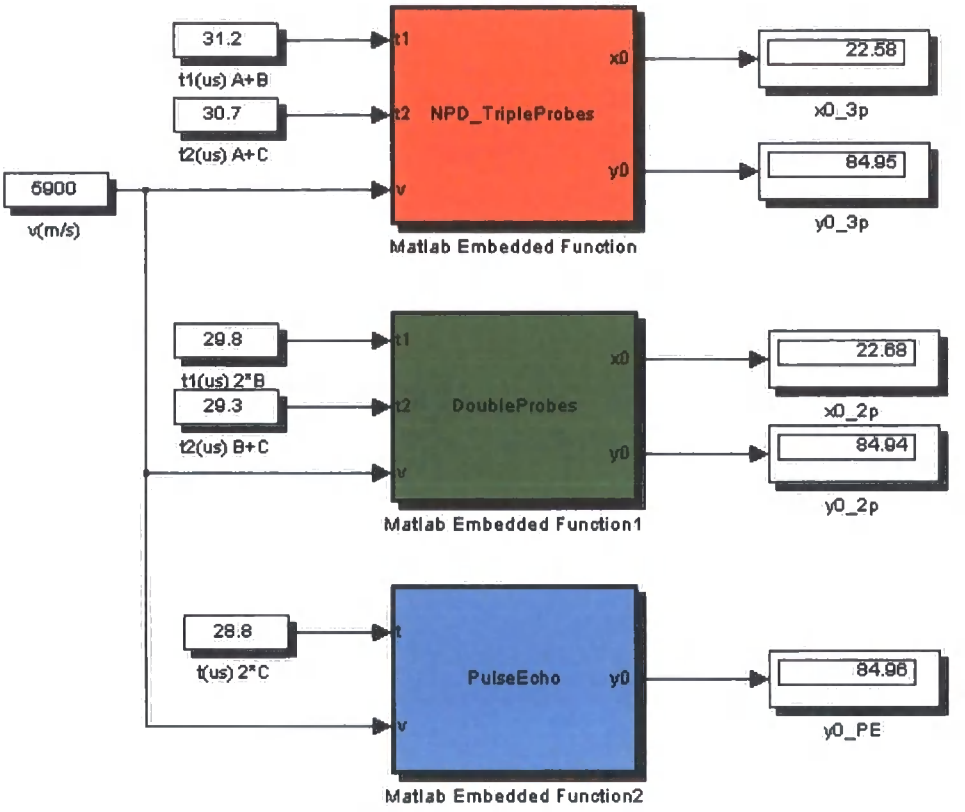

Figure 7 NPD Algorithm Simulation Model

3. DSP System

3.1Hardware

- TMS320C6713 DSK
- AED_330 Analog Expansion Daughterboard
- High Voltage High Frequency Amplifier
-

3.2Software

- Matlab and Simulink
- Code Composer Studio

3.3 System Architecture

Figure 8 depicts the architecture of a rapid Digital Signal Processing (DSP) prototype for the real-time testing system. Firstly a Simulink model is built using the MATLAB

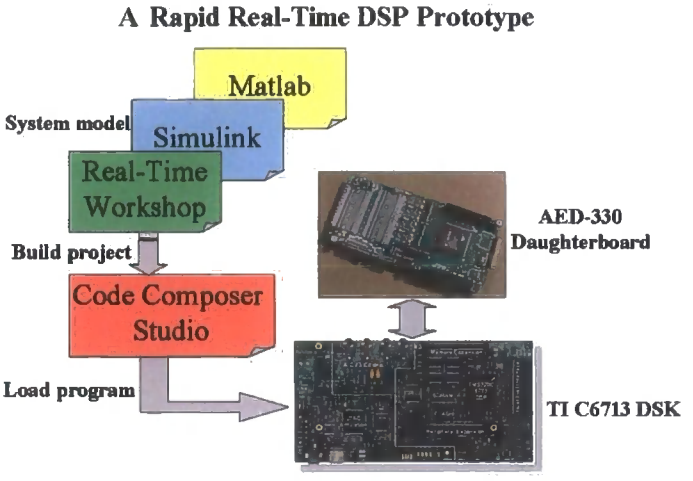

Figure 8 A Rapid Real-Time DSP Prototype

Embedded Target for DSP and DSP blockset which enable the rapid prototyping of real-time software for the TMS320C6713 floating-point processor and generates efficient code for the processor directly from the Simulink model. The generated code is readable and editable for manual optimization. The Embedded Target automates the creation of a link to the Integrated Development Environment, IDE, which provides board support software for the DSK board. It then invokes the compiler and linker to create a DSP executable file and finally downloads the executable to the DSK board and sets it running for real-time algorithm evaluation. An AED-330 analogue expansion daughterboard is mounted on the DSK to gain high speed digital to analogue and analogue to digital conversion for the desired high frequency pulse signal. Variable frequency and wave shape pulse signals can be used in order to gain the optimum testing conditions. A high voltage power amplifier is also designed to get a good response from the transducers (3). To remove the randomly distributed background noise that disturbs the recognition of the defect echoes and increase the behaviour of the system, several DSP algorithms such as correlation are applied and different filters including FIR filter and IIR filter can be chosen for real-time analysis as well (4).

4. Conclusion

The real-time system leads to a great improvement in verifying and realising NPD. Much information discarded by conventional test methods of ultrasonic billet inspection can be used due to modern advances in DSP. Therefore, the system not only improves the test integrity and sensitivity, but also makes the experiment data easy to acquire, analyze and visualise. After the successful simulation of the signal-channel system, a probe array based on the geometry in a typical ultrasonic defect detection system is being built and driven using sequential transmitter and parallel receiver processing units. The electronic hardware to achieve this goal has been designed and constructed.

References

1. P C Snowdon, S Johnstone, S Dewey, (2003), A 2D static ultrasonic array of passive probes for improved Probability of Detection, Nondestructive Testing and Evaluation, 19(3), pp. 111-120

2. PC Snowdon, S Johnstone, S Dewey, (2003), Improving the probability of detection for a 2D ultrasonic array using digital signal processing techniques, Insight 45(11)

3. R. L. Tutwiler, S Madhavan, K. V. Mahajan, (1999), Design of a Test System to Characterize Very High-Frequency Ultrasound Transducer Arrays, SPIE 3664(182)

4. R. Venteris, (2002) Exploration of DSP architectures in ultrasonic measurement application, Ultragarsas Journal 42(1)

Normal Probe Diffraction – Improving the capability of industrial ultrasonic probe arrays

Lei Zhang, Sherri Johnstone, Paul C. Snowdon, School of Engineering, University of Durham, DH1 3LE
Steve Dewey, STC, Rotherham, Corus

Abstract

In bloom and billet mills, on-line defect detection systems exist, in which each probe is sequentially used to produce a radio frequency pulse, which is then reflected from the defect and detected by the same probe. The work carried out in this project shows that extra information can be obtained about the defect if the diffracted signal is also collected by neighbouring probes and digital signal processing algorithms are applied to improve the signal to noise ratio. This technique is similar to time-of-flight diffraction, but does not require angled probes, and is thus referred to as normal probe diffraction, NPD. The advantage of this method is that it is possible to apply it in real-time thus giving the possibility of improved on-line defect detection, sizing and orientation. This paper describes the physical principles of NPD together with the hardware and software development required to implement the system in real time. The results on a simulated defect show that it can be detected from a distance of 41mm using NPD as opposed to 15mm with the sequential single probe pulse-echo method.

Key words: Normal Probe Diffraction (NPD), Digital Signal Processing (DSP), real-time, ultrasonic detection, non-destructive testing (NDT)

1. Introduction

The defects of steel mainly include inclusions, bubbles and cracks, all of which can affect the quality of the steel to some degree, therefore their detection and recognition is becoming increasingly significant, due to the customer lead demand for higher quality products. In steel making, on-line defect position and real-time size detection are desired. Many methods have been tried and developed for achieving a reliable cost-effective solution. Ultrasonic detection is commonly used in this field of non-destructive testing (NDT) in the steel industry. Traditional ultrasonic defect detection systems use an array of probes in which each probe pulses and receives sequentially. One new ultrasonic detection technology-Normal Probe diffraction (NPD) has been proven to enhance the probability of detection for steel testing in the previous research[1]. In this work, the necessary real-time system is simulated with software and the corresponding hardware is to be realised and tested to demonstrate the result. In order to gain the best testing effect, an ultrasonic pulser is designed to generate a variable frequency and pulse shape, which can be completely and flexibly controlled in real-time. A high voltage power amplifier is also designed to get a good response from the transducers. To remove the randomly distributed background noise that disturbs the recognition of the defect echoes and increase the behaviour of the system, several Digital Signal Processing (DSP) algorithms are applied and different filters can be chosen for real-time analysis as well. The developed real-time system will help increase the probability of detection of defects in steel billets and produce low-cost system solution for ultrasonic billet inspection in steel industry.

2. Previous Research

The previous research has investigated the potential within a current multi-probe ultrasonic detection system installed at a steel mill. Extensive laboratory experiments were carried out using the transducer array geometry, to extract additional information from passive probes. The apparatus was set up as shown in Figure1 [2].

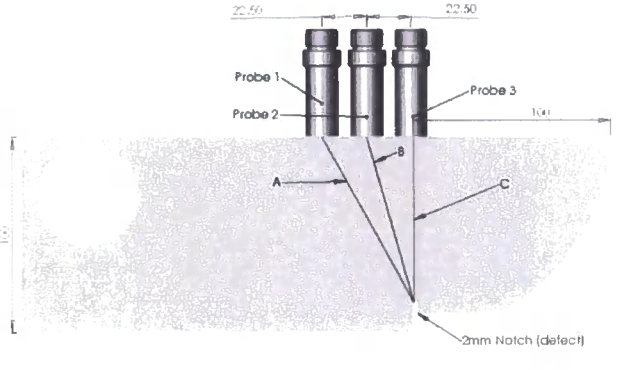

Figure 1 Probe Geometry

Figure 2 shows the increase of probability of detection using the standard single-probe-multi-receiver (SPMR) system over the conventional single-probe-single-receiver (SPSR) system. It shows that the NPD system starts detecting the defect at a lateral distance of 41mm from the defect whereas the pulse-echo probe needs to be within a range of 15mm. The physical principle behind this system uses diffracted waves from the edge of the defects and thus it is particularly effective for the increased detection and sizing of centre-line defects. This technique is defined as Normal Probe Diffraction (NPD), which has been successfully applied offline on a V1 calibration block and a single billet, but has not yet been applied for real-time control.

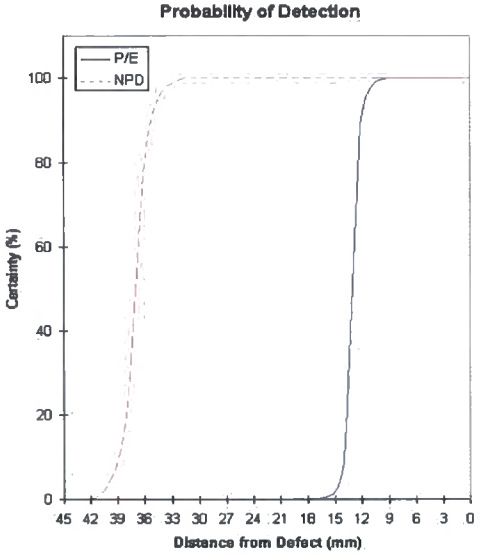

Figure 2 Comparison of Detection Range for NPD and Pulse-Echo techniques

Experiments show that the defect detection range can be increased by collecting the diffracted pulse on all the neighbouring probes. This is due to the defect being detected several times per pulse. The research project involves in developing a real-time laboratory based prototype which can detect defects using two methods: the standard single probe pulse echo technique and NPD, and testing the system on a V1 calibration block and a steel billet. In this project, the transmitting and receiving electronics are developed to enable the NPD technique to be applied in real-time.

3. Real Time Implementation

A good real-time implementation should be reliable, low power consuming, compact and always runs in real-time [3]. Sufficient amount of instructions per second and quick enough transport speed must be considered and calculated during the design procedure to meet the requirement of short delays between inputs and outputs in real-time implementation. This system uses general purpose digital signal processing microprocessors for solving signal processing problems in real-time, particularly focus on using the Texas Instruments (TI) TMSC6713 DSK (Digital Signal Processing Starter Kit) with the C6713 kernel floating processor to implement programs written in assembly and C. The TI C6713 DSK is for general real-time signal processing applications. The main applications taking place in this project are digital filter design using different DSP algorithms. These filters are characterized and applied on the received data. TI Hardware/software development tools (Code Composer Studio and DSP/BIOS) provide I/O channels for data exchange with Matlab in real-time.

System testing applies MATLAB and Simulink including several toolboxes. The MATLAB Embedded Target for TI C6000 DSP enables the rapid prototyping of real-time software for C6713 floating-point processor and generates efficient code for the processor directly from a Simulink model using MATLAB Real-Time Workshop. The generated code is readable and editable, and the code profiler identifies regions of generated code that may benefit from manual optimisation. The Embedded Target for TI C6000 DSP automates the creation of Link for Code Composer Studio project, provides board support for the C6713 DSK board, invokes Link for Code Composer Studio to create a DSP executable and downloads the executable to the DSK board for real-time algorithm evaluation. It also employs the link to enable interactive debugging and systematic testing of the DSP programs.

4. System Architecture

The system is available for testing single input and output channels with dual transducers (transmitter/receiver) and can be expanded for multi-channel testing as well. This system combines analogue and digital electronics technology together. The digital part consists of pulser generation and signal processing, while the analogue part includes pulse amplification and A/D (Analogue-to-Digital), D/A (Digital-to-Analogue) conversion. A single channel system is illustrated in figure 3. The digital pulse signal generated by C6713DSK, with a variable

Figure 3 Single Channel Test System Block

pulse repetition frequency (PRF), is converted to analogue signal by AED330 analogue daughter-card and amplified by a high voltage high frequency amplifier. The custom amplifier is designed and fabricated to give out a high voltage output above 200V. The echoed signal is received, digitised and buffered for the further use of data analysis by a program loaded on the DSK. The program implements the functions of frequency spectrum analysis, an IIR (Infinite Impulse Response) or FIR (Finite Impulse Response) filter and defect depth calculated from transceiver time delay.

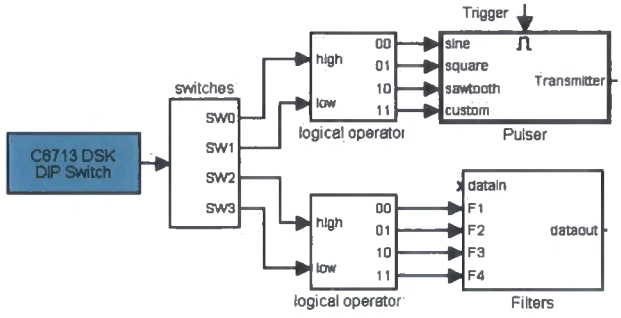

Figure 4 DIP Switches Controlling system

Table1 DIP Switches

D0	D1	PULSE	D2	D3	FILTER
0	0	Sinewave	0	0	IIR Band pass
0	1	Square	0	1	IIR Low pass
1	0	Sawtooth	1	0	FIR Band pass
1	1	Custom	1	1	FIR Low pass

The 6713DSK includes four DIP switches as a simple way to provide the user with flexible interactive control. These four switches are divided into two groups. One is used to control the waveforms of the generator's outputs; the other offers four different choices for the filter applying upon the echoed signal. Figure 4 Shows the controlling system built with Simulink and Table 1 indicates the corresponding switch setting modes.

6. Conclusion

The real-time system leads to a great improvement in verifying and realising NPD. Much information discarded by conventional test methods of ultrasonic billet inspection can be used due to modern advances in DSP. Therefore, the system not only improves the test integrity and sensitivity, but also makes the experiment data easy to acquire, analyze and visualise. After the successful simulation of the signal-channel system, a probe array based on the geometry in a typical ultrasonic defect detection system is to be built and driven by using sequential transmitter and parallel receiver processing units. The electronic hardware to achieve this goal is to be designed, constructed and tested in the following research.

7. Further Research

The single channel ultrasonic detection system discussed in this paper can be replicated to develop a multi-channel system by adding a software control structure for control and synchronization of single component [4]. FPGA architecture will give the multi-channel system the ability to perform in real-time. In NPD multi-channel system, each transducer is assigned to be the transmitter sequentially and the other transducers receive echoed signal. As multiple receivers can be set up to test in 3D, more diffracted signal are detected and more information is obtained. It is expected that the position and size of defect can be tested as well.

References

[1] PC Snowdon, S Johnstone, S Dewey, (2003), *A 2D static ultrasonic array of passive probes for improved Probability of Detection*, Nondestructive Testing and Evaluation, 19(3), pp. 111-120

[2]PC Snowdon, S Johnstone, S Dewey, (2003), Improving the probability of detection for a 2D ultrasonic array using digital signal processing techniques, Insight 45(11)

[3] R. Venteris, (2002) *Exploration of DSP architectures in ultrasonic measurement application*, Ultragarsas Journal 42(1)

[4] R. L. Tutwiler, S Madhavan, K. V. Mahajan, (1999), Design of a Test System to Characterize Very High-Frequency Ultrasound Transducer Arrays, SPIE 3664(182)

Poster presented at The 41st Annual British Conference on NDT held in Southport UK. September 2002.

Sponsored by corus

University of Durham School of Engineering

The Ultrasonic Detection of Discontinuities using Single Active and Multi-Passive Transducers

Paul C. Snowdon
Sherri Johnstone

E-mail
paul.snowdon@durham.ac.uk

Introduction

The manufacturer currently inspects its products using several methods. The main area of interest in this project is the core of the material, and for this the manufacturer uses a static immersion ultrasonic system. This ultrasonic flaw detection system operates in a standard pulse/echo mode. The system uses two static array banks of 8 probes, set at 90 degrees to each other (see fig.2). At present these probes operate independently of each other; that is the probe that transmits an ultrasonic pulse also receives the echo of that pulse. This gives complete flaw detection coverage of the selected area.

The Project

If however, more than one or all of the probes could be used simultaneously, the system would potentially have greater efficiency.

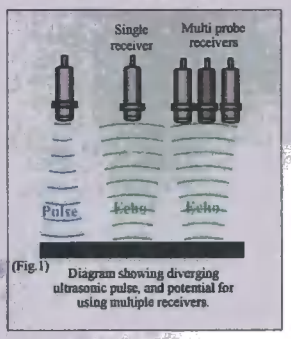

(Fig.1) Diagram showing diverging ultrasonic pulse, and potential for using multiple receivers.

The project research is to investigate the potential within the current system for using the passive (non pulsing) probes as receivers. This could lead theoretically to a faster throughput of material or a greater sensitivity of defect detection, and potentially higher reliability of defect detection.

(Fig.2) Photograph showing a typical probe array set-up.

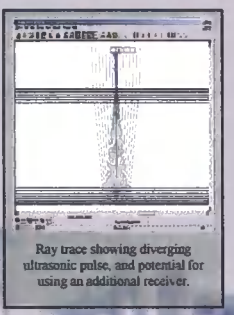

Ray trace showing diverging ultrasonic pulse, and potential for using an additional receiver.

The proposed system relies upon the divergence of the sound wave emitted from a transducer. However this signal, received at the passive probes, is required to be of sufficient strength, and carry additional information to the signal received at the active probe. The initial review of the project has been concentrating on this area, and the problems arising within the sound-field. This has included using several standard mathematical simulations of the sound field and its various properties.

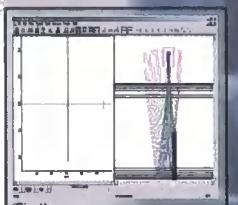

(Fig.4) Ray trace A scan showing pulse/echo signal from front and back-wall only. Ray trace showing pulse echo signal with signal of defect missing the receiver.

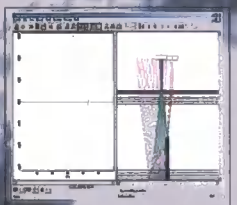

Ray trace A scan showing echo signal from defect only. Ray trace showing pulse/echo signal with echo signal from defect hitting the passive receiver.

Simulations

Initial simulation experiments have been completed using UTEX Scientific Instruments Inc. Imagine3D ray tracing software. Some of the results are displayed, and show that there is a potential for using these passive probes. Physical experiments are on going, using a standard immersion techniques and a single channel Socomate USPC 3100.

Ray trace showing the potential of using two probes set at 90 degrees in a pitch and mode.

(Fig.6) Ray traces produced using UTEX *Imagine3D*

Laboratory Experiment

The above experiment has been reproduced in the laboratory using two 5MHz immersion transducers set at 90 degrees and the stated flaw detection equipment. It was decided that the initial experiments would be carried out on an immersed round steel bar 8mm diameter.

The two A scans below show the traces of the 8mm bar. The first (Fig.8), is in standard pulse/echo mode. The next (Fig.9) is at 90 degrees to the pulsar. (see Fig.7)

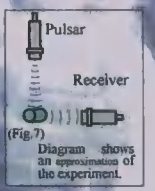

(Fig.7) Diagram shows an approximation of the experiment.

Traces from 8mm bar.

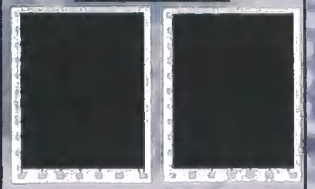

(Fig.8) Pulse echo trace (Fig.9) 90degree trace

Future Experiments

The next set of experiments is to include, tests on material with a side drilled hole, as the Imagination 3D, (Fig.6), with the probes arranged at 90degrees and adjacent to each other.

Background photograph of United States Steel Corporation, Gary Works, supplied by The University of Indiana

Poster presented at The 41st Annual British Conference on NDT held in Southport UK. September 2002.

Sponsored by corus

University of Durham School of Engineering

The Ultrasonic Detection of Discontinuities using Single Active and Multi-Passive Transducers

Paul C. Snowdon
Sherri Johnstone

E-mail
paul.snowdon@durham.ac.uk

Introduction

The manufacturer currently inspects its products using several methods. The main area of interest in this project is the core of the material, and for this the manufacturer uses a static immersion ultrasonic system. This ultrasonic flaw detection system operates in a standard pulse/echo mode. The system uses two static array banks of 8 probes, set at 90 degrees to each other (see fig.2). At present these probes operate independently of each other; that is the probe that transmits an ultrasonic pulse also receives the echo of that pulse. This gives complete flaw detection coverage of the selected area.

The Project

If however, more than one or all of the probes could be used simultaneously, the system would potentially have greater efficiency.

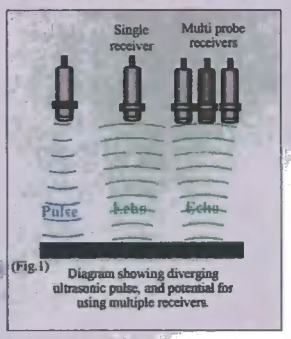

(Fig.1) Diagram showing diverging ultrasonic pulse, and potential for using multiple receivers.

The project research is to investigate the potential within the current system for using the passive (non pulsing) probes as receivers. This could lead theoretically to a faster throughput of material or a greater sensitivity of defect detection, and potentially higher reliability of defect detection.

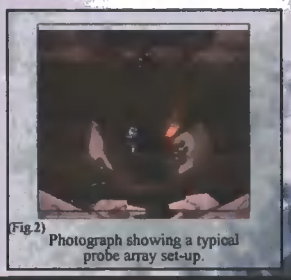

(Fig.2) Photograph showing a typical probe array set-up.

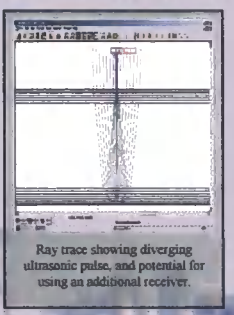

Ray trace showing diverging ultrasonic pulse, and potential for using an additional receiver.

The proposed system relies upon the divergence of the sound wave emitted from a transducer. However this signal, received at the passive probes, is required to be of sufficient strength, and carry additional information to the signal received at the active probe. The initial review of the project has been concentrating on this area, and the problems arising within the sound-field. This has included using several standard mathematical simulations of the sound field and its various properties.

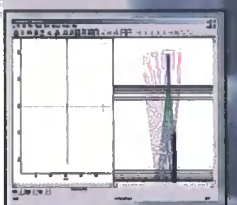

(Fig.4) Ray trace A scan showing pulse/echo signal from front and back-wall only. Ray trace showing pulse echo signal with signal of defect missing the receiver.

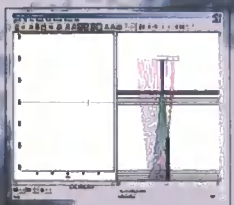

Ray trace A scan showing echo signal from defect only. Ray trace showing pulse/echo signal with echo signal from defect hitting the passive receiver.

Simulations

Initial simulation experiments have been completed using UTEX Scientific Instruments Inc. Imagine3D ray tracing software. Some of the results are displayed, and show that there is a potential for using these passive probes. Physical experiments are on going, using a standard immersion techniques and a single channel Socomate USPC 3100.

Ray trace showing the potential of using two probes set at 90 degrees in a pitch and mode.

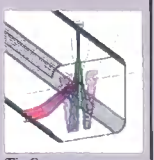

(Fig.6) Ray traces produced using UTEX *Imagine3D*

Laboratory Experiment

The above experiment has been reproduced in the laboratory using two 5MHz immersion transducers set at 90 degrees and the stated flaw detection equipment. It was decided that the initial experiments would be carried out on an immersed round steel bar 8mm diameter.

The two A scans below show the traces of the 8mm bar. The first (Fig.8), is in standard pulse/echo mode. The next (Fig.9) is at 90 degrees to the pulsar. (see Fig.7).

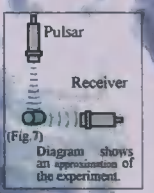

(Fig.7) Diagram shows an approximation of the experiment.

Traces from 8mm bar.

(Fig.8) Pulse echo trace (Fig.9) 90degree trace

Future Experiments

The next set of experiments is to include, tests on material with a side drilled hole, as the Imagination 3D, (Fig.6), with the probes arranged at 90degrees and adjacent to each other.

Background photograph of United States Steel Corporation, Gary Works, supplied by The University of Indiana

NPD, a low cost ultrasonic static array system for improved POD

Abstract

The aim of this project was to investigate the potential within a current multi-probe ultrasonic Non-Destructive Testing (NDT) system installed at a steel mill. Extensive laboratory experiments were carried out using an existing online transducer array geometry, to extract additional information from passive probes.

The technique devised involves the transmission from a single transducer and reception on several adjacent transducers, with the aim of detecting a diffracted signal from a discontinuity.

The technique has been termed Normal Probe Diffraction (NPD).

The process also employs Digital Signal Processing (DSP), to improve the Signal to Noise Ratio (SNR), which is essential for small signal recognition.

This paper describes the theory of NPD with reference to SAFT and TOFD and shows how the technique maximises the scanned volume within the material under inspection without the loss of resolution, and also how it can effectively locate defects using simple geometric methods.

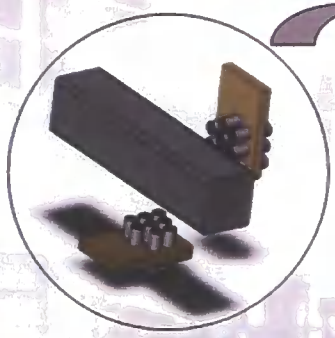

The project was progressed onto a section of material, with a known defect, and with a repeatable experimental set-up.

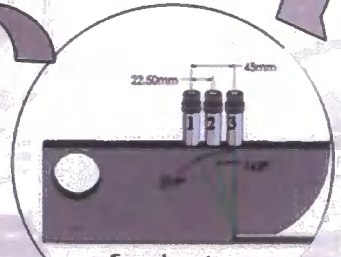

Experiment on V1 calibration block

The transducer array scanned the V1 block with probe 3 transmitting and probes 1 & 2 receiving. The received A-scans where compiled to produce a B-scan.

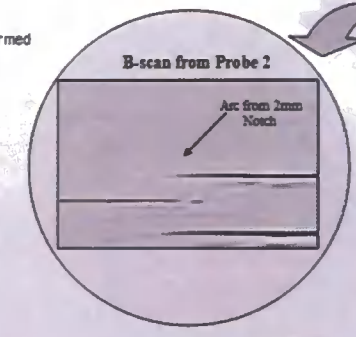

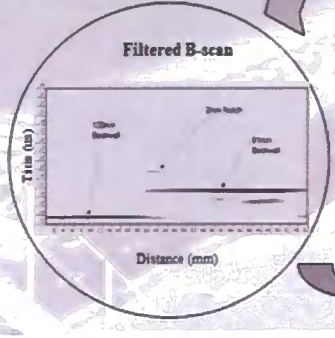

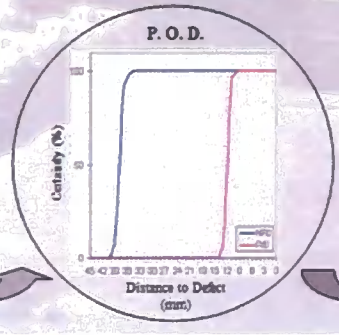

The project has shown that a diffracted signal can be produced and detected using probes normal to the inspection surface, using a V1 calibration block with improved P.O.D.

Poster presented at QNDE 2004